

**TWO DIMENSIONAL LOOP SHAPING CONTROLLER DESIGN FOR  
PAPER MACHINE CROSS-DIRECTIONAL PROCESSES**

By

Gregory Edward Stewart

B. Sc. (Honours Physics) Dalhousie University

M. Sc. (Mathematics) Dalhousie University

A THESIS SUBMITTED IN PARTIAL FULFILLMENT OF  
THE REQUIREMENTS FOR THE DEGREE OF  
DOCTOR OF PHILOSOPHY

in

THE FACULTY OF GRADUATE STUDIES  
DEPARTMENT OF ELECTRICAL AND COMPUTER ENGINEERING

We accept this thesis as conforming  
to the required standard

THE UNIVERSITY OF BRITISH COLUMBIA

August 2000

© Gregory Edward Stewart, 2000

In presenting this thesis in partial fulfilment of the requirements for an advanced degree at the University of British Columbia, I agree that the Library shall make it freely available for reference and study. I further agree that permission for extensive copying of this thesis for scholarly purposes may be granted by the head of my department or by his or her representatives. It is understood that copying or publication of this thesis for financial gain shall not be allowed without my written permission.

Department of Electrical and Computer Engineering  
The University of British Columbia  
2356 Main Mall  
Vancouver, Canada  
V6T 1Z4

Date:

August, 27, 2000

## Abstract

The objective of this work is the development of a practical technique for the design of feedback controllers for the cross-directional control of paper machines.

An industrial paper machine produces a wide sheet of paper which is required to be of uniform quality in terms of the weight, moisture content, and caliper (thickness). Modern machines produce a paper sheet which is up to 11 metres in width and is properly described as a two dimensional system. The direction perpendicular to the sheet travel is known as the cross-direction, and cross-directional control is implemented by arrays of up to 300 identical actuators evenly distributed across the sheet width. The sheet properties are measured by a scanning sensor at up to 2000 locations evenly spaced across the width of the moving paper sheet.

A constructive, computationally inexpensive, graphical controller design technique is developed for dynamical systems that are distributed in one spatial dimension and controlled by an array of identical actuators. The feedback controller is designed using a two dimensional loop shaping technique with reference to the process model and the model uncertainty such that the spatial and dynamical bandwidth limitations of the physical system are respected.

The two dimensional loop shaping design technique is then applied to the design of cross-directional feedback controllers for the paper making process. The two dimensional loop shaping approach is well-suited to address the wide variety of processes and conditions for which a cross-directional controller must perform well.

The design technique is demonstrated by successfully tuning an industrial cross-directional controller. The tuning results are confirmed by experiments with a real paper machine in a working mill.

# Table of Contents

<b>Abstract</b>	<b>ii</b>
<b>List of Figures</b>	<b>vi</b>
<b>Acknowledgements</b>	<b>x</b>
<b>1 Introduction</b>	<b>1</b>
1.1 Paper Machine Cross Direction Processes . . . . .	1
1.1.1 Basis Weight Control . . . . .	3
1.1.2 Moisture Control . . . . .	6
1.1.3 Caliper Control . . . . .	9
1.2 Industrial Cross-Directional Control . . . . .	11
1.3 Theoretical Work . . . . .	14
1.3.1 Complexity . . . . .	15
1.3.2 Large Scale Problem . . . . .	17
1.3.3 Ill-Conditioned System . . . . .	19
1.3.4 Model Uncertainty . . . . .	20
1.4 Related Applications . . . . .	23
1.5 Aims and Contributions of the Work . . . . .	24
<b>2 Problem Specifications</b>	<b>27</b>
2.1 Spatially Distributed Process Model . . . . .	27
2.2 Controller Implementation . . . . .	32
2.3 Performance . . . . .	36
2.4 Uncertainty and Robustness . . . . .	39

<b>3</b>	<b>Spatial Frequency Decomposition</b>	<b>43</b>
3.1	Circulant Extension of a Toeplitz System . . . . .	45
3.2	Generalized Plant and Linear Fractional Transformations . . . . .	48
3.3	Systems Composed of Symmetric Circulant Blocks . . . . .	51
3.4	Closed-Loop Performance . . . . .	56
3.5	Closed-Loop Robust Stability . . . . .	60
3.6	Example . . . . .	63
3.7	Graphical Interpretation . . . . .	66
3.7.1	Singular Values, Eigenvalues, and Spatial Frequencies . . . . .	67
3.7.2	Two Dimensional $\omega\nu$ -Plots . . . . .	69
<b>4</b>	<b>Two Dimensional Loop Shaping</b>	<b>74</b>
4.1	Traditional Loop Shaping . . . . .	75
4.2	Two Dimensional Frequency Domain Specifications . . . . .	78
4.3	Controller Spatial Order Reduction with Stability Requirement . . . . .	83
4.4	Two Dimensional Loop Shaping Design Procedure . . . . .	89
<b>5</b>	<b>Industrial Paper Machine Control</b>	<b>93</b>
5.1	Prototype Tuning Tool . . . . .	93
5.2	Field Test: Consistency Profiling for Newsprint . . . . .	95
5.2.1	Process Model . . . . .	99
5.2.2	Design Specifications . . . . .	101
5.2.3	Two Dimensional Open-Loop Shaping . . . . .	104
5.2.4	Paper Mill Results . . . . .	116
<b>6</b>	<b>Conclusions</b>	<b>120</b>

**Bibliography**

**123**

**A Fourier Matrices**

**130**

# List of Figures

1.1	Wide view of the paper machine showing relative positions of the various actuator arrays and scanning sensor(s). (Artwork courtesy of Honeywell-Measurex.) . . . . .	2
1.2	Steady-state response of basis weight to slice lip actuators on a heavy grade 200gsm linerboard machine. This is one of the wider weight responses in CD control. (Data courtesy of Honeywell-Measurex.) . . . . .	5
1.3	Steady-state response of basis weight to consistency profiling actuators on a 45gsm newsprint machine. (Data courtesy of Honeywell-Measurex.) . . . . .	7
1.4	Steady-state response of moisture to steam box profiling actuators on a machine making 50gsm paper with 6% moisture target. (Data courtesy of Honeywell-Measurex.) . . . . .	9
1.5	Steady-state response of moisture to rewet shower profiling actuators on a machine making 50gsm paper with 6% moisture target. (Data courtesy of Honeywell-Measurex.) . . . . .	10
1.6	Steady-state response of caliper to induction heating profiling actuators on a machine making newsprint with $78\mu\text{m}$ caliper target. (Data courtesy of Honeywell-Measurex.) . . . . .	12
1.7	The flow of information for an industrial cross-directional control system. . . . .	13
2.1	(a) Column of the matrix $B \in \mathcal{R}^{73 \times 73}$ in (2.8) identified from a basis weight process controlled by $n = 73$ slice lip actuators. (b) The singular value decomposition of $B$ . (Data courtesy of Honeywell-Measurex.) . . . . .	31
2.2	Feedback controller configuration. . . . .	34
2.3	The industrial cross-directional controller block diagram. . . . .	35

2.4	Singular values of the process model $G(e^{i\omega}) \in \mathcal{C}^{73 \times 73}$ in (2.1) and model uncertainty $l(\omega) = 10^{-2}$ in (2.26) for the basis weight process illustrated in Figure 2.1. . . . .	41
3.1	Non-zero elements of a banded symmetric circulant matrix $M$ , the associated band-diagonal Toeplitz symmetric matrix $M_t$ , and the difference described by the ‘ears’ in $\delta M_t = M - M_t$ . . . . .	47
3.2	Block diagram of the linear fractional transformation $\mathcal{F}_l(P, K)$ in (3.9). . .	50
3.3	Geometric interpretation of the decomposition of a SISO transfer function $g(z)$ in terms of dynamical frequencies $g(e^{i\omega})$ . The $\mathcal{H}_2$ and $\mathcal{H}_\infty$ norms of the original transfer function $g(z)$ may be represented in the frequency domain. As indicated, the square of the $\mathcal{H}_\infty$ -norm, $\ g(z)\ _\infty^2$ , is given by the maximum height of the curve. The square of the $\mathcal{H}_2$ -norm, $\ g(z)\ _2^2$ , is proportional to the area under the curve. . . . .	72
3.4	$\omega\nu$ -plot for the symmetric circulant transfer matrix $G(z)$ in terms of spatial and dynamical frequencies $FG(e^{i\omega})F^T = \tilde{G}(e^{i\omega}) = \text{diag}\{\tilde{g}(\nu_j, e^{i\omega})\}$ . The $\mathcal{H}_2$ and $\mathcal{H}_\infty$ norms of the original transfer matrix $G(z)$ may be represented in this domain. As indicated, the square of the $\mathcal{H}_\infty$ -norm, $\ G(z)\ _\infty^2$ , is given by the maximum height of the surface as indicated at $(\nu, \omega) \approx (0.7, 1.3)$ . The square of the $\mathcal{H}_2$ -norm, $\ G(z)\ _2^2$ , is proportional to the volume bounded by the surface. . . . .	73
4.1	Traditional multivariable open-loop singular value shaping. The performance requirement places a lower bound on $\sigma(GK)$ for low frequencies $\omega < \omega_l$ . The safety requirements (robust stability, limited control action, etc.) place an upper bound on $\bar{\sigma}(GK)$ for high frequencies $\omega > \omega_h$ . . . . .	77
4.2	The analogous open-loop $\omega\nu$ -surface shaping. Note that contrary to traditional loop shaping, the performance constraint is not selected to cover all singular values $j \in \{1, \dots, n\}$ . The roll-off of the gain of the plant $\tilde{g}(\nu_j, z)$ for high spatial frequencies $\nu_j$ places a limit on the spatial bandwidth of a closed-loop system. . . . .	81

4.3	The $\omega\nu$ contour plot shows that this design was too aggressive. The robustness condition (4.4) is not satisfied for all $\{\nu_j, \omega\} \in \Omega_h$ , as the $ \tilde{g}(\nu_j, e^{i\omega})\tilde{k}(\nu_j, e^{i\omega})  = w_h$ contour intersects $\Omega_h$ . . . . .	83
4.4	The $\omega\nu$ contour plot shows that this design was too conservative. The performance condition (4.3) is not satisfied for all $\{\nu_j, \omega\} \in \Omega_l$ , as the $ \tilde{g}(\nu_j, e^{i\omega})\tilde{k}(\nu_j, e^{i\omega})  = w_l$ contour intersects $\Omega_l$ . . . . .	84
4.5	The $\omega\nu$ contour plot illustrates a design which has successfully traded off the conflicting requirements. . . . .	85
5.1	Model identification: The upper plot illustrates the actuator profile shape used to excite the process during the model identification. The second plot indicates the ‘true’ measured basis weight response profile. The last plot indicates the modelled response. The lower plot contains the residual signal due to process disturbances and model uncertainty. . . . .	100
5.2	Contour plot of the open-loop basis weight frequency response $ \tilde{g}(\nu_j, e^{i\omega}) $ for the model in (5.1)–(5.8). The area outside the 0.1 contour indicates the region of the $\omega\nu$ -plane for which there is more than 100% relative model uncertainty. Even at steady-state, over a quarter of the spatial frequencies (60 out of 226 singular vectors) are uncontrollable. . . . .	102
5.3	Contour plots in $\omega\nu$ of the sets $\Omega_l$ in (5.21) and $\Omega_h$ in (5.24). The performance condition (5.22) is satisfied if the contour(s) $ \tilde{k}(\nu_j, e^{i\omega})  = 22.0$ lie outside the set $\Omega_l$ . The robust stability condition (5.25) is satisfied if the contour(s) $ \tilde{k}(\nu_j, e^{i\omega})  = 5.0$ lie outside the set $\Omega_h$ . The contours of the full-matrix controller $K(z)$ obtained in the ‘Controller Synthesis’ step are illustrated as the solid lines. The contours of the controller $K_l(z)$ obtained by spatial order reduction are illustrated as the dashed lines. . . . .	107
5.4	The spectra $\tilde{s}(\nu_j)$ and $\tilde{c}(\nu_j)$ resulting from the controller synthesis for the controller $\tilde{k}(\nu_j, z)$ in (5.17) and (5.19). The dashed line represents the spectrum of $\tilde{c}_l(\nu_j)$ obtained by spatial order reduction. . . . .	111

5.5	The central row of the full circulant matrices $C(113, :)$ and $I - S(113, :)$ resulting from the spectrum $\tilde{c}(\nu_j)$ and $\tilde{s}(\nu_j)$ in Figure 5.4 and $C = F^T \text{diag}\{\tilde{c}(\nu_1), \dots, \tilde{c}(\nu_{226})\}F$ and $S = F^T \text{diag}\{\tilde{s}(\nu_1), \dots, \tilde{s}(\nu_{226})\}F$ . . . . .	112
5.6	The central row of the banded circulant matrix $C_l(113, :)$ resulting from the spatial order reduction (5.34). The central row of the banded circulant matrix $I - S_l(113, :)$ is also shown, due to the structure of the industrial controller $S_l = S$ and no spatial order reduction was required. . . . .	114
5.7	An $\omega\nu$ contour plot showing the controller $ \tilde{k}_b(\nu_j, z) $ in (5.43) relative to the sets $\Omega_l$ in (5.21) and $\Omega_h$ in (5.24). The performance criterion is violated since the contour $ \tilde{k}_b(\nu_j, e^{i\omega})  = 22.0$ intersects the set $\Omega_l$ . . . . .	117
5.8	The steady-state of the measured paper profiles under closed-loop control, (a) with the controller $K_b(z)$ in (5.41) which was designed according to the more traditional industrial tuning rules, and (b) with the controller $K_t(z)$ in (5.39) which was designed according to two dimensional loop shaping procedure in Chapter 4. . . . .	118
5.9	Spatial frequency power spectra of the steady-state error profiles of the closed-loop system with the controller $K_b(z)$ in (5.41) shown as the dashed line, and the controller $K_t(z)$ in (5.39) shown as the solid line. . . . .	119

## Acknowledgements

This work was performed as a collaboration between the industrial partner Honeywell-Measurex and the University of British Columbia. I would like to thank my supervisors, Dr Dimitry Gorinevsky at Honeywell-Measurex and Dr Guy Dumont at UBC for their guidance, advice, and friendship throughout the course of this project.

The efforts of my committee members and readers, Drs Michael Davies, Peter Lawrence, Dale Cherchas, Peter Wellstead, Tim Salcudean, André Ivanov, and Bruce Dunwoody, are gratefully acknowledged.

A number of people at the University of British Columbia has been very enjoyable and productive. In particular, I would like to thank Lisa Brandly, Brenda Dutka, Georgina White, Brian MacMillan, Rita Penco, Ken Wong, and Debbie Lin for being there to help with any problems that I encountered while studying there.

This work would not have been possible without the support (both financial and technical) of the industrial partner Honeywell-Measurex. This collaboration has been a very valuable experience for myself. I am very grateful to the following people for all of their help: Cristian Gheorghe, Johan Backstrom, Bob Vyse, Mike Heaven, Gary Burma, Stephen Chu, Paul Baker, Dan Stevens, Scott Morgan, Max Kean, Chris Sung, Rob Spinner, Tom Steele, Salim Ladak, Jahan Ghofraniha, Ali Arya, Kevin Carlson, Sharon Phillips, Rebecca Mulhern, Sandra Dick, Howard Robinson, Peter Ponter, and Mike Yuswack.

The technical material concerning the characteristics of industrial paper machines in Section 1.1 is based on discussions with the experienced engineers at Honeywell-Measurex. Special thanks to Jonathan Crawford, Thomas Congdon, Eric Passiniemi, Johan Backstrom, and Bob Vyse.

Over the past years, I have benefited from technical discussions/arguments with a large number of people. I have been very lucky to meet and work with my fellow students at UBC, Kayvan Najarian, Jan Bergstrom, Ahmed Ismail, Stevo Mijanovic, Michael

Chong Ping, and Shiro Ogawa. In addition, Mihai Huzmezan, Stephen Duncan, Michael Safonov, Karl Astrom, Elisabeth Paul, Rob Leitch, and Glen Viau, have all provided technical input that shaped this work.

I would like to thank my parents James and Heather Stewart for their support and advice. The last few years have been made much easier as a result.

Finally, I owe a great deal to my new wife Elisabeth Paul. She is a wonderful partner and a tremendous inspiration in my life. Her patience, thoughtfulness, and love have made everything else possible. Je suis ton amoureux pour toujours.

# Chapter 1

## Introduction

### 1.1 Paper Machine Cross Direction Processes

The job of a paper machine is to transform a slurry of water and wood cellulose fibres into a saleable sheet of paper as efficiently as possible. The following description of its operation is very brief and more complete discussions of this complex process may be found in [9, 57]. Figure 1.1 illustrates the main parts of a typical configuration of a Fourdrinier style paper machine. The slurry enters the headbox at the left of the figure and the dry paper is wound up on a roll at the far right in the figure.

Wet pulp at about 0.5% consistency (0.5% fibres and 99.5% water) is pumped into the headbox of the paper machine. The job of the headbox is to distribute the slurry such that the fibres are evenly distributed over the wide flow area (up to 11m). The slurry is then deposited on to an endless wire mesh belt which may be moving at speeds in excess of 100km/h. The wet pulp is dewatered as water is lost through the mesh due to blades and suction boxes placed under the wire screen. The sheet, now composed of approximately 20% solids, is heated by steam boxes before and during the press section where it is pressed and dewatered between counter-rotating rollers. The sheet, now about 40% dry, then enters the dryer section and a series of steam heated dryer cans. The sheet of paper exiting the dryer section typically contains 5-9% water content by weight. The dry sheet then enters a series of rotating rollers known as the calendar stack where the sheet thickness, or caliper, is controlled. In paper production, the three most important properties of the finished product are (1) the sheet weight per unit area in terms of grams per square metre (gsm), (2) the sheet moisture content expressed as a percentage of the sheet weight (%), (3) the caliper or thickness of the sheet expressed here in  $\mu\text{m}$ . These properties are each measured by a scanning sensor which traverses back and forth across the moving paper sheet.

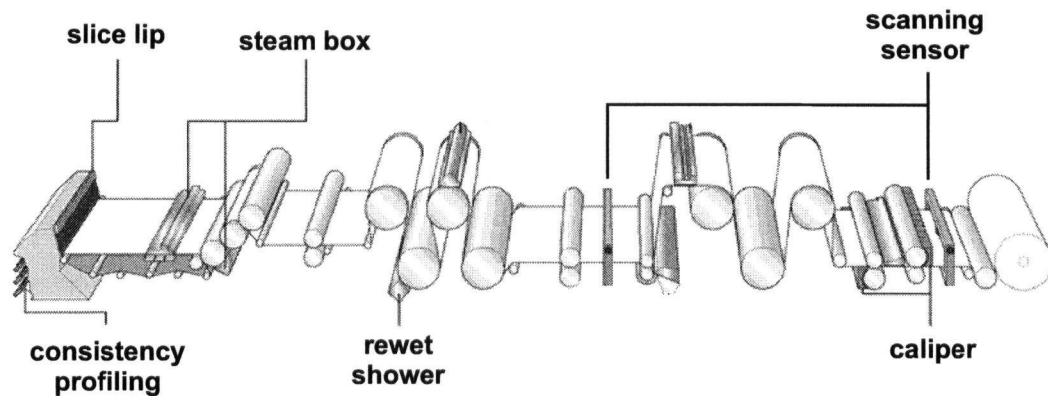


Figure 1.1: Wide view of the paper machine showing relative positions of the various actuator arrays and scanning sensor(s). (Artwork courtesy of Honeywell-Measurex.)

The quality of the paper sheet is defined in terms of the variance of these properties [1]. If a roll of paper is produced which is measured by the scanning sensor at  $m$  locations and the roll consists of  $T$  scans, then the sheet measurements are given by  $x(i, j)$  where  $i = 1, \dots, m$  and  $j = 1, \dots, T$ , and the average is given by,

$$\bar{x} := \sum_{i=1}^m \sum_{j=1}^T \frac{x(i, j)}{mT} \quad (1.1)$$

The variance of the two-dimensional measured paper sheet is known within the industry as ‘two-sigma’ and is defined by

$$2\sigma := 2 \cdot \sqrt{\sum_{i=1}^m \sum_{j=1}^T \frac{(x(i, j) - \bar{x})^2}{mT - 1}} \quad (1.2)$$

and is an important quality factor. Many control strategies have posed the CD control problem in terms of a minimization of (1.2) with the setpoint  $r$  substituted for the profile average  $\bar{x}$  in (1.2).

In order to define the control problem, some definitions and orientation is required. The direction of sheet travel is known as the machine direction or MD and is from the left to right in Figure 1.1. The direction perpendicular to the sheet travel is known as the cross direction or CD. Due to the process design and nature of the actuators, the

industrial approach to paper machine control considers the MD and the CD problems separately.

MD control is concerned with controlling the average value of each scan. The control of the dynamically varying, but zero-mean, error profile is known as CD control and is the task of arrays of actuators distributed across the width of the paper machine, as shown in Figure 1.1. However, as the sensor is scanning a moving sheet, it traces a diagonal path across the paper sheet, and thus it does not measure pure MD and CD paper profiles. Filtering of the sensor signal is used to aid in the separation of the MD and CD components.

The majority of industrial paper machines possess at least one CD actuator array for each of the three main paper properties. The most common CD control techniques are outlined below.

### 1.1.1 Basis Weight Control

The weight per unit area of a sheet of paper, is an important factor in the quality of the finished product, the metric measurement is grams per square metre (gsm). Variations in the weight of the paper sheet will affect most other properties [9]. A sheet of newsprint has a weight of about 45gsm, a paperback book cover may have a weight of about 300gsm, and cardboard may weigh 450gsm.

CD control of the weight of a paper sheet is accomplished by actuators at the headbox (Figure 1.1). The job of weight control actuators is to achieve an even distribution of the pulp fibres across the width of the wire belt, despite changing pulp properties. Since the weight control actuators are located the furthest upstream, the dynamics of weight control often require the consideration of a significant dead time component, as the paper sheet must travel through the entire machine before reaching the scanning sensor.

Since the raw material used is wood, it happens that the pulp stock characteristics change over time. The consistency and drainage properties of the delivered stock are kept as constant as possible by the approach system, but variability inevitably occurs. In addition, the flow of the pulp stock through the headbox and on the wire belt can

distribute the wood fibres unevenly in the cross-direction. Basis weight profile control is important not only for paper strength reasons, but also due to the fact that a poor quality weight profile will propagate downstream and appear as disturbances in both the moisture and caliper profiles.

The operation of the two most common weight control actuators is described next.

### **Slice Lip**

The use of a slice lip is the traditional method of controlling the CD profile of basis weight of a paper sheet. The slurry exits the headbox through an opening which is as wide as the paper machine (up to 11m) but only 1cm–2cm tall for fine paper and 4cm–6cm tall for linerboard. The amount of pulp exiting the headbox is controlled by locally changing the height of this opening by bending its flexible upper lip. A taller opening is used to allow more pulp on to the wire thus increasing the amount of fibres at that location and increasing the basis weight.

The bending of this upper lip is controlled by an array of force actuators distributed along its length. A typical slice lip installation has  $n = 50$  of such actuators in the array, but there exist installations with  $n = 118$  or more slice lip actuators. The actuator spacing is quite variable depending on the installation and is anywhere from 7.0cm to 20cm.

The response of the basis weight profile to the slice lip actuators varies widely. Moving a slice lip actuator in a 45gsm newsprint installation results in changing the weight profile only for a strip about as wide as the actuator zone itself. Heavy grade paper is altogether different. Bending the slice lip for a slow moving heavy weight paper process produces a very wide response with significant negative gain side lobes as shown in Figure 1.2. The response to a single actuator may cover over a third of the entire width of the paper machine.

The slice lip itself is quite expensive, and much care is taken to prevent damaging it due to excessive flexing and bending. Depending on the lip material, each actuator has a range of at most 0.17mm–0.75mm. The industrial controller contains many safety interlocks and an actuator setpoint profile is prevented from violating the bending constraints specified

for the slice lip.

Modern slice lip actuator dynamics are very fast compared with the scan time. The process dynamics are thus dominated by the sensor filtering and the dead time due to the transport delay from the actuators to the scanning sensor.

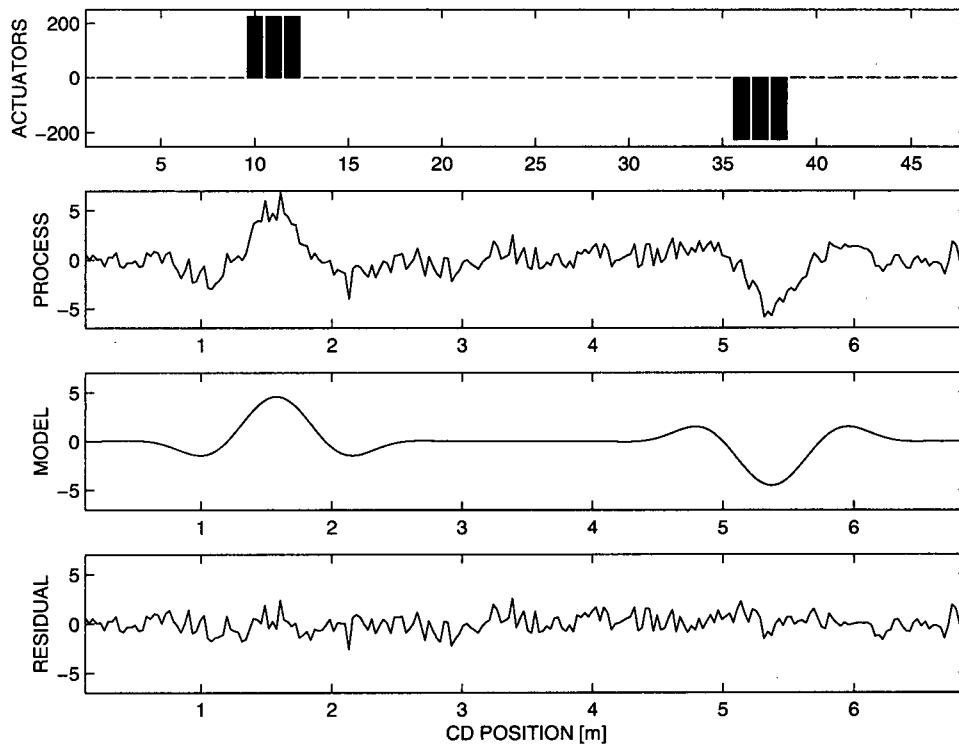


Figure 1.2: Steady-state response of basis weight to slice lip actuators on a heavy grade 200gsm linerboard machine. This is one of the wider weight responses in CD control. (Data courtesy of Honeywell-Measurex.)

### Consistency Profiling

A newer method for basis weight control, known as consistency profiling or dilution control, is described in [65]. These actuators change the basis weight profile by locally altering the concentration of pulp fibres in the headbox. This is accomplished by an array of dilution actuators distributed across the back of the headbox. The consistency of the pulp stock is changed by injecting it with a stream of low consistency water as it enters the

headbox. An increase in the flow of a dilution actuator reduces the local concentration of pulp fibres and thus locally reduces the resulting basis weight.

The industrial implementation of consistency profiling falls into several different configurations. One configuration typically has  $n = 150 - 200$  actuators with up to  $n = 298$  actuators installed on 3.5cm centres. A second configuration typically has  $n = 60 - 80$  actuators installed on 6.0cm-7.0cm centres. Within the industry, there exist other consistency profiling systems with different configurations.

The response of the weight profile to a consistency profiling actuator is typically very well localized with none of the side lobes that may be observed in slice control, compare Figures 1.2 and 1.3. The typical effect of a consistency profiling actuator is confined to a 12.5cm strip centred on the actuator, and most of its influence being concentrated in the central 7.5cm.

As with the slice lip, the consistency profiling actuator dynamics are very fast compared with the scan time and the process dynamics are dominated by the sensor filtering and the transport delay.

### 1.1.2 Moisture Control

The moisture content of a sheet of paper is a very important factor in determining paper strength [9]. Typical moisture content targets are 5–9% of the total weight of the paper sheet. Overdrying a paper sheet will reduce its strength as the fibres are damaged. An excessively variable moisture profile leads to a variable temperature profile and thus increases the demand on the caliper profiling actuators.

The dewatering and drying of the paper sheet as it passes through the paper machine is very complex and is affected by many factors. The fibre slurry exiting the headbox is approximately 0.5% fibres and 99.5% water. The paper which is wound up on the reel is about 95% fibres and 5% water. This impressive feat is accomplished through a well designed process. The goal of feedback CD control of moisture is to perform the fine control and level a variable moisture profile.

Disturbances in the moisture profile may be introduced by a variety of sources. The

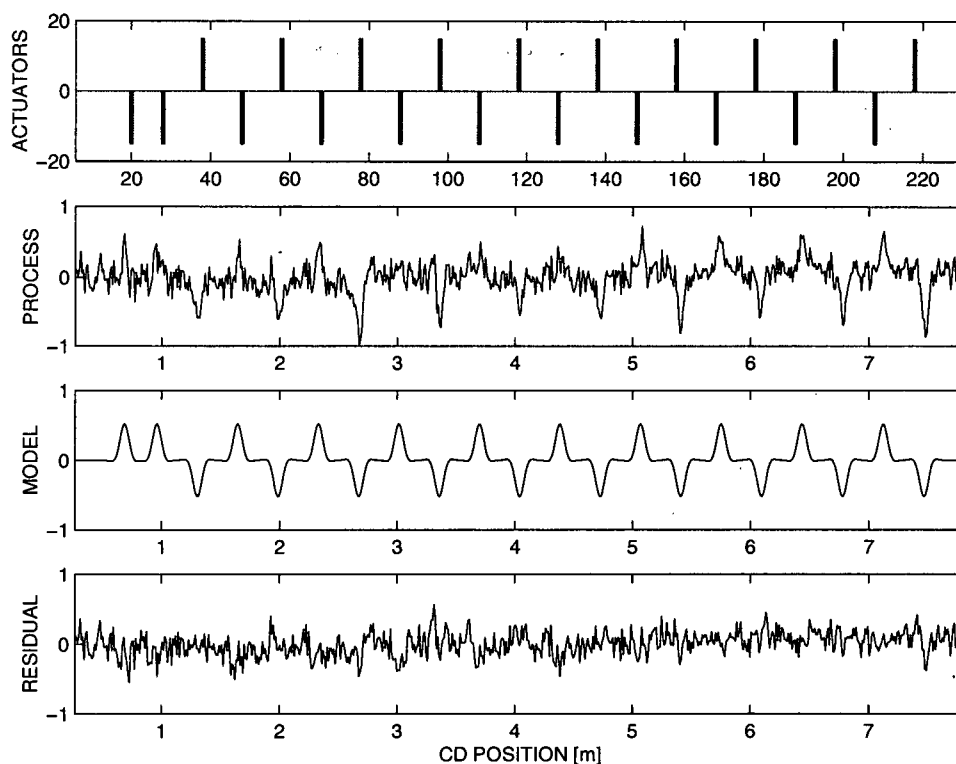


Figure 1.3: Steady-state response of basis weight to consistency profiling actuators on a 45gsm newsprint machine. (Data courtesy of Honeywell-Measurex.)

cross-coupling of actuation between processes means that weight actuation appears in the measured moisture profile<sup>1</sup>.

Steady-state or dynamically varying disturbances may be introduced by plugging of the mesh or uneven tension in the felt (the wire screen belt which is used to guide and support the newly-formed paper sheet), malfunctioning water drainage from dryer cans, or uneven suction from vacuum boxes placed across the sheet.

Analogous to the weight profile, an uncorrected moisture disturbance will propagate downstream and appear in the caliper profiles.

<sup>1</sup>This 'disturbance' may sometimes be used to our advantage. For example slice lip actuators are used to control the moisture profile in [3].

## Steam Boxes

Counter-intuitively the addition of steam to a wet paper sheet is used to help dry the sheet (see [48] and references therein). The steam-heated water in the wet paper sheet has a lower viscosity than cooler water and is more easily extracted from the paper sheet by the presses.

Industrial steam showers are implemented in an array of  $n = 55$  actuators on average, and up to  $n = 171$  in some wide paper machine installations. The actuator separation is between 7.5cm–15cm depending on the specific installation. The response of the paper sheet to the application of steam depends on many factors but its main lobe is typically between 30cm–60cm wide. The process also responds with smaller-amplitude side lobes, resulting in a total response width between 60cm–120cm wide, see Figure 1.4. A lighter weight paper sheet is more likely to have a narrower response, as the steam penetrates the thinner sheet more readily.

The steam box actuators are typically capable of providing up to 2% (or sometimes more) of the total sheet weight moisture content correction. The process response to steam box actuators is much slower than the pure time delay response dynamics of the basis weight actuators in Section 1.1.1. The response to the application of steam has a time constant around 200-250s. The paper sheet is in constant contact with many presses and rollers and the steam box must raise the temperature of all of these before the new equilibrium may be reached.

## Rewet Shower

Dry streaks in a paper sheet can be corrected through the use of a remoisturizing spray or rewet shower. These actuators are used to fill in the dry spots in a paper profile by applying an atomized water spray directly to the sheet. Rewet showers may be used on machines producing almost any grade of paper.

Industrial rewet showers are implemented in an array of  $n = 50$  actuators on average, and up to  $n = 120$  in some wide paper machine installations. The actuator separation is between 7cm-15cm and the typical response is confined to a 18cm strip centred on the

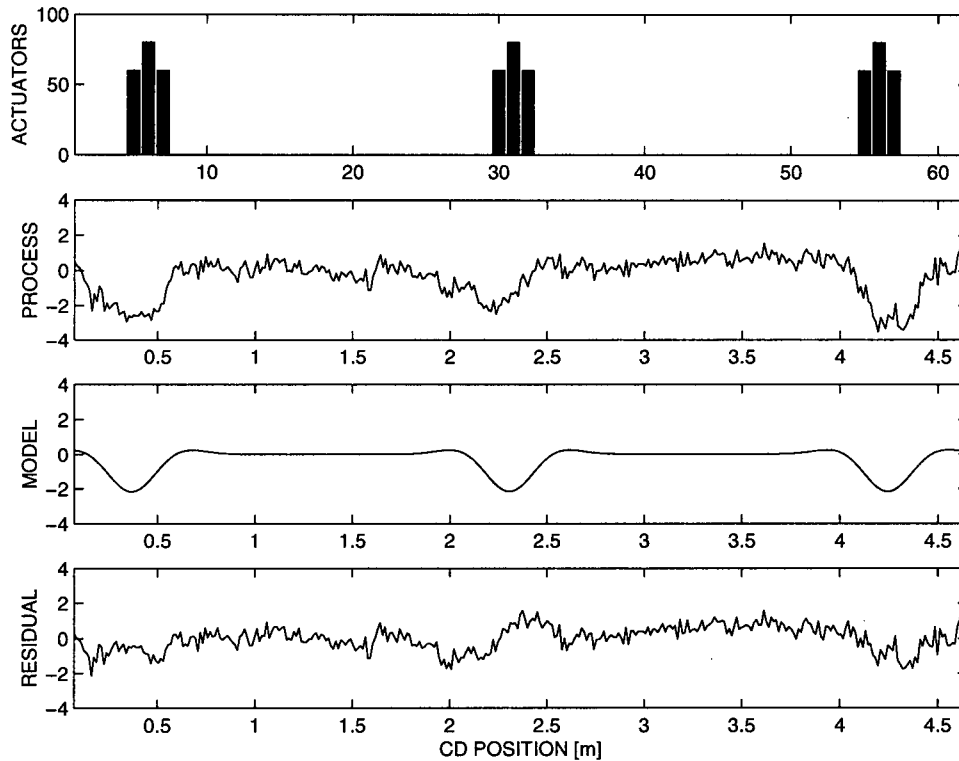


Figure 1.4: Steady-state response of moisture to steam box profiling actuators on a machine making 50gsm paper with 6% moisture target. (Data courtesy of Honeywell-Measurex.)

actuator, with 80% of the water occurring in the central 15cm. Figure 1.5 illustrates a typical response.

Typically the rewet shower actuators are capable of providing 1-2% moisture content correction. The rewet shower can work on some light weight installations to provide up to 3-4% moisture content adjustment.

The dynamics of the rewet shower actuators are very fast compared with the scan time and the process dynamics are dominated by the sensor filtering and the transport delay.

### 1.1.3 Caliper Control

The caliper of a sheet of paper is controlled by feeding the paper sheet through rotating rollers, known as the calendar stack. The pressure that the rolls exert on the paper sheet

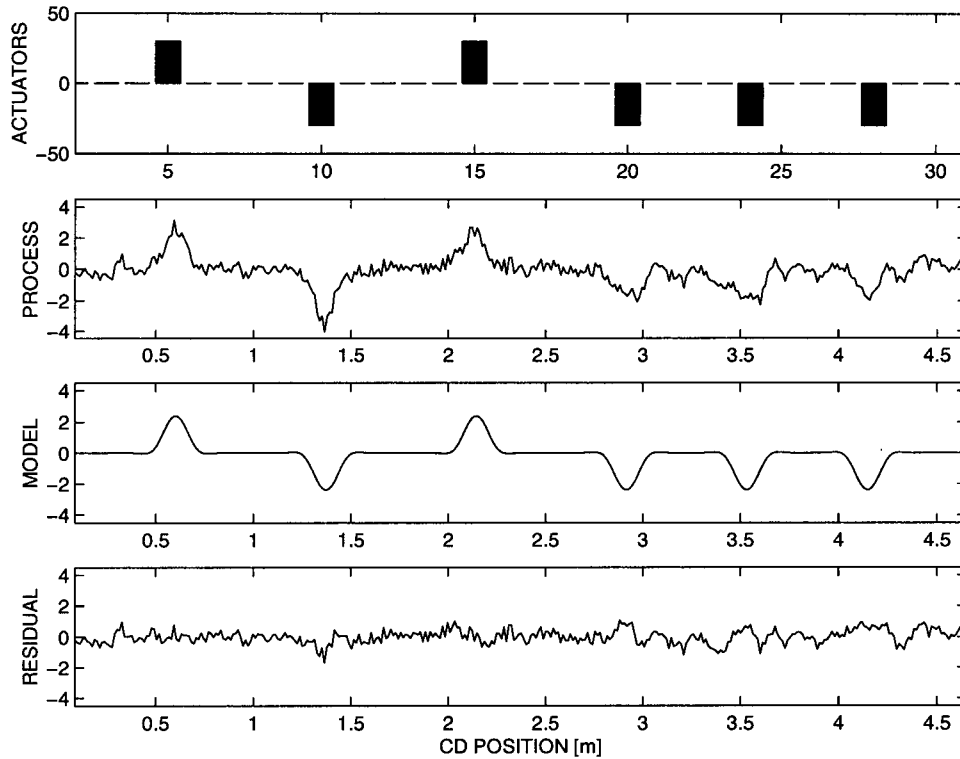


Figure 1.5: Steady-state response of moisture to rewet shower profiling actuators on a machine making 50gsm paper with 6% moisture target. (Data courtesy of Honeywell-Measurex.)

may be adjusted by locally heating (cooling) one of the rollers. As the temperature of the roller increases (decreases), its diameter also increases (decreases) due to thermal expansion, and thus the pressure on the paper sheet increases (decreases), leading to a decrease (increase) in the paper caliper [39].

The earliest CD caliper control was implemented through the use of hot and cold air showers on the roller. Modern caliper control is much more efficient and uses induction heating actuators. A high frequency alternating current is used to generate an oscillating magnetic field at the roller surface. The resulting eddy currents near the surface of the roller cause the temperature of the roller to rise, and subsequently an increase in roller diameter.

Industrial caliper control is implemented in an array of  $n = 100$  actuators on average, and up to  $n = 150$  in some wide paper machine installations. The actuator separation

is 7.5cm and the typical response has around 30cm–40cm wide main lobe and 10–15cm wide side lobes (Figure 1.6).

Caliper setpoint targets are typically in the range  $70\mu\text{m}$  to  $300\mu\text{m}$  depending on the grade. The induction heating actuators are capable of providing up to  $10\mu\text{m}$  caliper profile correction. Induction heating is the slowest of the actuators considered here. The response of the caliper to the actuator setpoints varies from very slow to an almost integrating response. Typically this rise time is the dominant factor in the process dynamics. The dead time due to the transport delay of the paper sheet is usually quite small due to the scanning sensor often being installed just after the calendar stack (Figure 1.1).

Disturbances in the caliper profile can be caused by variation in the moisture profile. A wet streak in the paper causes the roll temperature (and hence compression on the paper) to decrease close to the streak.

Other caliper disturbances may be induced by the set-up of the calendar stack. An uneven pressure profile may be caused by uneven calendar stack loading or uneven roll diameter in the CD. This will appear as a steady-state disturbance in the measured caliper profile.

## 1.2 Industrial Cross-Directional Control

The industrial implementation of an industrial cross-directional profile control scheme involves a large engineering effort. The components of the control system - the scanning sensor, the control processor, and the actuators are often located a large distance apart. In a paper mill, the control processor is located in the control room within sight of the paper machine. The scanning sensor sends the measured sheet profiles of weight, moisture, and caliper via a network connection (e.g. LAN) to the controlling computer. The error profiles are processed by the computer and the actuator setpoint arrays are downloaded, via the LAN network, into the relevant actuators. A block diagram indicating the relative positions of each of the operations in an industrial cross-directional control system is illustrated in Figure 1.7.

The scanning sensor measures up to 2000 locations across the width of the paper sheet.

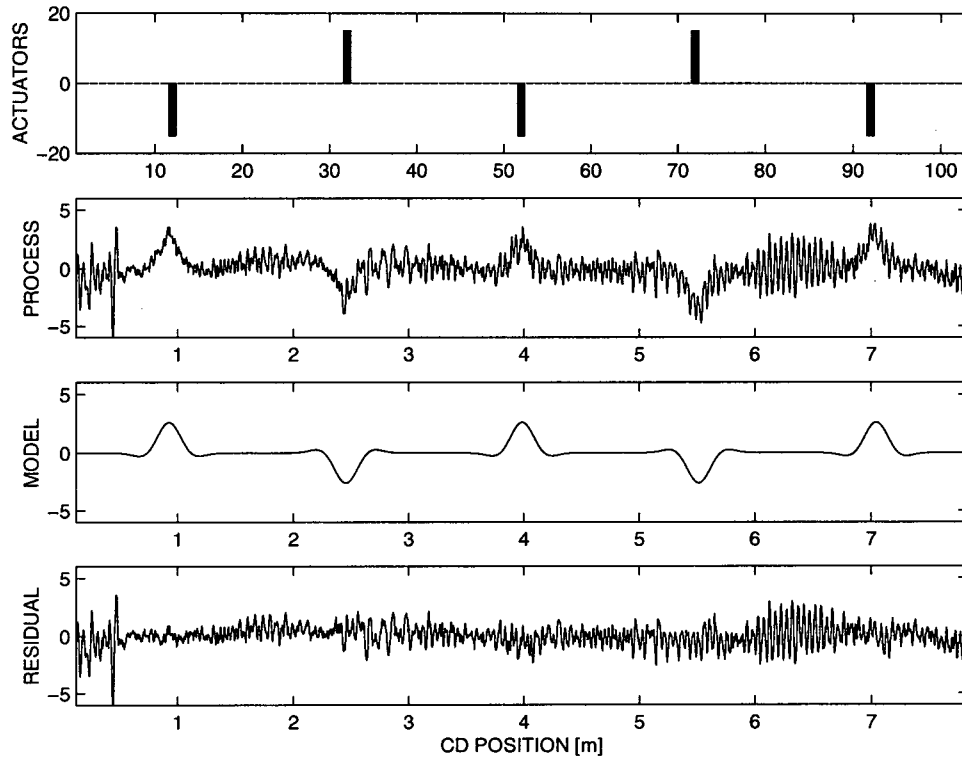


Figure 1.6: Steady-state response of caliper to induction heating profiling actuators on a machine making newsprint with  $78\mu\text{m}$  caliper target. (Data courtesy of Honeywell-Measurex.)

The measured profile is then dynamically filtered in order to separate the cross-direction (CD) and machine-direction (MD) components of the paper profile. The MD component of this signal is an estimate of the scanned profile averaged over the width of the sheet. The MD component is controlled by a separate feedback loop (not shown in Figure 1.7) and is assumed to be independent of the CD feedback loop. As this operation involves the use of a dynamical filter to separate the components of the profile, it has the effect of introducing additional dynamics into the CD process.

As the scanned profile contains many more measurements than actuators, the next operation in the chain is to reduce the dimension of the measurement profile to that of the actuator profile. In an analogy to time-domain signal downsampling, the signal is first passed through a spatial antialiasing filter in order to remove the high frequency components of the signal. Following this, the signal is then downsampled to the actuator

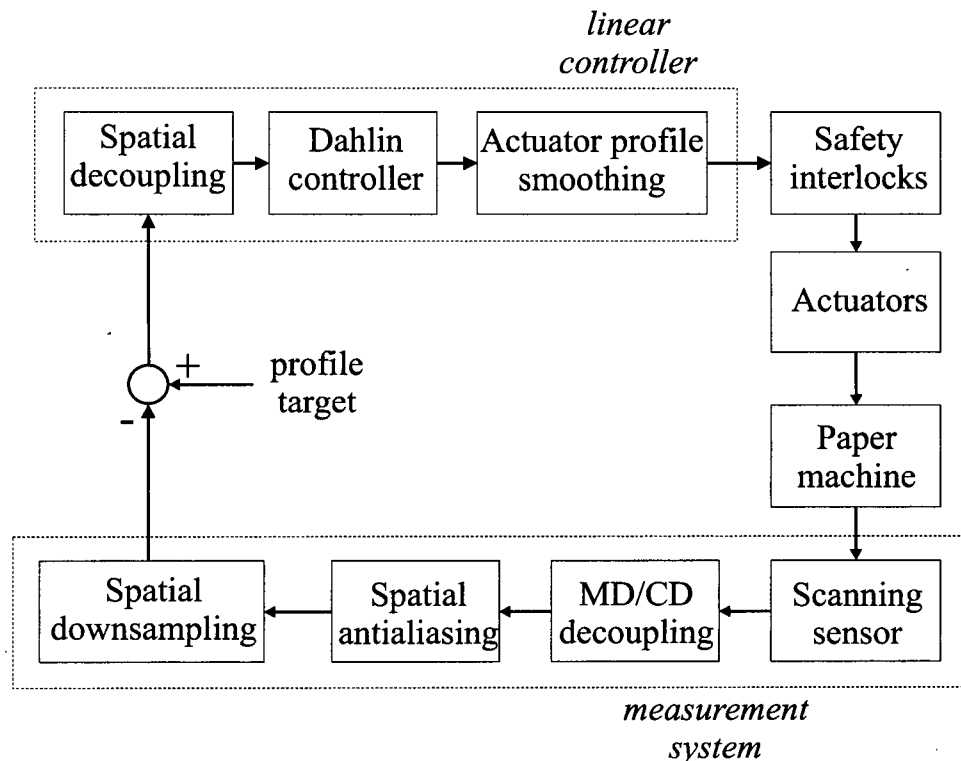


Figure 1.7: The flow of information for an industrial cross-directional control system.

dimension. Details concerning the optimal design of the spatial downsampling operation may be found in [19, 33]. The low resolution measured profile is then sent to the control processor usually through a LAN network connection.

The error signal is then constructed by subtracting the target profile from the down-sampled measurement profile. The linear controller is implemented via the algorithm blocks illustrated in Figure 1.7. The calculated actuator setpoints are then checked against the system's safety interlocks which ensure that the physical limitations of the actuators are respected. Finally, the new actuator setpoint are sent from the control processor, via the LAN connection, to the actuator array.

Industrial CD control design then involves tuning the parameters of the blocks comprising the *linear controller* shown in Figure 1.7. These algorithm blocks are described

in detail in Section 2.2 of this work. The tuning of the control law shown above requires the setting of around two dozen tuning parameters. These parameters represent the dynamical response of the Dahlin dead time compensator as well as the spatial convolution parameters used in the 'Spatial Filtering' and 'Actuator Profile Smoothing' blocks. Currently there only exist empirical rules (usually based on open-loop analysis) for the design of this controller and tuning requires a major effort on the part of site personnel. There is a need to present a controller design strategy that allows the tuning of the parameters of the industrial CD controller with respect to the issues of closed-loop performance, robustness, and practicality required by the industrial application.

### 1.3 Theoretical Work

The goal of this section is to present some of the important issues which arise when closing the feedback loop for profile control and outline the state of the art in control techniques for such a problem. The following discussion includes control techniques developed specifically to address the cross directional problem. Also included are control techniques that have been developed for related or more general applications, but are potentially applicable to the CD control problem.

The CD control problem considered herein is the regulation of disturbances. The objective is to manipulate the CD actuators to counteract the effect of process disturbances on the paper sheet. The success of the disturbance attenuation is measured by the reduction of the variance in the sheet properties (1.2). Several features of the CD process make it a challenging and interesting control problem. The following features are inherent in the physical process and must be considered by any modelling or control design technique.

Many of the theoretical developments considered below have a practical use. As will be discussed below, the theoretical aspects of ill-conditioned, uncertain multivariable systems, and especially cross-directional control systems, have been very well-studied. However, the theoretical contributions are usually limited to the consideration of a few isolated aspects of the whole engineering problem.

There exists a significant gap between the body of theoretical work that may be

applicable to the cross-directional control problem, and the implementation of advanced control strategies in working mills. There is a genuine need for a complete solution to the problem, starting from the principles of multivariable control engineering and ending with a practical tool that can be used to design cross-directional controllers on industrial paper machines.

### 1.3.1 Complexity

Cross-directional control of paper machines is a distributed parameter control problem in which the process' response to the actuator array could be possibly modelled by partial differential equations. Section 1.1 describes the wide range of possible spatial and dynamical responses which commonly occur on a working paper machine. Figures 1.2–1.6 demonstrate that the spatial response to a single actuator can be as narrow as a few centimetres (e.g. consistency profiling) or as wide as several metres (slice lip control on a heavy grade). In addition the dynamical responses range from 'instantaneous' (e.g. basis weight control or rewet shower for moisture control) to an almost integrating process (e.g. caliper control or steam box for moisture control). The transport delay from the actuators to the scanning sensor (process dead time) can be less than one sample time or over 90 seconds in longer paper machines.

Practical control strategies have relied on a simplified model of the CD process. A common assumption is that the process has a separable dynamical and spatial response. In other words, a discrete-time model of the process is given by,

$$y(z) = G(z) \cdot u(z), \quad G(z) = g(z) \cdot G, \quad (1.3)$$

where  $y(t) \in \mathcal{R}^m$  is the profile measured at  $m$  locations across the paper sheet,  $u(t) \in \mathcal{R}^n$  is the array of  $n$  actuator setpoints,  $g(z)$  is a scalar dynamical operator and  $G \in \mathcal{R}^{m \times n}$  is a constant matrix.

The constant matrix  $G$  in (1.3) is obtained by a spatial discretization of the continuous model of the spatial response in [19, 21, 26, 34] by careful consideration of the appropriate basis functions with which to represent the spatial component of the process interaction.

Other schemes start with the assumption of a spatially discretized response  $G$  in (1.3). The interaction between a discrete set of  $n$  inputs and a discrete set of  $m$  outputs may be interpreted as a multivariable problem and this implicit discretization is used in [5, 24, 40, 41].

There exists a separate line of work which considers sheet forming processes as a two-dimensional system ([11, 35] and references therein). The representation is quite general and the process is not necessarily assumed to have a separable spatial and dynamical components. It is neatly described as a two-dimensional polynomial in shift operators, both dynamical  $z^{-1}x(i, j) = x(i, j - 1)$  and spatial  $w^{-1}x(i, j) = x(i - 1, j)$ , where  $i$  and  $j$  are the spatial and dynamical indices of the two-dimensional array  $x(\cdot, \cdot)$ .

In practice, the process dynamics  $g(z)$  in (1.3) are usually represented as low order, stable, and minimum phase except for the transport delay. Some authors have restricted attention to the steady-state problem, by simply neglecting the process dynamics in the control design [7, 21, 64]. One of the earliest studies on the dynamics found that dynamics described by first order polynomials in the numerator and denominator was sufficient [5].

In [19, 20, 24, 41] a continuous-time model of the dynamics is used with

$$g(s) = \frac{e^{-\theta s}}{s + a} \quad (1.4)$$

being defined in terms of a transport delay  $\theta$  and a single pole  $-a < 0$ .

The discrete-time model, often identified from discrete-time input/output data arrays, has a similar form

$$g(z) = \frac{z^{-d}}{1 - az^{-1}} \quad (1.5)$$

with  $0 \leq a \leq 1$ , and has been used by [3, 32, 33, 40, 50]. Dynamics of the form (1.5) were used throughout the course of the current work, and were found sufficient for the majority of industrial paper making processes.

### 1.3.2 Large Scale Problem

Industrial CD control processes have up to  $n = 300$  actuators in a single array and are measured at up to 2000 locations across the paper sheet. Following the spatial discretization, there are potentially 600000 interactions to consider. If considered in its full generality, this is a potentially intractable problem for control design and implementation. Efforts for a tractable controller design procedure have been concentrated in two directions: (1) design for a reduced model of the process or (2) model diagonalization. Efficient implementation of the controller has been addressed by the reduced model design and more recently by controller localization.

The controller design may be simplified by expanding the spatial response of the process model in terms of orthogonal basis functions. An  $n_r \times n_r$  multivariable controller is then designed for a reduced process model representing the response of  $n_r \ll n$  of the ‘low-order’ spatial components. This technique has been used to achieve dimensionality reduction with various basis function representations in [26, 34, 40, 50].

Diagonalization strategies represent the second approach to controller design for these large scale processes. In general, multivariable control problems cannot be transformed into a one-loop-at-a-time design due to the non-analytic nature of the singular values of a dynamical system [16]. However, as described in [37] two classes of problems may be so diagonalized, separable systems (such as (1.3)) and circulant systems (described in detail in Chapter 3). It is interesting to note that CD processes have been modelled as each of these at one time or another. These strategies work by pre- and post-multiplying the plant model by unitary matrices, such that a diagonal transfer matrix remains,

$$\text{diag}\{g_1(z), \dots, g_n(z)\} = U^H \cdot G(z) \cdot V \quad (1.6)$$

where for separable or circulant matrices,  $U$  and  $V$  are independent of dynamical frequency, the matrix  $U^H$  denotes the conjugate transpose of  $U$ . Since  $U$  and  $V$  are unitary, they do not disrupt the singular value spectrum, and the controller design may proceed in terms of  $n$  SISO problems, designing one  $k_j(z)$  for each  $g_j(z)$  for  $j \in \{1, \dots, n\}$  in (1.6).

The multivariable controller is then recovered by writing,

$$K(z) = V^H \cdot \text{diag}\{k_1(z), \dots, k_n(z)\} \cdot U \quad (1.7)$$

Diagonalization techniques have been used for CD control in paper making by [20, 21, 24, 33, 41] and for a steel rolling application in [51]. A diagonal design for systems with one dynamical and two spatial dimensions were investigated in [15], with an application to optics. Diagonalization techniques for a more general class of multivariable systems may be found in [37, 38] and for spatially distributed systems in [4].

In addition to the controller design problem, there is a current interest in producing feedback controllers which may be implemented efficiently. Many controller design techniques produce controllers  $K(z)$  which are full  $n \times n$  matrices. In CD control applications, the process model transfer matrix  $G(z)$  typically has a sparse band-diagonal structure and this has led to the consideration of implementing the feedback control in terms of similarly sparse, banded transfer matrices  $K(z)$ .

CD control in terms of band-diagonal matrices  $K(z)$  has long been the industrial practice [36]. A control scheme where each actuator move is based on information from nearby sensor measurements and neighbouring actuator positions has become known as *localized control* [4].

Current theoretical work [4] has justified this practice by demonstrating that feedback controllers  $K(z)$  obtained from a quadratic optimization with a spatially distributed process  $G(z)$  will possess an almost-localized structure. The possibility of obtaining a truly localized controller from such a structure has been investigated for CD control of paper machines in [64]. More theoretical and general studies of the controller localization problem have been presented in [4, 10, 14, 46].

It should be noted that advances in processor speed are helping mitigate the problem of high dimensionality. Recently, a successful constrained model predictive control scheme has been implemented in real time on an industrial paper machine using all information from the model by the use of sparse arithmetics optimization calculations [3].

### 1.3.3 Ill-Conditioned System

The majority of industrial CD processes are strongly ill-conditioned [33, 36, 40]. The process response is strongly dependent on the direction of actuation. In many industrial CD control installations well over half of the process' singular values are vanishingly small, even at steady-state  $\omega = 0$  [62]. In Section 2.4, Figure 2.4 contains a typical example. For such a system, it is very important to consider the directionality of the feedback controller.

If a feedback controller  $K(z)$  is developed without consideration of the ill-conditioning of the process, then a potentially dangerous problem can arise where the controller provides larger and larger magnitudes of actuation in the weakly controllable directions of the process [43, 55]. For example, a controller with integral action will continually increase the magnitude of the actuator setpoint signal  $u(t)$  in a low-gain direction due to the fact that the measured error signal is persisting despite the 'corrective' action taken by the actuators [36]. The literature for the control of ill-conditioned multivariable processes involves one of two philosophies, full control or partial control.

Full control requires performance specifications to be satisfied for all directions of the closed-loop process. For example, the disturbance attenuation specification for a stable discrete-time control system may require that

$$\sigma_j \left( [I - GK(e^{i\omega})]^{-1} \right) < p(\omega) \quad \text{for all } j \in \{1, \dots, n\} \\ \omega \in [-\pi, \pi] \quad (1.8)$$

where  $p(\omega) < 1$  at low  $\omega$  and  $p(\omega) > 1$  at high  $\omega$  [56]. This approach leads to a control scheme applying a large control signal in the low-gain directions of the plant [43, 55]. Caution must be taken in applying this technique in industrial situations since a large control signal can lead to actuator saturation. In addition, it has been shown that the use of full control for ill-conditioned processes is especially vulnerable to stability problems caused by model uncertainty [55, 56]. The combination of a large controller gain with a small plant gain reduces the tolerance of the closed-loop system to model uncertainty.

Partial control of an ill-conditioned process means that the closed-loop system satisfies

performance specifications for a subset of the closed-loop singular values. The goal is to be aggressive in the well-controllable directions of the process and conservative in the low gain directions. One possible partial control performance specification is to simply modify the full control specification (1.8), to apply to a subset of  $n_r < n$  singular values, such that

$$\sigma_j \left( [I - GK(e^{i\omega})]^{-1} \right) < p(\omega) \quad \text{for all } j \in \{n - n_r + 1, \dots, n\} \\ \omega \in [-\pi, \pi] \quad (1.9)$$

where  $p(\omega)$  is as in (1.8).

The modal truncation strategies discussed in the previous section are a partial control scheme, in which a controller is designed for a subset  $n_r \ll n$  directions of the process. The  $n_r$ -dimensional controlled subspace is not necessarily defined in terms of the singular vectors (as in (1.9) and [51, 26]), and more general orthogonal function expansions of large multivariable transfer matrix models of the CD process are found in [34, 40, 50].

A second, softer, partial control approach is achieved by simply tuning the multivariable controller  $K(z)$  such that its gain is low, but not necessarily zero, in the weakly-controllable directions of the process. Various methods exist for detuning a controller in this way. Optimization based design techniques have been used with a penalty on the closed-loop actuation in the weakly-controllable directions. These include signal-based optimization approaches [7, 21] in which some norm of  $u(t)$  is penalized, and also system based approaches [60] in which some norm of the controller  $K(z)$  is penalized in the low-gain directions of the plant model.

### 1.3.4 Model Uncertainty

The almost-universal assumption made when modelling a CD process, is that the response of the measured paper sheet properties to the actuators is described by a linear, time invariant transfer matrix of low dynamical order. Each of these assumptions, as well as the separability of dynamical and spatial responses (1.3), is only an approximation to the real industrial paper machine CD process. A non-exhaustive list of the main sources of

model uncertainty in a CD process are:

- **Alignment.** The paper sheet may wander or shrink over time, leading to a mismatch between the true location of an actuator's effect and its predicted location. This is the spatial analogue to phase uncertainty in a dynamical system's response.
- **MD-CD cross coupling.** The scanning sensor is traversing back and forth across the moving paper sheet and is actually tracing a diagonal path on the sheet. Thus, in addition to the usual measurement noise, the sensor will also alias certain MD variations into the CD profiles. These variations are generally not controllable by the CD actuator array [9].
- **CD response shape.** The spatial response shape is often modelled as the same (but shifted) for each actuator (see Figures 1.2–1.6). However, the CD response shape may be very different at the sheet edges [28]. It varies with conditions such as machine speed and stock properties.
- **Actuator failure.** The model assumes that all actuators have the same response. However, these are industrial processes subject to uneven wear and tear and occasionally actuators may fail or partially fail (e.g. plugging in steam valves).
- **Process dynamics.** Rise time and transport delay may change over time, with changing paper machine conditions such as speed. Also, the process may be of higher dynamical order than the low-order model used (often first-order-plus-deadtime as in (1.5)).
- **Actuator nonlinearities.** For several CD actuators, the incremental process gain depends on the current actuator position  $u(t)$  and rate  $u(t) - u(t - 1)$ . Examples exist for basis weight control using slice lip, moisture control using steam, and caliper control using induction heating of rolls.

Since no modelling strategy is capable of accurately capturing all features of an industrial paper machine, any practical approach to CD controller design must tolerate process-model mismatch. The combination of an ill-conditioned process with model uncertainty is especially dangerous since the low gain directions can easily become swamped

by the model uncertainty [34, 43, 55, 62]. A robustly stable system is one in which closed-loop stability is maintained for all process models included in the uncertainty description. Robust performance is achieved if the closed-loop satisfies performance specifications for the set of possible process models. Very general studies in the mathematics of robust control for spatially distributed systems exist, and the interested reader is referred to [4, 49].

In CD control applications, it has been noted [24, 30, 40] that even the *sign* of the process steady-state gain is unknown for certain directions (for example see Figure 2.4 in Section 2.4). In practical applications, the sign uncertainty corresponds to the directions of the process with a high spatial frequency component. A problem occurring in industrial CD control installations is that the actuator array will slowly develop a large-amplitude 'picket fence' appearance [36]. As will be shown, this problem is due simply to the application of a control signal in a direction of low process gain and high model uncertainty.

Robust multivariable control has matured to the point where the design techniques can easily handle an ill-conditioned, uncertain process, provided the design specifications are reasonable [56, 66]. For example, no benefit may be obtained by attempting to control any singular vector direction of the error which has a gain smaller than the associated model uncertainty. Many of these issues are closely related to the philosophy of partial control described in Section 1.3.3 above.

Initial work on robust CD control may be found in [19]. It was later developed into a graphical design technique for a CD controller which is robustly stable to multiplicative model uncertainty [20]. The question of robust performance of a CD control scheme was addressed in [41] where a highly structured parametric uncertainty structure was used. However, neither of these designs considered the possibility of uncertainty of the sign of the gain of the modes of the process models.

In [24, 30] it was demonstrated that the performance specification of zero steady-state error in all directions was incompatible with the CD control problem. Robust stability of the closed-loop cannot be guaranteed if integral control action is applied in all directions. This is a result of the fundamental rule for feedback control that the steady-state gain of

an integrating controller must have the same sign as the steady-state gain of the process. Closed-loop instability results if the sign of these gains are not matched. Therefore, if the process' steady-state gain is uncertain, then the stability of the closed-loop with an integrating controller is also uncertain.

As a result, practical control strategies must be modified to provide more conservative control in the low-gain directions. This philosophy is followed in the current work and the closed-loop requirements on the controller design are specified only after considering the capabilities of the open-loop process.

#### 1.4 Related Applications

Much work is currently being done for large scale systems in which the control is implemented through large arrays of identical actuators. Cross-directional control of paper machines is an industrially important example of such systems. However, there exist many more applications in which a process is described by a spatially distributed structure. The following discussion outlines some of the other applications, which may not seem to be 'related' at first sight.

Sheet forming is the most closely related application to papermaking. The formation of plastic film is a fascinating process whose control has been studied in [19]. Steel making is another process control application requiring consideration of the spatial distribution of the material [29, 49, 51].

The growth of semiconductor crystals is considered in [2] where arrays of heating elements maintain a uniform temperature distribution throughout the furnace.

The active control of vibrations in spatially-distributed structures has been achieved by arrays of identical sensors (e.g. accelerometer or piezoelectric strain) and actuators (e.g. point force or piezoelectric strain) [25]. A closely related application is the control of a sound field in an enclosure in which the sensing is performed by an array of identical microphones and the actuation is achieved with several identical loudspeakers [22, 25].

Newer applications, which at the time of writing are still in the experimental stages, include inflatable structures whose shape is controlled by arrays of force actuators [53].

Micro-electromechanical systems (MEMS) are an emerging technology in which thousands of tiny actuators distributed over a large structure must be coordinated in terms of global control goals [4, 31, 46].

Older applications include the automated control of a long line of vehicles on a highway, known as platoons have been studied in [4, 42, 54]. It is interesting to note that today's open problem of designing a localized control strategy for a spatially distributed system was discussed as an open problem as far back as 1966 in [42].

The control of unmanned aerial vehicles flying in formation has been considered in [12, 17, 52], and is as far from papermaking as this discussion will stray.

### **1.5 Aims and Contributions of the Work**

This work considers the control of linear dynamical systems distributed in one spatial dimension and discretized both dynamically and spatially. The systems under consideration are controlled through an array of identical actuators evenly spaced throughout the spatial domain. The process output is measured in the spatial domain at an evenly distributed number of discrete locations. Each location is assumed to be measured by an identical sensor.

The process response is further assumed to be almost invariant to shifts in space and time. This idealization is quite rare in practice and the design procedure includes provisions for the disruption of these invariance properties by boundary conditions which occur in physical systems. A more specific classification of the problems under consideration is included in the process model specifications of Section 2.1.

Cross-directional control of paper machines is an industrially important application of such processes. One of the aims of this work is in bridging the gap between the existing theoretical work and the industrial implementation of cross-directional control strategies. As discussed in Section 1.3 there is an abundance of academic work existing for designing controllers for multivariable systems. In addition, much work has focussed on the cross-directional control problem specifically. However, as discussed in Section 1.2, the current industrial state of the art for cross-directional controller design is, for the most part,

independent of the body of theoretical work and is largely governed by empirical tuning rules.

The main contributions of this work are summarized as follows:

- The development of a constructive, computationally inexpensive, graphical controller design technique for dynamical systems that are distributed in one spatial dimension and controlled by an array of identical actuators. The feedback controller is designed using a two dimensional loop shaping technique with reference to the process model and the model uncertainty such that the spatial and dynamical bandwidth limitations of the physical system are respected.
- Application of the loop shaping technique as a tool for the design of feedback controllers for paper machine cross-directional processes. The two dimensional loop shaping approach is well-suited to address the wide variety of such processes for which a cross-directional controller must perform well.
- The demonstration of the loop shaping design technique by tuning an industrial cross-directional controller. The tuning results are confirmed by experiments with a real paper machine in a working mill.

An outline of the structure of the thesis follows. Chapter 2 presents cross-directional controller design requirements of performance, robust stability, and localized implementation in a mathematical form suitable for a control design strategy.

Chapter 3 presents an overview of existing techniques for two-dimensional frequency domain decomposition in order to improve the design both computationally and conceptually. The frequency domain is familiar territory for control engineers, and a spatial frequency decomposition allows for the  $n \times n$  multivariable control synthesis problem to be restated in terms of  $n$  SISO control design problems. In addition, the graphical nature of spatial frequencies is shown to provide a richer insight into the large multivariable control system than the common approach in multivariable control of studying only the system's maximum and minimum singular values.

Chapter 4 describes the constructive design technique that is central to this work. Dynamical systems distributed in one spatial dimension are considered and the controller

design may be interpreted as a two-dimensional generalization of the well-known loop shaping design technique for multivariable (and SISO) control systems in a two-step graphical design procedure. The first step is the synthesis of a high-performance robust controller. The second step is a spatial order reduction in which the full matrix controller is approximated by sparse, banded matrices to obtain a localized feedback controller.

Finally, the loop shaping design technique is applied to an industrial paper machine cross-directional control problem. The modelling, design, and implementation are the subject of Chapter 5. Closed-loop data were collected for the industrial system running under the loop shaping controller design. The performance is then compared to the performance of a more traditional controller design based on empirical tuning rules.

## Chapter 2

### Problem Specifications

The goal of this chapter is to define the conditions upon which the proposed design technique is based. A general structure is presented for the class of discretized, spatially distributed process models under consideration. The same structure is used to define the feedback controllers to be designed. The duality between the process model transfer matrices and controller transfer matrices provided by this framework is beneficial throughout the closed-loop analysis and design described in Chapters 3 and 4.

Next, the design specifications for closed-loop performance and closed-loop robustness are presented. In general, performance and robustness are conflicting requirements requiring aggressive and conservative control, respectively. The trade-off of these specifications forms the central design problem considered in this work.

The cross-directional control problem described in Chapter 1 is an important industrial application of the models and design specifications described herein and forms the demonstration in Chapter 5. Therefore each of the general problem specifications is also discussed in terms of the special case of the industrial CD control problem.

#### 2.1 Spatially Distributed Process Model

This section presents the class of process models for which the subsequent analysis (Chapter 3) and design (Chapter 4) are valid. The class of problems under consideration are modelled by linear dynamical systems distributed in one spatial dimension and discretized both dynamically and spatially. The control is effected through an array of identical actuators evenly spaced throughout the spatial domain. The process output is measured in the spatial domain at an evenly distributed number of discrete locations. Each location is assumed to be measured by an identical sensor.

The process response is further assumed to be almost-invariant to shifts in space and time. This idealization is quite rare in practice and the design procedure includes provisions for the disruption of these invariance properties by boundary conditions which occur in physical systems.

The model structure presented here is familiar from its use in discretization of partial differential equation models of spatially distributed systems. Its practical use in this work is justified by its ability to capture the relevant features of all processes in Section 1.1.

Several features of the spatially distributed control process must be described by the model. The actuator dynamics, the process response, and the scanning sensor spatial and dynamical responses will all be described by the linear transfer matrix model,

$$y(z) = G(z)u(z) \quad (2.1)$$

where  $u(z) \in \mathcal{C}^n$  is the  $\mathcal{Z}$ -transform of the actuator setpoint profile,  $G(z) \in \mathcal{C}^{n \times n}$  is the process transfer matrix containing both the dynamical and the spatial responses of the sensor array to the actuator array.

In an effort to gain physical insight into the structure of the process model, it is helpful to factor the transfer matrix  $G(z)$  in (2.1) as

$$G(z) = [I + A(z)]^{-1}B(z) \quad (2.2)$$

where  $B(z)$  and  $A(z)$  are strictly causal operators, so that the process model in (2.1) may be written as

$$y(z) = B(z)u(z) - A(z)y(z) \quad (2.3)$$

A further structure is imposed on the  $n \times n$  transfer matrix factors  $B(z)$  and  $A(z)$  in (2.3). Motivated by the form of discretized systems of linear, constant coefficient, partial differential equations, the  $n \times n$  transfer matrix factors  $B(z)$  and  $A(z)$  are given by the

expansion,

$$B(z) = \sum_{i=1}^{m_b} B_i \cdot b_i(z), \quad A(z) = \sum_{j=1}^{m_a} A_j \cdot a_j(z) \quad (2.4)$$

Each  $b_i(z)$  and  $a_j(z)$  in (2.4) is a scalar transfer function. Each of the constant matrices  $B_i, A_j \in \mathcal{R}^{n \times n}$  is a symmetric, band-diagonal Toeplitz matrix.

For example, a constant  $n \times n$  band-diagonal symmetric Toeplitz matrix with  $q$  independent elements is given by,

$$B = \begin{bmatrix} b_1 & b_2 & \cdots & b_q & 0 & \cdots & \cdots & \cdots & \cdots & 0 \\ b_2 & b_1 & b_2 & \cdots & b_q & 0 & \ddots & \ddots & \ddots & \vdots \\ \vdots & \ddots & \ddots & \ddots & \vdots & \ddots & \ddots & \ddots & \ddots & \vdots \\ b_q & \cdots & b_2 & b_1 & b_2 & \ddots & \ddots & \ddots & \ddots & \vdots \\ 0 & b_q & \cdots & b_2 & b_1 & \ddots & \ddots & \ddots & \ddots & \vdots \\ \vdots & 0 & \ddots & 0 \\ \vdots & \ddots & b_q \\ \vdots & \ddots & \vdots \\ \vdots & \ddots & \ddots & \ddots & 0 & b_q & \cdots & b_2 & b_1 & b_2 \\ 0 & \cdots & \cdots & \cdots & \cdots & 0 & b_q & \cdots & b_2 & b_1 \end{bmatrix} \quad (2.5)$$

This matrix structure will occur repeatedly throughout the text, and henceforth is abbreviated using Matlab's representation of symmetric Toeplitz matrices

$$B = \text{toeplitz}\{b_1, \dots, b_q, 0, \dots, 0\} \quad (2.6)$$

In Section 1.1, Figures 1.2–1.6 illustrate that the CD actuators have localized authority. In other words, the effect of each actuator is localized to a nearby region of the sheet. In addition, due to the continuous nature of a paper sheet, the measured sheet properties  $y_i(t)$  with  $i = 1, \dots, n$  are correlated spatially to nearby measurements  $y_{i\pm 1}(t)$ ,  $y_{i\pm 2}(t)$ , etc. Therefore, considerable physical motivation exists to model the process with band-diagonal transfer matrices  $B(z)$  and  $A(z)$  in (2.2)–(2.4). Furthermore, since an array of identically constructed actuators is being used to control a uniform product (paper

sheet), it is sensible to exploit this redundant information when modelling the process. Therefore, the nominal process model is constructed by assuming that each actuator in the array has the same effect on the paper sheet.

The most commonly used model for the CD control processes on the paper machine assumes the spatial and dynamical process responses to be separable (1.3). The dynamics of the process are further modelled as first-order-plus-deadtime [3, 32, 33, 40, 50]. This model is given by the general structure (2.1)–(2.4) with  $m_b = m_a = 1$  in (2.4) and

$$B(z) = B \cdot z^{-d}, \quad A(z) = A \cdot z^{-1} \quad (2.7)$$

where Toeplitz symmetric matrices model the spatial correlation of the process response,

$$B = \text{toeplitz}\{b_1, \dots, b_q, 0, \dots, 0\}, \quad A = \text{toeplitz}\{-a_1, 0, \dots, 0\} \quad (2.8)$$

Typical industrial paper machine processes are described in Section 1.1 and may be roughly translated into ranges on the model parameters of the transfer matrices in (2.7)–(2.8). The process deadtime  $d$  is due to the transport delay is typically in the range  $1 \leq d \leq 4$ . Due to its location, see Figure 1.1, caliper has the shortest time delay, weight control the longest, and moisture control somewhere in the middle. The process pole is in the range  $0 < a_1 < 1$ . The process models for slow actuators such as induction heating for caliper control or steam boxes for moisture control typically result in  $a_1 \approx 1$ . The time constant for the faster actuators is negligible, see Section 1.1, but industrial sensors include a filter to limit the introduction of high frequency sensor noise into the feedback loop, resulting in  $a_1 > 0$  for all actuators.

The spatial response width of a CD process will result in  $2 \leq q \leq 20$  for the symmetric Toeplitz matrix  $B$  in (2.8.) A large value of  $q \approx 20$  will occur for slice lip control of heavy grade paper, narrower responses with  $q \approx 2$  are obtained for consistency profiling, rewet showers, and some light weight slice lip installations. The vast majority of practical CD control applications result in a process model with the constant matrix  $B$  in (2.8) being ill-conditioned. The majority of industrial CD control installations have several singular values of  $B$  in (2.8) indistinguishable from zero, see Figure 2.1. (In the case of slice lip

control of heavy weight paper, this may be more than two-thirds of the singular values of the process model.) Therefore the corresponding input directions will be uncontrollable at all dynamical frequencies  $\omega$ . It is demonstrated in Chapter 4, this ill-conditioning requires the modification of the performance specifications on the closed-loop system.

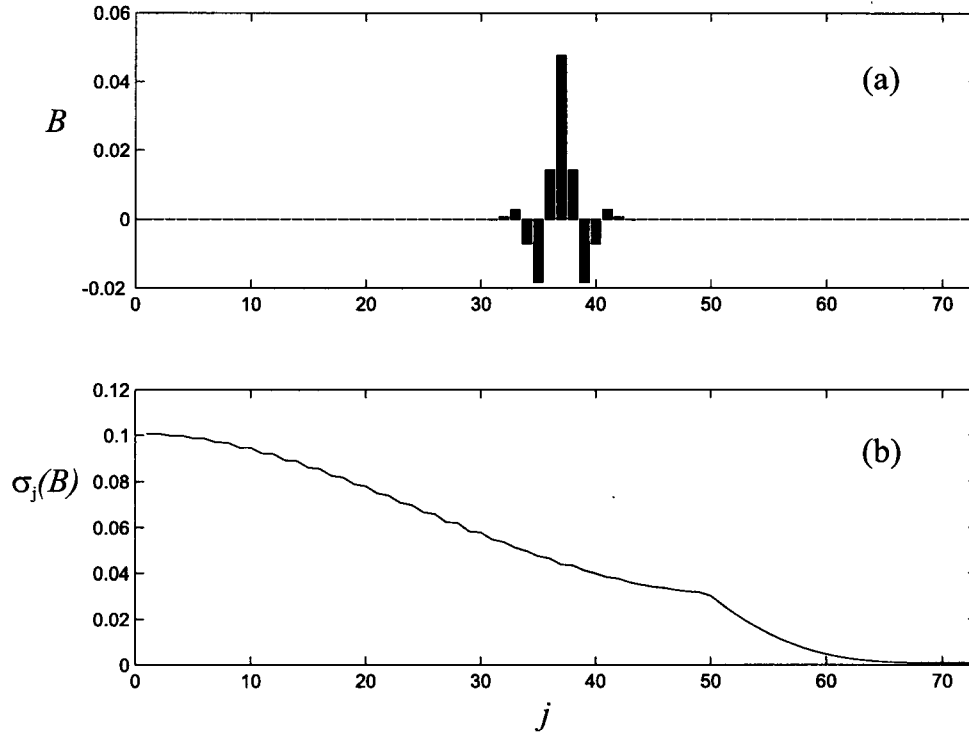


Figure 2.1: (a) Column of the matrix  $B \in \mathcal{R}^{73 \times 73}$  in (2.8) identified from a basis weight process controlled by  $n = 73$  slice lip actuators. (b) The singular value decomposition of  $B$ . (Data courtesy of Honeywell-Measurex.)

It is interesting to note that the transfer matrix model structure shown in (2.3), with band-diagonal symmetric Toeplitz matrices as coefficients of a polynomial in the delay operator  $z^{-1}$ , is a familiar discretization of spatially distributed partial differential equations. Equations with structure (2.3)–(2.4) have been used to describe spatial discretizations of the well-known heat equation and wave equation in [6, 63]. For example, if one neglects actuator and sensor responses, the heat equation may be discretized [6, 63] as  $B(z) = B \cdot z^{-1}$  and  $A(z) = A \cdot z^{-1}$  with  $B = \text{toeplitz}\{b, 0, \dots, 0\}$  and  $A = \text{toeplitz}\{a_1, a_2, 0, \dots, 0\}$ . In fact, the CD control problem is a practical example of a sampled distributed parameter system. The real-world hardware accesses the spatially distributed process through  $n$

discrete actuator setpoints and the scanning sensor returns a profile of  $n$  discrete profile measurements. It is not surprising to discover that this physical discretization results in a similar description of these processes.

## 2.2 Controller Implementation

This section presents the structure of the feedback controllers considered throughout this work. Multivariable transfer matrices may be represented in many equivalent forms [56]. The particular factorization described below was chosen for three main reasons. First, the feedback is to be applied to spatially distributed processes as described by the models in Section 2.1. The proposed feedback controller has a structure which is dual to the spatially distributed process model described in (2.1)–(2.4). As described in Chapter 3, this fact allows for the convenient representation and calculation of the various properties of the closed-loop system.

Second, this form closely resembles the proposed implementation of the feedback as algorithms in the control processor. In Chapter 4, it will be seen that the practical issue of controller localization (defined in this section) is more accessible throughout the controller design procedure.

Finally, the algorithm structure of the industrial cross-directional feedback controller (comprising the *linear controller* shown in Figure 1.7 in Section 1.2) is a specific realization of this factorization of the transfer matrix. The industrial controller was designed via years of extensive field testing and validation. Currently, there are several thousand installations of this particular controller performing feedback for paper machine profiles throughout the world.

In this work, the feedback controller is represented by the output feedback transfer matrix relation,

$$u(z) = K(z)v(z) \quad (2.9)$$

where  $u(z) \in C^n$  is the  $\mathcal{Z}$ -transform of the actuator setpoint profile, the controller is

represented by the transfer matrix  $K(z) \in \mathcal{C}^{n \times n}$ . The error profile is given at time  $t$  by,

$$v(t) = y(t) - r(t) \quad (2.10)$$

where  $y(t) \in \mathcal{R}^n$  is the sensor profile measured at time  $t$  and  $r(t) \in \mathcal{R}^n$  is the profile target at time  $t$ .

A further specification must be satisfied in the implementation of the feedback controller  $K(z)$  in (2.9) and Figure 2.2. It is required that the feedback controller be constructed from band-diagonal Toeplitz transfer matrices. This practical requirement is related to the spatially 'localized' controller design currently being studied in [4, 10, 46]. In this work the feedback controller  $K(z)$  in (2.9) is referred to as localized if it is factored as

$$K(z) = [I + S(z)]^{-1}C(z) \quad (2.11)$$

and implemented as

$$u(z) = C(z)v(z) - S(z)u(z) \quad (2.12)$$

where  $C(z), S(z) \in \mathcal{C}^{n \times n}$  are band-diagonal transfer matrices, such that

$$C(z) = \sum_{i=1}^{m_c} C_i \cdot c_i(z), \quad S(z) = \sum_{j=1}^{m_s} S_j \cdot s_j(z) \quad (2.13)$$

Each  $c_i(z)$  and  $s_j(z)$  in (2.13) is a scalar transfer function. Each of the constant matrices  $C_i, S_j \in \mathcal{R}^{n \times n}$  is a symmetric, band-diagonal Toeplitz matrix.

The degree of controller localization is defined in terms of the constant Toeplitz matrices  $C_i$  and  $S_j$  in (2.13). Let the 'widest' of the  $m_c$  (respectively  $m_s$ ) matrices  $C_i$  (respectively  $S_j$ ) be given for  $i = i^*$  (respectively  $j = j^*$ ) such that

$$C_{i^*} = \text{toeplitz}\{c_1, \dots, c_{n_c}, 0, \dots, 0\}, \quad S_{j^*} = \text{toeplitz}\{s_1, \dots, s_{n_s}, 0, \dots, 0\}, \quad (2.14)$$

where the notation 'toeplitz{.}' is borrowed from Matlab's representation for symmetric

Toeplitz matrices and is displayed for the process model in (2.5).

The band-diagonal structure of  $C(z)$  means that the actuator setpoint for the  $i^{\text{th}}$  actuator, given by  $u_i(t)$ , is based on the signals from only sensors  $v_{i+j}(z)$  where  $j = 0, \pm 1, \dots, \pm n_c$ , rather than the entire sensor array of  $v(z) \in \mathcal{C}^n$ . A similar interpretation follows for the actuator array, each actuator is receiving information from only the  $2(n_s - 1)$  neighbouring actuators, rather than from all  $n$  actuators in the array.

The controller localization requirement is analogous to the familiar practical specification of low order implementations of dynamical controllers. A controller with a low dynamical order acts only on the recent values of the error signal (defined by the order of the transfer function's numerator) and recent values of the control signal (defined by the order of the denominator). A localized controller has a low 'spatial order' in which the controller acts on nearby values of the error signal  $v(z)$  (defined by the spatial order of  $C(z)$ , given by  $n_c$  in (2.14) and nearby values of the actuator setpoint signals (defined by the spatial order of  $S(z)$ , given by  $n_s$  in (2.14)).

The industrial CD control algorithms considered herein have a fixed structure which is a special case of the general structure (2.9)–(2.13). The configuration for a closed-loop CD control system is illustrated in Figure 2.2 for the process modelled with output disturbances (described in Section 2.3). The error profile is processed by a series of

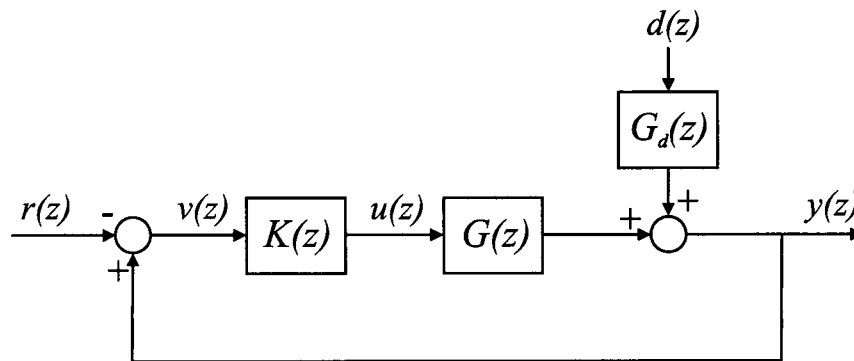


Figure 2.2: Feedback controller configuration.

blocks which either spatially filter the error profile by multiplying it with a constant

band-diagonal matrix, or by dynamically filtering it by passing the array through a scalar transfer function, see Figure 1.7 in Section 1.2. Figure 2.3 indicates the block diagrams which process the measured error signal  $v(t)$  and transform it into the actuator setpoint profile  $u(t)$ .

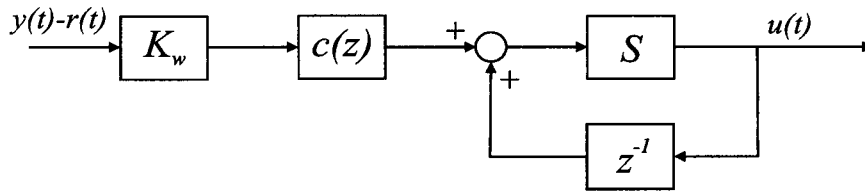


Figure 2.3: The industrial cross-directional controller block diagram.

The feedback controller in Figure 2.3 is constructed from a scalar dynamical term  $c(z)$  and two constant  $n \times n$  symmetric Toeplitz matrices  $K_w$  and  $S$  and is written in terms of the general structure (2.9)–(2.13) with  $m_c = m_s = 1$  and

$$\begin{aligned} C(z) &= S \cdot K_w \cdot c(z) = C \cdot c(z) \\ S(z) &= -S \cdot z^{-1} \end{aligned} \quad (2.15)$$

The scalar dynamical part  $c(z)$  of the controller in (2.15) is the Dahlin's dead time compensator [18, 59] implemented in velocity form<sup>1</sup>.

$$c(z) = \frac{(1 - \alpha_c)[1 - a_c z^{-1}]}{1 + (1 - \alpha_c) \sum_{i=1}^{d_c-1} z^{-i}} \quad (2.16)$$

The controller parameters  $\alpha_c$ ,  $a_c$  and  $d_c$  defining  $c(z)$  in (2.16) are required to be tuned.

The industrial implementation requires the two constant matrices  $K_w$  and  $S$  to be

<sup>1</sup>The more familiar expression of the Dahlin controller is its position form  $c_d(z) = c(z)/[1 - z^{-1}]$  where

$$c_d(z) = k \cdot \frac{(1 - \alpha_c)[1 - a_c z^{-1}]}{1 - \alpha_c z^{-1} - (1 - \alpha_c)z^{-d_c}}$$

symmetric band-diagonal Toeplitz matrices,

$$\begin{aligned} K_w &= \text{toeplitz}\{k_1, \dots, k_{n_k}, 0, \dots, 0\} \\ S &= \text{toeplitz}\{s_1, \dots, s_{n_s}, 0, \dots, 0\} \end{aligned} \quad (2.17)$$

Therefore the design of the  $n \times n$  constant matrices  $K_w$  and  $S$  in (2.15) is a matter of selecting  $n_k$  and  $n_s$  coefficients respectively. For practical CD control,  $n_k, n_s \ll n$ , resulting in  $K_w$  and  $S$  in (2.15) being sparse matrices.

Multiplication of a profile by a symmetric band-diagonal Toeplitz matrix is often referred to as ‘spatial filtering’ by CD control practitioners. In fact, the constant matrix  $S$  in (2.15) is further parameterized in terms of a Blackman convolution window filter,  $H(n_s)$ ,

$$S = \lambda \cdot H(n_s) + (1 - \lambda) \cdot I \quad (2.18)$$

where  $0 \leq \lambda < 1$  and  $n_s$  defines the width of  $S_t$  in (2.17) because,

$$H(n_s) = \text{toeplitz}\{h_1, \dots, h_{n_s}, 0, \dots, 0\} \quad (2.19)$$

The elements  $h_k$  of  $H(n_s)$  defined by a lowpass Blackman window of order  $n_s$  normalized such that  $h_1 + 2 \cdot h_2 + \dots + 2 \cdot h_{n_s} = 1$ . Consider for example  $n_s = 3$  in (2.19), then  $\{h_1, h_2, h_3\} = \{0.3968, 0.2500, 0.0516\}$ , so that  $h_3 + h_2 + h_1 + h_2 + h_3 = 1$ .

Chapters 3 and 4 present a general design technique for spatially distributed controllers with the structure (2.9)–(2.13). Chapter 5 demonstrates the application of this design for the special case of the industrial cross-directional controller (2.15)–(2.19).

### 2.3 Performance

This section presents the closed-loop performance requirements for which the feedback controller  $K(z)$  in (2.9) is to be designed. The design technique, developed in Chapters 3 and 4, defines closed-loop performance in the language of loop shaping design. In other

words, the performance of the feedback controller  $K$  is summarized by achieving high gains of the multivariable loop transfer function  $KG$  in the appropriate bandwidths and directions.

The industrial requirement for controller performance is defined by the variance of the measured output signal as defined in (2.22). The industrial specification is reworked to a form amenable to control design. The effect of the disturbances on the output profile is written in terms of a closed-loop transfer matrix. The performance objective for the controller is then given by the  $\mathcal{H}_2$ -norm of said matrix. Designing a controller  $K$  to make this norm small requires that the loop transfer matrix  $KG$  has a large gain at those dynamical frequencies and directions for which the disturbances are significant [56, 66]. This idea will be expanded upon in Chapter 4.

The production of a sheet of paper is largely a regulation problem. The task of the feedback control is the removal of disturbances from the sheet profile. The profile setpoint array is constant  $r(t) = r$  for the vast majority of the industrial operation, only changing when a different grade of paper is to be produced.

It is assumed that disturbances enter the process at the output, as shown in Figure 2.2. In equation form, the open-loop transfer matrix representation of the process is given by,

$$y(z) = G(z)u(z) + G_d(z)d(z) \quad (2.20)$$

where  $G(z)$  is described in (2.1). The disturbances,  $d(t) \in \mathcal{R}^n$ , entering the system are assumed to be independent, identically distributed white noise with identity covariance matrix  $I_n$ . The transfer matrix  $G_d(z) \in \mathcal{C}^{n \times n}$  models the spatial and dynamical correlation of the process' disturbances.

The industrial definition of paper quality was presented in (1.2) where deviations of the paper property from the average value for the roll should be small. However, this is necessarily an off-line performance index as the paper roll average  $\bar{x}$  in (1.2) may be computed only after the completion of the roll. The control design is based on a modified version of the quality index (1.2) and compares the sensor profile  $y(t)$  with the setpoint

profile  $r(t)$ . The performance will then be defined in terms of the variance of the error profile  $v(t) = y(t) - r(t)$ .

An expression for the error profile signal in closed-loop is obtained from (2.9) and (2.20),

$$v = [I - GK]^{-1}G_d \cdot d - [I - GK]^{-1} \cdot r \quad (2.21)$$

where the argument  $z$  has been suppressed in favor of neatness.

The cross-directional controller design strategy will concentrate on the contribution of the first term in (2.21) to the error signal  $v(t)$ . The second term in (2.21) is usually zero in industrial CD control systems due to two facts. First, the profile targets  $r(t)$  are usually a flat paper sheet such that each element  $r_i(t) = r$  for all  $i = 1, \dots, n$ . Second, as described in Section 1.1, the industrial practice is to use the machine direction (MD) actuators to control the average sheet properties. In other words, the mean value of the error profile at time  $t$  is  $\sum_i v_i(t) = \sum_i y_i(t) - r_i(t)$  is removed and used in the MD feedback loop - it is not present in the CD loop.

The design of the CD controller is motivated by the minimization of the effect of the uncorrelated disturbances  $d(t)$  on the variance of the error profile  $v(t)$ . If the contribution of the second term in (2.21) is neglected, then the expected value of the variance of the error profile is given by,

$$E [v(t)^T v(t)] = \|[I - G(z)K(z)]^{-1}G_d(z)\|_2^2, \quad (2.22)$$

where the discrete-time  $\mathcal{H}_2$  norm of a stable transfer matrix,  $T(z)$ , is defined as

$$\|T(z)\|_2^2 = \frac{1}{2\pi} \int_{-\pi}^{\pi} \sum_{j=1}^n \sigma_j [T(e^{i\omega})]^2 d\omega, \quad (2.23)$$

which may be interpreted as a measure of the gain of the multivariable transfer function  $T(z)$  summed over all singular values  $\sigma_j$  with  $j = 1, \dots, n$  and all dynamical frequencies  $\omega \in [-\pi, \pi]$ .

The expected variance of the error profile (2.22) may then be translated into a mathe-

mathematical specification for the control system's performance. The feedback controller  $K(z)$  in (2.9) is to be designed such that the closed-loop is internally stable and the  $\mathcal{H}_2$  norm,

$$\| [I - G(z)K(z)]^{-1}G_d(z) \|_2^2 \rightarrow \text{small} \quad (2.24)$$

This performance objective is achieved if a stabilizing controller  $K(z)$  is designed such that the gain of the loop transfer matrix  $GK(e^{i\omega})$  is large for frequencies  $\omega$  for which the gain of  $G_d(e^{i\omega})$  is also large [56]. The directionality of these transfer matrices is usually stated in terms of their singular vectors, and is a crucial consideration of the feedback design. However, the directionality of the systems described in Sections 2.1 and 2.2 is the subject of Chapter 3 and is discussed thoroughly there.

## 2.4 Uncertainty and Robustness

As discussed in Section 2.3 above, a closed-loop performance requirement such as (2.24) may be satisfied with an aggressive feedback controller  $K(z)$  in (2.9) designed such that  $\underline{\sigma}(K)$  is large. The controller  $K(z)$  will then generate a large control signal  $u(t)$  in order to counteract the effect of the disturbances  $d(t)$  on the error signal  $v(t)$ . However, a large control signal  $u(t)$  is undesirable in an industrial application where physical limitations on actuators must be considered. Processes that are described by ill-conditioned transfer matrices such as  $G(z)$  in (2.1) are especially sensitive to high-gain controllers and care must be taken to avoid excessive actuation in the directions of the singular vectors which correspond to small singular values of the process.

A large actuation signal is not the only concern when designing a high loop gain. The tolerance of the closed-loop to model uncertainties is an essential part of any practical control scheme. In general the closed-loop robust stability of open-loop stable systems is guaranteed by designing the controller  $K(z)$  such that the gain of the loop transfer matrix  $KG$  is sufficiently small. However, a small loop gain is in direct conflict with the closed-loop performance specification as discussed in Section 2.3. This is a fundamental trade-off in designing feedback control. A successful design is one in which the loop gain  $\sigma_j(GK(e^{i\omega}))$  is high at those dynamical frequencies  $\omega$  and directions (indexed by  $j$ )

for which performance is important, and is small at those dynamical frequencies  $\omega$  and directions  $j$  for which the robust stability is important [56, 66]. This is possible due to the fact that for many physical applications, these specifications apply at quite different frequency ranges. The performance/robustness trade-off is revisited within the context of spatially distributed systems in Chapter 4.

Next, the presence of uncertainty in the modelling of the cross-directional process is discussed. The physical interpretation of the main sources of model uncertainty was discussed in Section 1.3.4. The most striking effect of model uncertainty in the CD control problem arises due to its interaction with an ill-conditioned process model  $G(z)$  in (2.1), as discussed in Section 1.3.4. In most practical CD control applications, one does not know the *sign* of the gain of the process for all of the singular vector directions of the transfer matrix  $G(z)$  even at steady-state with  $\omega = 0$  [24, 33]. In other words, the small model gain combines with the model uncertainty such that the relative uncertainty is larger than 100% for certain singular values at all  $\omega$ . This is a rather rare situation for multivariable feedback control and a design technique specifically tailored to this problem is presented in Chapter 4.

In order to describe the model uncertainty in the CD process, it is assumed that the true process response is not perfectly modelled by the linear transfer matrix  $G(z)$  in (2.1). Following the traditional approach used in robust control for representing model uncertainty [56, 66], the true process  $G_p(z)$  is assumed to belong to a set of possible response models,

$$G_p(z) \in \Pi_g \quad (2.25)$$

For the CD process this family is assumed to be described by an additive unstructured perturbation on the nominal transfer matrix model,

$$\Pi_g := \{G(z) + \delta G(z) : \bar{\sigma}(\delta G(e^{i\omega})) < l(\omega)\} \quad \forall \omega \in [-\pi, \pi] \quad (2.26)$$

where  $l(\omega)$  is a positive scalar function which limits the perturbed transfer matrix  $G_p(z)$  to a neighbourhood of the nominal model  $G(z)$  in (2.1).

The additive uncertainty structure is used here due to its ability to model sign uncertainty in the process model's singular values even at low frequencies  $\omega$ . Figure 2.4 plots the singular values of a typical CD process as a function of dynamical frequency  $\omega$ . The model uncertainty bound  $l(\omega) = 0.01$  is also included, and it can be seen that one must carefully consider the directionality of the control signal even at  $\omega = 0$ . There are a total of  $n = 73$  singular values in this process model and 17 of them are smaller than  $l(\omega) = 0.01$  for all dynamical frequencies  $\omega$ . Figure 2.4 also illustrates the need for a better graphical representation of the frequency response of the CD process. It is apparent that plotting all  $n$  singular values is unnecessary and leads to a cluttered diagram. The representation of these large scale transfer matrices is the subject of Section 3.7.

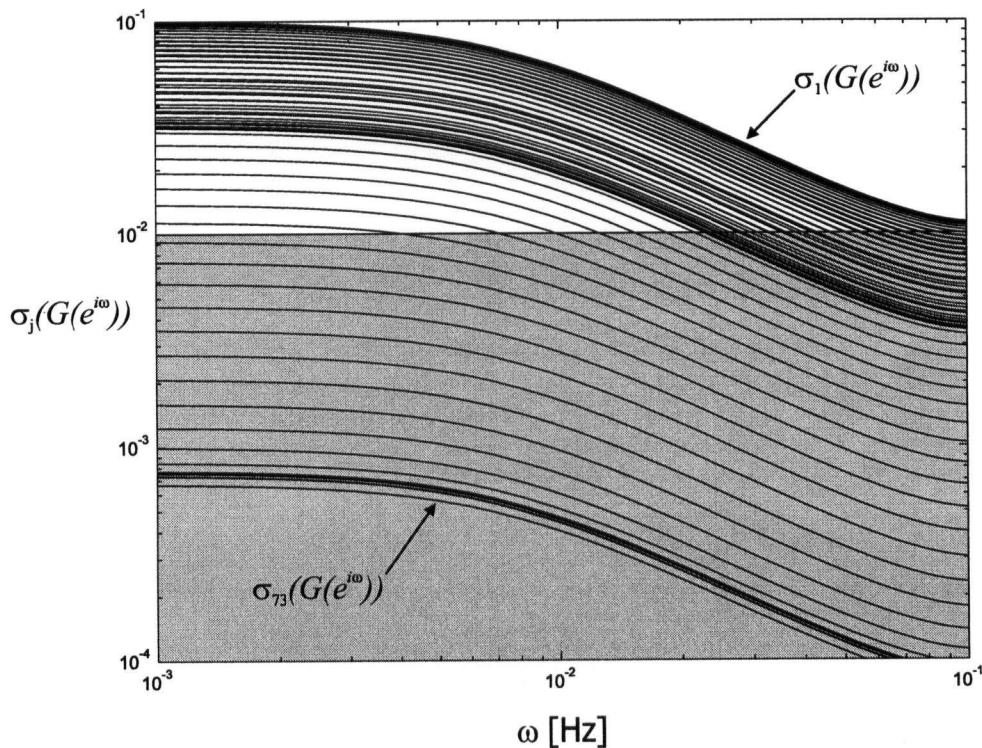


Figure 2.4: Singular values of the process model  $G(e^{i\omega}) \in \mathcal{C}^{73 \times 73}$  in (2.1) and model uncertainty  $l(\omega) = 10^{-2}$  in (2.26) for the basis weight process illustrated in Figure 2.1.

The final specification on the design of the feedback controller  $K(z)$  in (2.9) is that of robust stability of the closed-loop. The feedback controller  $K(z)$  is to be designed such

that the closed-loop is internally stable and the  $\mathcal{H}_\infty$ -norm

$$\|\delta G(z) \cdot K(z)[I - G(z)K(z)]^{-1}\|_\infty < 1 \quad (2.27)$$

where the discrete-time  $\mathcal{H}_\infty$  norm of a stable transfer matrix is defined as

$$\|T(z)\|_\infty^2 = \sup_{\omega \in [-\pi, \pi]} \bar{\sigma} [T(e^{i\omega})]^2 \quad (2.28)$$

This norm may be interpreted as the largest gain of the transfer matrix  $T(z)$  with respect to all input directions and all dynamical frequencies  $\omega \in [-\pi, \pi]$ .

For the unstructured model uncertainty in (2.26), the condition (2.27) is equivalent to the frequency-by-frequency condition,

$$\bar{\sigma} (K(e^{i\omega})[I - G(e^{i\omega})K(e^{i\omega})]^{-1}) < 1/l(\omega) \quad \forall \omega \in [-\pi, \pi] \quad (2.29)$$

Notice that the robust stability requirement in (2.29) may be satisfied by  $\bar{\sigma}(K) \rightarrow 0$ , but that the performance requirement of (2.24) requires a large controller gain  $\underline{\sigma}(K)$ . This fundamental trade-off in feedback control is central to the loop shaping approach for controller design [56, 66]. Chapter 4 presents a technique for the class of spatially distributed control problems, described in Section 2.1 and 2.2, that allows the designer to quantify the performance/robustness trade-off during the design of the feedback controller  $K(z)$  in (2.9).

## Chapter 3

### Spatial Frequency Decomposition

The problem statement of Chapter 2 requires a spatially distributed feedback controller to be designed for a spatially distributed process to satisfy closed-loop performance and robust stability specifications. The class of process models,  $G(z)$  in Section 2.1, was composed of symmetric band-diagonal Toeplitz matrix factors. The feedback controller,  $K(z)$  in Section 2.2, is required to possess the same structure as the process models and is also to be constructed using symmetric Toeplitz matrix factors. The justification for the use of these structures in describing and controlling spatially distributed processes is presented in Chapter 2.

Spatially distributed systems are often of very large scale. For example, in Chapter 5, the cross-directional control of an industrial paper machine is considered where the input array consists of  $n = 226$  evenly-spaced actuators distributed across an 7.91 metre wide paper sheet. Such a large size discourages the direct use of off-the-shelf optimal controller synthesis methods. The computational complexity of  $\mathcal{H}_2$  and  $\mathcal{H}_\infty$  optimal controller synthesis increases rapidly as a function of the dimension.

In addition, the large size of these systems inhibits the conceptual understanding of the problem. Figure 2.4 in Section 2.4 illustrates the open-loop singular value plot of a typical slice lip basis weight cross-directional control process with  $n = 73$  actuators. It is not an easy task to begin sorting the 73 directions as ‘controllable’ or ‘uncontrollable’.

Recently, there has been much interest in the design of feedback controllers for spatially distributed systems whose properties are invariant in space and time [4, 38]. It has been demonstrated that the design of feedback controllers for these systems may be decoupled into consideration of independent single-input-single-output (SISO) controller design problems. In addition, in the case of dynamical systems distributed in one spatial dimension, the eigenfunction directions coincide with the singular vector directions and

are in fact the spatial Fourier components of the system<sup>1</sup>. This feature provides an intuitive insight into the problem as each eigenfunction of the process may be characterized by its dynamical frequency  $\omega$  and its spatial frequency  $\nu$ . Spatially-invariant systems with a finite number  $n$  of degrees of freedom are defined via  $n$  discrete spatial frequency components  $\nu \in \{\nu_1, \dots, \nu_n\}$ . Frequency-domain design is familiar to control engineers from experience with dynamical systems.

As described in Section 2.1, the processes under consideration are time-invariant and *almost* spatially-invariant. The truncated Toeplitz matrices, forming the plant model (2.4) and feedback controller and (2.13), are related to spatially-invariant *circulant* matrices by a small perturbation. It is therefore proposed that the design problem of Chapter 2 be replaced by a spatially-invariant system. In Section 3.1, each of the Toeplitz matrices, in both the plant and controller models (2.4) and (2.13), is replaced by an appropriate symmetric circulant matrix. The controller design may now proceed with the computationally and conceptually simpler problem of designing  $n$  independent SISO problems, one for each spatial frequency  $\nu_j \in \{\nu_1, \dots, \nu_n\}$ . In terms of the cross-directional paper machine control problem, this approximation may be interpreted physically as imposing spatially-periodic boundary conditions on the process. In other words, instead of producing a flat sheet of paper, it is assumed that the machine is producing a 'tube' of paper whose circumference is equal to the cross-directional width of the original sheet.

This chapter includes a summary of the main properties of symmetric circulant systems that may be found in [4, 13, 38]. In Sections 3.4 and 3.5, it is demonstrated that a circulant symmetric controller is sufficient to control a symmetric circulant process. In other words, there is no risk of degrading performance or robustness by restricting attention to the design of a symmetric circulant feedback controller.

In Section 3.6, an example is shown that demonstrates the convenience of designing an  $n \times n$  circulant controller in terms of  $n$  independent SISO problems. Finally, Section 3.7 provides a graphical interpretation of the spatial and dynamical frequency decomposition of circulant systems as a generalization of dynamical frequency representation of SISO dynamical problems. Two dimensional loop shaping controller design, in terms of spatial

---

<sup>1</sup>Analogous results also exist for dynamical systems distributed in more than one spatial dimension, but are outside the scope of this work. See [4, 15] for more details.

and dynamical frequencies, is the subject of Chapter 4 and will be explored in more detail there.

### 3.1 Circulant Extension of a Toeplitz System

The class of process models and feedback controllers in Sections 2.1, 2.2 were defined in terms of truncated Toeplitz matrix factors (2.4) and (2.13) respectively. The goal of this section is to illustrate the relationship between these truncated symmetric Toeplitz matrix factors and the associated symmetric circulant matrix factors. The closeness of this relationship is exploited to allow the controller synthesis to proceed in terms of a symmetric circulant design problem. The advantages of performing controller design for a circulant system are the subject of Sections 3.4–3.7.

The design procedure in Chapter 4 performs closed-loop stability, performance, and robustness calculations on the associated symmetric circulant system - not on the ‘true’ system of truncated Toeplitz matrices. A small gain argument is presented in this section that relates the internal stability of the idealized spatially-invariant system to the internal stability of the true system subjected to disruptions of the spatial-invariance by the boundary conditions of the physical process.

The problem statement in Chapter 2 requires to design a feedback controller  $K_t(z) = [I + S_t(z)]^{-1}C_t(z)$  in (2.11) for the process modelled as  $G_t(z) = [I + A_t(z)]^{-1}B_t(z)$  in (2.2). The process is modelled with the transfer matrix factors  $B_t(z)$  and  $A_t(z)$  in (2.4) having a band-diagonal symmetric Toeplitz structure. The design requirements for the feedback controller  $K_t(z)$  specify the same structure for the transfer matrices  $C_t(z)$  and  $S_t(z)$  in (2.13).

It is proposed to proceed with the design of the band-diagonal transfer matrices  $C_t(z)$  and  $S_t(z)$  by restating the problem in terms of the circulant extension of this system as will be defined below. First the band-diagonal system matrices  $B_t(z)$  and  $A_t(z)$  are replaced with their circulant extensions  $B(z)$  and  $A(z)$  as in (3.2). Next, the procedure described in Chapter 4 is used to generate banded symmetric circulant transfer matrices  $C(z)$  and  $S(z)$  satisfying the design requirements. Finally, the band-diagonal Toeplitz

factors  $C_t(z)$  and  $S_t(z)$  in the controller  $K_t(z)$  are recovered by extracting the non-zero diagonal bands from  $C(z)$  and  $S(z)$ .

The circulant extension is proposed to be used in the solution of this problem for two reasons. First, the difference between narrow band-diagonal Toeplitz matrices and banded circulant matrices is small. Second, the design of controllers for circulant systems has many advantages over the Toeplitz version. These advantages are discussed in detail in Sections 3.4–3.7, but are previewed here:

1. All symmetric circulant systems of the same size are diagonalized with the *same* unitary matrix  $F$  (defined as the real Fourier matrix in Appendix A in (A.4)) by pre- and post-multiplication by  $F(\cdot)F^T$ .
2. The singular values of a symmetric circulant matrix are equal to the magnitude of the eigenvalues. This fact allows for the  $n \times n$  multivariable controller to be designed in terms of a family of  $n$  independent single variable problems.
3. The singular vectors of symmetric circulant matrices possess an intuitive physical interpretation as harmonic functions of the spatial variable (the rows of the real Fourier matrix  $F$ ).

Let us now define exactly what is meant by the term ‘circulant extension’. A symmetric Toeplitz matrix is defined completely in terms of its first row. The  $n \times n$  band-diagonal symmetric Toeplitz matrices that are important in this work (Sections 2.1 and 2.2) may be written as,

$$M_t = \text{toeplitz}\{m_1, m_2, \dots, m_{n_m}, 0, \dots, 0\} \quad (3.1)$$

Herein, typically the width of the band-diagonal is much smaller than the order of the matrix so that  $n_m \ll n$ .

Next, define the circulant extension to the band-diagonal symmetric Toeplitz matrix  $M_t$  in (3.1) by the  $n \times n$  symmetric circulant matrix,

$$M = \text{toeplitz}\{m_1, m_2, \dots, m_{n_m}, 0, \dots, 0, m_{n_m}, \dots, m_2\} \quad (3.2)$$

where the difference between these two matrices is then given by,

$$\begin{aligned}\delta M_t &= M - M_t \\ &= \text{toeplitz}\{0, \dots, 0, m_{n_m}, \dots, m_2\}\end{aligned}\quad (3.3)$$

and contains the ‘ears’ of the circulant matrix  $M$  as illustrated in Figure 3.1.

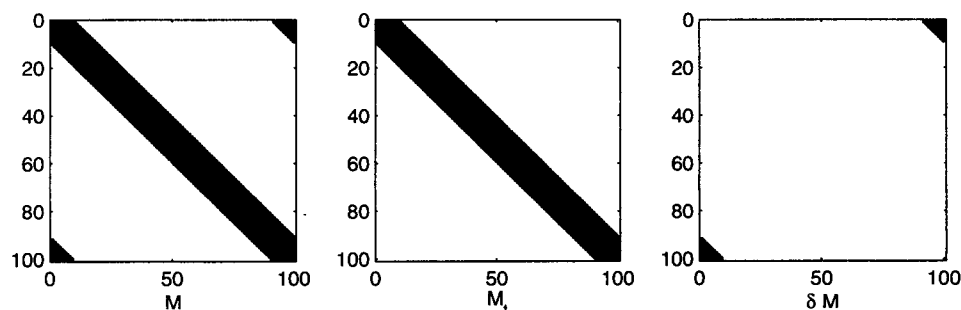


Figure 3.1: Non-zero elements of a banded symmetric circulant matrix  $M$ , the associated band-diagonal Toeplitz symmetric matrix  $M_t$ , and the difference described by the ‘ears’ in  $\delta M_t = M - M_t$ .

The first design requirement on any feedback controller for any application is that it provides an internally stable closed-loop. Since the design of the feedback is performed on the circulant extension of the ‘true’ system, a result is required to relate the internal stability of the true system to the internal stability of the circulant approximation.

Assume that a feedback controller  $K(z) = [I + S(z)]^{-1}C(z)$  has been designed with banded circulant factors  $C(z)$  and  $S(z)$  to be internally stable with the plant  $G(z) = [I + A(z)]^{-1}B(z)$  with factors  $B(z)$  and  $A(z)$  being the circulant extensions of  $B_t(z)$  and  $A_t(z)$  respectively. Internal stability of this circulant closed-loop is equivalent to the condition that the  $2n \times 2n$  transfer matrix

$$L(z) := \begin{bmatrix} I + S(z) & C(z) \\ B(z) & I + A(z) \end{bmatrix}\quad (3.4)$$

is invertible in  $\mathcal{RH}_\infty$  for all  $|z| \geq 1$ .

The corresponding ‘true’ system has band-diagonal transfer matrices  $A_t(z)$ ,  $B_t(z)$ ,

$C_t(z)$ ,  $S_t(z)$  which are related to the symmetric circulant transfer matrices  $A(z)$ ,  $B(z)$ ,  $C(z)$ ,  $S(z)$  as in (3.1), (3.2),

$$\begin{aligned} L_t(z) &:= \begin{bmatrix} I + S_t(z) & C_t(z) \\ B_t(z) & I + A_t(z) \end{bmatrix} \\ &= \begin{bmatrix} I + S(z) & C(z) \\ B(z) & I + A(z) \end{bmatrix} - \begin{bmatrix} \delta S_t(z) & \delta C_t(z) \\ \delta B_t(z) & \delta A_t(z) \end{bmatrix} \end{aligned} \quad (3.5)$$

The internal stability of the ‘true’ closed-loop system is equivalent to the invertibility of  $L_t(z)$  in (3.5) in  $\mathcal{RH}_\infty$  for all  $|z| \geq 1$ .

However, a computationally more attractive result may be found by appealing to robust control theory for the stability of feedback systems with perturbations. A sufficient condition for the internal stability of the true system defined by  $L_t(z)$  in (3.5) follows from the small gain theorem. The closed-loop system with  $L_t(z)$  in (3.5) is stable if

$$\left\| \begin{bmatrix} \delta S_t(z) & \delta C_t(z) \\ \delta B_t(z) & \delta A_t(z) \end{bmatrix} \cdot \begin{bmatrix} I + S(z) & C(z) \\ B(z) & I + A(z) \end{bmatrix}^{-1} \right\|_\infty < 1 \quad (3.6)$$

The systems under consideration (i.e. arising from paper machine process models) are typically described by transfer matrices with relatively narrow non-zero bands such as that shown in Figure 3.1. For example, Chapter 5 contains an industrial example in which the Toeplitz symmetric transfer matrix  $B_t(z)$  is  $n \times n$  with  $n = 226$  but has only 5 non-zero diagonals. Intuitively speaking, the narrower the band, the smaller is the size of the perturbation introduced by the circulant extension (3.3). A smaller perturbation corresponds to less error introduced by neglecting the edge effects of the original system while designing the feedback controller in terms of the symmetric circulant system (3.4).

### 3.2 Generalized Plant and Linear Fractional Transformations

Prior to analyzing the closed-loop performance and robustness of systems composed of symmetric circulant blocks, in Sections 3.4 and 3.5, it is necessary to define a general structure upon which to base an analysis. A standard technique in multivariable con-

trol system design and analysis is to reorganize the control problem into the generalized plant format. The following discussion is based on the representation in [56] for feedback controller analysis and design.

As described below, the generalized plant is a transfer matrix  $P(z)$  containing all process model, disturbance model, and performance weighting transfer functions. The loop is closed with the feedback controller  $K(z)$  and the generalized transfer function is compactly represented by a linear fractional transformation (LFT) of  $P(z)$  and  $K(z)$ .

The convenience of this format lies in the fact that a wide variety of practical control problems find a compact representation as a LFT. Sections 3.4 and 3.5 of this work discuss quite general performance and robust stability results for control systems composed of symmetric blocks, for which this format is essential.

The general statement of the feedback control problem is: given exogenous inputs  $w(z)$  to a system, find a controller  $K(z)$  which uses sensor data  $y(z)$  to calculate actuator inputs  $u(z)$  which counteract the influence of  $w(z)$  on the signal  $e(z)$  [56]. The generalized input  $w(z)$  will contain external inputs such as disturbances  $d(z)$  and setpoint references  $r(z)$ . The generalized output  $e(z)$  will usually contain signals such as the difference between measurement and setpoint  $y(z) - r(z)$  and the control signal  $u(z)$ . The problem of keeping the generalized error  $e(z)$  small may be stated in terms of some norm on the closed-loop transfer function from the inputs  $w(z)$  to  $e(z)$ . A generalized plant is often used to describe the path from the exogenous inputs to the outputs of a feedback control system [8, 56].

The open-loop generalized plant  $P(z)$  is introduced such that

$$\begin{bmatrix} e(z) \\ v(z) \end{bmatrix} = P(z) \begin{bmatrix} w(z) \\ u(z) \end{bmatrix} = \begin{bmatrix} P_{11}(z) & P_{12}(z) \\ P_{21}(z) & P_{22}(z) \end{bmatrix} \begin{bmatrix} w(z) \\ u(z) \end{bmatrix} \quad (3.7)$$

where  $P(z)$  contains, not only the open-loop plant  $G(z)$  in (2.1), but also includes all transfer matrices associated with disturbances and performance weights.

The feedback control is then described by,

$$u(z) = K(z)v(z) \quad (3.8)$$

where  $u(z)$  is the control signal and  $v(z)$  is the feedback signal. The equations (3.7) and (3.8) are illustrated in Figure 3.2.

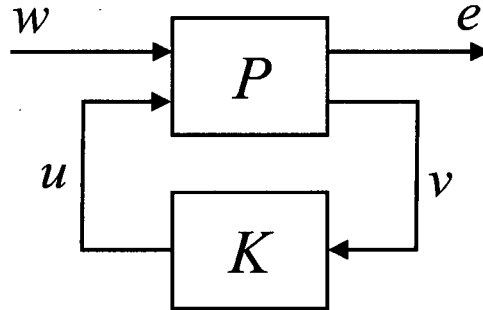


Figure 3.2: Block diagram of the linear fractional transformation  $\mathcal{F}_l(P, K)$  in (3.9).

In feedback control an important transfer matrix is given by the closed-loop transfer matrix from exogenous inputs  $w(z)$  to the generalized error  $e(z)$  and is denoted by  $T_{ew}(z)$ . This transfer matrix is related to the generalized plant  $P(z)$  in (3.7) and feedback  $K(z)$  in (3.8) by the linear fractional transformation (LFT),

$$T_{ew}(z) = P_{11}(z) + P_{12}(z)K(z) [I - P_{22}(z)K(z)]^{-1} P_{21}(z) := \mathcal{F}_l(P, K) \quad (3.9)$$

where the  $l$  in  $\mathcal{F}_l(P, K)$  indicates that this is a *lower* LFT [56].

Most practical feedback control problems may be written in terms of the generalized plant  $P(z)$  in (3.7) and the feedback  $K(z)$  in (3.8) [56]. For example the performance specification in (2.24) may be written as

$$\|\mathcal{F}_l(P, K)\|_2^2 \rightarrow \text{small} \quad \mathcal{F}_l(P, K) = [I - G(z)K(z)]^{-1} G_d(z) \quad (3.10)$$

Where the generalized plant  $P(z)$  in (3.7) is constructed by defining the generalized output signal  $e(z)$  as the error signal,  $e(z) = v(z) = y(z) - r(z)$ . The exogenous inputs  $w(z)$  to the closed-loop system are the disturbances  $d(z)$ . Then the generalized plant  $P(z)$  in

(3.7) is

$$P(z) = \begin{bmatrix} P_{11}(z) & P_{12}(z) \\ P_{21}(z) & P_{22}(z) \end{bmatrix} = \begin{bmatrix} G_d(z) & G(z) \\ G_d(z) & G(z) \end{bmatrix} \quad (3.11)$$

and the loop is closed with  $u(z) = K(z)v(z)$  as above.

Including other signals in the optimization is straightforward. For instance, the weighted actuator signal  $W(z)u(z)$  may be penalized in the optimization

$$\|\mathcal{F}_l(P, K)\|_2^2 = \|[I - G(z)K(z)]^{-1}G_d(z)\|_2^2 + \|W(z) \cdot K(z)[I - G(z)K(z)]^{-1}\|_2^2 \quad (3.12)$$

then the generalized plant  $P(z)$  is simply augmented such that the error signal and the generalized plant are given by

$$e(z) = \begin{bmatrix} v(z) \\ W(z)u(z) \end{bmatrix}, \quad P(z) = \begin{bmatrix} G_d(z) & G(z) \\ 0 & W(z) \\ \hline G_d(z) & G(z) \end{bmatrix} \quad (3.13)$$

The important feature to note in this section is the appearance of the system transfer matrices in the generalized plant  $P(z)$ . The generalized plant  $P(z)$  is a block transfer matrix containing all of the component transfer matrices that are important to the performance of the feedback controller.

The following section discusses the discretized spatially-distributed feedback control problem in terms of the generalized plant described by  $P(z)$  in (3.7). Sections 3.4 and 3.5 analyze the closed-loop based on the LFT description of the closed-loop system  $\mathcal{F}_l(P, K)$  in (3.9).

### 3.3 Systems Composed of Symmetric Circulant Blocks

This section considers dynamical systems such that the generalized plant  $P(z)$  in (3.7) in Section 3.2 is composed of symmetric circulant transfer matrices. The class of process models considered in Section 2.1 is composed of symmetric truncated Toeplitz matrices

which are approximated by symmetric circulant transfer matrices as shown in Section 3.1. The goal of this section is to demonstrate the decoupling of matrices of symmetric circulant blocks into block diagonal matrices. In the language of dynamical systems, this decoupling represents a modal decomposition, such that the large scale dynamical system may be represented by a family of SISO subsystems. This decomposition is central to the closed-loop performance and robustness analysis of symmetric circulant systems presented in Sections 3.4 and 3.5.

For control system analysis and design, one of the most convenient properties of a system described by a circulant matrix is that every circulant matrix of the same size may be diagonalized with the same constant matrix [13, 38]. This diagonalizing matrix is very closely related to the Fourier transform operator.

The discrete Fourier transform [45] of an array consisting of  $n$  discrete elements is equivalent to a multiplication by a unitary complex matrix  $\mathcal{F} \in \mathcal{C}^{n \times n}$  (see Appendix A for its construction). As described in [13, 45] for example, the constant matrix  $\mathcal{F}$  may be used to diagonalize circulant matrices. *Symmetric* circulant matrices, such as those important in this study, have a further advantage. Any symmetric circulant matrix  $A \in \mathcal{C}^{n \times n}$ , is diagonalizable with the real Fourier matrix,  $F \in \mathcal{C}^{n \times n}$  given in (A.4), such that,

$$A = F^T \tilde{A} F, \quad \tilde{A} = \text{diag}\{\tilde{a}(\nu_1), \dots, \tilde{a}(\nu_n)\} \quad (3.14)$$

where each  $\tilde{a}(\nu_j) \in \mathcal{C}^{1 \times 1}$  [13]. The variable  $\nu_j$  indexes the spatial frequency of the  $j^{\text{th}}$  spatial mode and is given by  $\nu_j = 2\pi(j-1)/n$  (see Appendix A).

The set of symmetric circulant transfer matrices is included here and is especially important for the feedback control applications under consideration. It is important that the same diagonalizing matrix  $F$  may be used to decouple a transfer matrix  $A(e^{i\omega})$  at all dynamical frequencies  $\omega$  such that,

$$A(z) = F^T \tilde{A}(z) F, \quad \tilde{A}(z) = \text{diag}\{\tilde{a}(\nu_1, z), \dots, \tilde{a}(\nu_n, z)\} \quad (3.15)$$

where  $\tilde{a}(\nu_j, z) \in \mathcal{C}^{1 \times 1}$  for each  $j \in \{1, \dots, n\}$  is a scalar, rational transfer function [4, 6, 13].

In multivariable control terminology, one would say that the directionality of symmetric circulant transfer matrices is independent of the dynamical frequency  $\omega$ . The transfer matrix has the same singular vectors at all frequencies and it will be shown that this fact will be very beneficial when designing feedback controllers for symmetric circulant plants.

To be considered next are matrices composed of symmetric circulant blocks. These matrices have a direct application to the system models that are being considered in this work. It was stated above that the generalized plant transfer matrix  $P(z)$  in (3.7) will be considered to be composed of symmetric circulant blocks. The goal of this section is to show how a matrix composed of symmetric circulant blocks may be transformed into a block diagonal matrix. In particular, the transformation may be interpreted completely in terms of pre- and post-multiplication by unitary matrices. The benefit of this property becomes clear in the following section, where it is used to simplify the calculation of the optimal feedback controller  $K(z)$  in (2.9).

For the purposes of this explanation, the following  $3n \times 2n$  generalized plant  $P(z)$  will be used as an example,

$$\begin{bmatrix} e_1(z) \\ e_2(z) \\ v(z) \end{bmatrix} = P(z) \begin{bmatrix} w(z) \\ u(z) \end{bmatrix} = \begin{bmatrix} A_1(z) & A_2(z) \\ A_3(z) & A_4(z) \\ A_5(z) & A_6(z) \end{bmatrix} \begin{bmatrix} w(z) \\ u(z) \end{bmatrix}, \quad (3.16)$$

where each  $A_i(z) \in \mathcal{C}^{n \times n}$  is assumed to be a symmetric circulant transfer matrix.

Next, the diagonalizing matrix is introduced. It was shown above that the real Fourier matrix  $F$  in (A.4) may be used to diagonalize symmetric circulant matrices. In order to demonstrate the block-diagonalization of a transfer matrix composed of symmetric circulant blocks, the following block-diagonal matrix operator is introduced,

$$I_3 \otimes F := \begin{bmatrix} F & 0 & 0 \\ 0 & F & 0 \\ 0 & 0 & F \end{bmatrix} \quad (3.17)$$

where  $\otimes$  denotes the Kronecker product and  $I_3$  is an  $3 \times 3$  identity matrix. In general, the Kronecker product ( $I_H \otimes F$ ) results in an  $nH \times nH$  block-diagonal matrix, with  $H$  copies

of  $F$  comprising the blocks (but is more difficult to draw than the third-order example shown in (3.17)).

Next, form a new system by pre-multiplying both sides of the system (3.16) by  $(I_3 \otimes F)$

$$(I_3 \otimes F) \begin{bmatrix} e_1(z) \\ e_2(z) \\ v(z) \end{bmatrix} = (I_3 \otimes F) \begin{bmatrix} A_1(z) & A_2(z) \\ A_3(z) & A_4(z) \\ A_5(z) & A_6(z) \end{bmatrix} (I_2 \otimes F)^T (I_2 \otimes F) \begin{bmatrix} w(z) \\ u(z) \end{bmatrix}, \quad (3.18)$$

where the product  $(I_2 \otimes F)^T (I_2 \otimes F) = I_{2n}$  due to the unitarity of the operator  $(I_H \otimes F)$ .

The new system (3.18) may be re-written as

$$\begin{bmatrix} \tilde{e}_1(z) \\ \tilde{e}_2(z) \\ \tilde{v}(z) \end{bmatrix} = \begin{bmatrix} \tilde{A}_1(z) & \tilde{A}_2(z) \\ \tilde{A}_3(z) & \tilde{A}_4(z) \\ \tilde{A}_5(z) & \tilde{A}_6(z) \end{bmatrix} \begin{bmatrix} \tilde{w}(z) \\ \tilde{u}(z) \end{bmatrix} \quad (3.19)$$

where the transformed signal  $\tilde{u}(z) := Fu(z) \in \mathcal{C}^n$ . There exists a similar definition for all remaining signals in (3.19). The transformed transfer matrices  $\tilde{A}_i(z) := FA_i(z)F^T$ . Since each  $A_i(z) \in \mathcal{C}^{n \times n}$  is symmetric circulant, then as in (3.14), each  $\tilde{A}_i(z)$  in (3.19) is a diagonal transfer matrix,

$$\tilde{A}_i(z) = \text{diag}\{\tilde{a}_i(\nu_1, z), \dots, \tilde{a}_i(\nu_n, z)\} \quad (3.20)$$

Next the system composed of diagonal blocks (3.19), will be transformed into a block-diagonal system. The matrix algebra required for this transformation is quite straightforward, but is difficult to show all of the steps neatly. Let it be summarized, by saying that there exist permutation matrices  $M_1$  and  $M_2$  of appropriate dimension, such that the transformation

$$M_1 \begin{bmatrix} \tilde{e}_1(z) \\ \tilde{e}_2(z) \\ \tilde{v}(z) \end{bmatrix} = M_1 \begin{bmatrix} \tilde{A}_1(z) & \tilde{A}_2(z) \\ \tilde{A}_3(z) & \tilde{A}_4(z) \\ \tilde{A}_5(z) & \tilde{A}_6(z) \end{bmatrix} M_2^T M_2 \begin{bmatrix} \tilde{w}(z) \\ \tilde{u}(z) \end{bmatrix} \quad (3.21)$$

where using the fact that each  $\tilde{A}_i(z)$  is diagonal (3.20), allows (3.19) to be re-written as



that the block-diagonal transfer matrix  $\tilde{P}(z)$  is related to the original  $P(z)$  by pre- and post-multiplication by unitary matrices such that the  $\mathcal{H}_2$  and  $\mathcal{H}_\infty$  norms are unaffected by the transformation. In general, the  $\mathcal{H}_2$  norm of an  $(M+1)n \times (N+1)n$  transfer matrix  $P(z)$  composed of  $n \times n$  symmetric circulant blocks is given by,

$$\|P(z)\|_2^2 = \sum_{j=1}^n \|\tilde{p}(\nu_j, z)\|_2^2 \quad (3.25)$$

where the  $(M+1) \times (N+1)$  transfer matrix  $\tilde{p}(\nu_j, z)$  is obtained by a transformation such as (3.24).

The  $\mathcal{H}_\infty$  norm of the same transfer matrix  $P(z)$  is given by,

$$\|P(z)\|_\infty^2 = \max_{j \in \{1, \dots, n\}} \|\tilde{p}(\nu_j, z)\|_\infty^2 \quad (3.26)$$

In practical applications, each of the subsystems  $\tilde{p}(\nu_j, z)$  in (3.24) is significantly smaller than the original generalized plant  $P(z)$ . For example, there exist real-world applications in which there are  $n = 300$  actuators. Assume a typical control application requiring the consideration of  $N = 2$  exogenous inputs (say setpoint and disturbances  $w(z) = [r(z)^T \ d(z)^T]^T$ ) and  $M = 1$  output signals (say deviation from setpoint  $e(z) = y(z) - r(z)$ ). Since the subsystems  $\tilde{p}(\nu_j, z)$  are a factor  $n$  smaller than the generalized plant  $P(z)$ , then each subsystem is of size  $1 \times 2$ , and the original system is of size  $300 \times 600$ . The following section demonstrates that it is sufficient to consider each of these subsystems independently during the controller synthesis and analysis stages of design.

### 3.4 Closed-Loop Performance

The control problem defined in Chapter 2 involves very large transfer matrices. There are up to  $n = 300$  actuators in an industrial cross-directional control system. The proposed design technique (Chapter 4) first diagonalizes the problem as in Section 3.3 and then proceeds to design  $n$  independent SISO controllers one for each  $j \in \{1, \dots, n\}$ . This approach assumes that the designed controller  $K(z)$  will be diagonalizable with the real Fourier matrix  $F$  in (A.4). In other words, a symmetric circulant structure is imposed on

the feedback controller  $K(z)$  before the controller design begins.

The goal of this section is to collect the results available in a variety of sources [4, 13, 38] in order to justify the a priori selection of a symmetric circulant controller for a symmetric circulant process. It is demonstrated that if the problem is stated in terms of symmetric circulant transfer matrices (i.e. each  $n \times n$  transfer matrix comprising the generalized plant  $P(z)$  in (3.7)), then  $\mathcal{H}_2$ - and  $\mathcal{H}_\infty$ -optimal performance is achievable with a symmetric circulant controller (Theorem 1).

These results are helpful even if one is not performing a strict  $\mathcal{H}_2$  or  $\mathcal{H}_\infty$  based synthesis. The decoupling of a multivariable control design problem into independent SISO design problems is useful in many synthesis techniques. It is comforting to know that the restriction of the structure of the controller is not restricting the achieved performance.

In the previous section, a technique was shown for transforming a large transfer matrix composed of symmetric circulant blocks into a block-diagonal matrix. The goal of this section is to demonstrate the use of this transformation in the analysis and design of feedback controllers for systems modelled by symmetric circulant transfer matrix blocks. It will be shown that the problem of designing a large multivariable feedback controller  $K(z) \in \mathcal{C}^{n \times n}$  in (2.9) for the  $(M+1)n \times (N+1)n$  generalized plant  $P(z)$  may be reduced to the consideration of designing a family of  $n$  independent SISO feedback controllers one for each  $(M+1) \times (N+1)$  subsystem  $\tilde{p}(\nu_j, z)$  with  $j \in \{1, \dots, n\}$  as in (3.23).

It should be noted that this is not an approximation technique. Designing a controller for the decoupled process  $\tilde{p}(\nu_j, z)$  will satisfy the  $\mathcal{H}_2$  and  $\mathcal{H}_\infty$  optimality conditions for the full process  $P(z)$ . There is no 'extra performance' available through designing directly with the full generalized plant  $P(z)$ .

Define the decoupled generalized plant as in (3.23), partitioned in the same way as the original multivariable plant in (3.7),

$$\begin{bmatrix} \tilde{e}(\nu_j, z) \\ \tilde{v}(\nu_j, z) \end{bmatrix} = \tilde{p}(\nu_j, z) \begin{bmatrix} \tilde{w}(\nu_j, z) \\ \tilde{u}(\nu_j, z) \end{bmatrix} = \begin{bmatrix} \tilde{p}_{11}(\nu_j, z) & \tilde{p}_{12}(\nu_j, z) \\ \tilde{p}_{21}(\nu_j, z) & \tilde{p}_{22}(\nu_j, z) \end{bmatrix} \begin{bmatrix} \tilde{w}(\nu_j, z) \\ \tilde{u}(\nu_j, z) \end{bmatrix} \quad (3.27)$$

the closed-loop systems under consideration are described by the one-degree-of-freedom

error feedback controller

$$\tilde{u}(\nu_j, z) = \tilde{k}(\nu_j, z)\tilde{v}(\nu_j, z) \quad (3.28)$$

ensuring that  $\tilde{p}_{22}(\nu_j, z)$  is always a  $1 \times 1$  transfer matrix for each mode  $j \in \{1, \dots, n\}$ . The size of the other three transfer matrices in (3.27) depends on the dimension of the signals  $\tilde{e}(\nu_j, z)$  and  $\tilde{w}(\nu_j, z)$ .

Next, the modal closed-loop transfer function  $\tilde{t}_{ew}(\nu_j, z)$  is defined in terms of an LFT of the modal generalized plant  $\tilde{p}(\nu_j, z)$  in (3.27) and the modal feedback controller  $\tilde{k}(\nu_j, z)$  in (3.28),

$$\begin{aligned} \tilde{t}_{ew}(\nu_j, z) &:= \mathcal{F}_l(\tilde{p}(\nu_j, z), \tilde{k}(\nu_j, z)) \\ &= \tilde{p}_{11}(\nu_j, z) + \tilde{p}_{12}(\nu_j, z)\tilde{k}(\nu_j, z) \left[1 - \tilde{p}_{22}(\nu_j, z)\tilde{k}(\nu_j, z)\right]^{-1} \tilde{p}_{21}(\nu_j, z) \end{aligned} \quad (3.29)$$

where  $\tilde{t}_{ew}(\nu_j, z)$  is a  $M \times N$  transfer matrix with  $j \in \{1, \dots, n\}$ , the linear fractional transformation  $\mathcal{F}_l(\cdot, \cdot)$  is defined in (3.9).

Now that the terms have been defined, it is necessary to show how the modal transfer functions are related to the full multivariable problem.

**Theorem 1** (cf. [4, 38]) ( **$\mathcal{H}_2$  and  $\mathcal{H}_\infty$  Optimality**) Consider a generalized plant  $P(z)$  in (3.7) that is composed of symmetric circulant transfer matrices and the modal generalized plants  $\tilde{p}(\nu_j, z)$  for  $j \in \{1, \dots, n\}$ , related by the transformation (3.24).

(i)  **$\mathcal{H}_2$  optimality.** If the multivariable optimal feedback is given by,

$$K_m(z) = \arg \inf_{K(z) \text{ stabilizing}} \|\mathcal{F}_l(P(z), K(z))\|_2 \quad (3.30)$$

and the optimal feedback for the subsystems is given by,

$$\tilde{k}_s(\nu_j, z) = \arg \inf_{k(z) \text{ stabilizing}} \|\mathcal{F}_l(\tilde{p}(\nu_j, z), k(z))\|_2 \quad (3.31)$$

for each  $j \in \{1, \dots, n\}$ . Then

$$\begin{aligned} K_m(z) &= K_s(z), \\ K_s(z) &:= F^T \text{diag}\{\tilde{k}_s(\nu_1, z), \dots, \tilde{k}_s(\nu_n, z)\}F, \end{aligned} \quad (3.32)$$

and trivially,

$$\|\mathcal{F}_l(P(z), K_s(z))\|_2 = \|\mathcal{F}_l(P(z), K_m(z))\|_2 \quad (3.33)$$

(ii)  $\mathcal{H}_\infty$  optimality. If the multivariable optimal feedback is given by,

$$K_m(z) = \arg \inf_{K(z) \text{ stabilizing}} \|\mathcal{F}_l(P(z), K(z))\|_\infty \quad (3.34)$$

and the optimal feedback for the subsystems is given by,

$$\tilde{k}_s(\nu_j, z) = \arg \inf_{k(z) \text{ stabilizing}} \|\mathcal{F}_l(\tilde{p}(\nu_j, z), k(z))\|_\infty \quad (3.35)$$

for each  $j \in \{1, \dots, n\}$ . Then writing  $K_s(z) = F^T \text{diag}\{\tilde{k}_s(\nu_1, z), \dots, \tilde{k}_s(\nu_n, z)\}F$ , gives the result

$$\|\mathcal{F}_l(P(z), K_s(z))\|_\infty = \|\mathcal{F}_l(P(z), K_m(z))\|_\infty \quad (3.36)$$

*Proof.*

The transformation decoupling the generalized plant  $P(z)$  outlined in (3.18)–(3.22) is independent of the feedback controller  $K(z)$  and involves pre- and post-multiplication by unitary matrices, leaving the  $\mathcal{H}_2$  and  $\mathcal{H}_\infty$  unaffected. The remainder of the proof involves proving that a decentralized controller is optimal for a decentralized plant and is detailed in [37].

□

**Remark.** As described in [38], in general  $K_s(z) \neq K_m(z)$  for the  $\mathcal{H}_\infty$  optimal con-

trollers defined in (3.34) and (3.35). This is due to the fact that the  $\mathcal{H}_\infty$  optimum is defined as minimizing the magnitude of the ‘worst direction’ of the closed-loop transfer matrix  $\mathcal{F}_l(P, K)$  in (3.9). The remaining  $n - 1$  directions are not considered. However, the  $\mathcal{H}_\infty$  optimal controller  $K_s(z)$ , obtained by modal optimization in (3.35), has optimized the  $\mathcal{H}_\infty$  norm of  $\mathcal{F}_l(P, K)$  in all  $n$  directions, so that  $K_s(z)$  is known as the ‘super-optimal’ solution to the multivariable optimization problem (3.34).

### 3.5 Closed-Loop Robust Stability

The previous section presented results justifying, in terms of achievable closed-loop performance, the use of symmetric circulant feedback controllers for the control of systems modelled by symmetric circulant transfer matrix blocks. The goal of this section is to justify the use of symmetric circulant controllers for symmetric circulant systems in terms of the achievable robust stability margins. First, a general result for the existence of  $\mathcal{H}_\infty$ -admissible controllers is proved. Second, the robust stability condition for the cross-directional control problem in Section 2.4 is described in terms of the spatial frequency decomposition of Section 3.3.

A common representation of model uncertainty is to state it in terms of bounded perturbations on the transfer matrix process models in the feedback loop [16, 44, 56, 66]. The robust stability conditions for such systems may then be stated in terms of an admissibility condition on the gain of one of the closed-loop transfer matrices.

The following theorem considers the existence of  $\mathcal{H}_\infty$ -admissible feedback controllers for systems composed of symmetric circulant transfer matrix blocks as described in Section 3.3. It is shown that if *some*  $\mathcal{H}_\infty$ -admissible feedback controller exists for such a system, then a *symmetric circulant*  $\mathcal{H}_\infty$ -admissible feedback controller also exists.

**Theorem 2** (cf. [4]) ( $\mathcal{H}_\infty$  admissibility) *Consider a generalized plant  $P(z)$  in (3.7) that is composed of symmetric circulant transfer matrices and the modal generalized plants  $\tilde{p}(\nu_j, z)$  for  $j \in \{1, \dots, n\}$ , related by the transformation (3.24). The following statements are equivalent:*

(i) There exists a multivariable controller  $K_m(z)$  stabilizing the generalized plant  $P(z)$  such that,

$$\|\mathcal{F}_l(P(z), K_m(z))\|_\infty \leq \gamma \quad (3.37)$$

(ii) There exists a symmetric circulant controller  $K_c(z)$  stabilizing  $P(z)$  such that,

$$\|\mathcal{F}_l(P(z), K_c(z))\|_\infty \leq \gamma \quad (3.38)$$

(iii) There exist SISO feedback controllers  $\tilde{k}_s(\nu_j, z)$  stabilizing  $\tilde{p}(\nu_j, z)$  such that,

$$\|\mathcal{F}_l(\tilde{p}(\nu_j, z), \tilde{k}_s(\nu_j, z))\|_\infty \leq \gamma \quad (3.39)$$

for each  $j \in \{1, \dots, n\}$ .

*Proof.*

(i)  $\Rightarrow$  (ii): By the result for  $\mathcal{H}_\infty$  optimality in Theorem 1, there exists a symmetric circulant  $K_c(z)$  stabilizing  $P(z)$  such that

$$\|\mathcal{F}_l(P(z), K_c(z))\|_\infty \leq \|\mathcal{F}_l(P(z), K(z))\|_\infty \quad (3.40)$$

for any  $K(z)$ . Then

$$\|\mathcal{F}_l(P(z), K_c(z))\|_\infty \leq \|\mathcal{F}_l(P(z), K_m(z))\|_\infty \leq \gamma \quad (3.41)$$

for the case  $K(z) = K_m(z)$ .

(ii)  $\Rightarrow$  (iii): Factor the symmetric circulant transfer matrix  $K_c(z)$  in (3.38) as

$$K_c(z) = F^T \tilde{K}_c(z) F, \quad \tilde{K}_c(z) = \text{diag}\{\tilde{k}_c(\nu_1, z), \dots, \tilde{k}_c(\nu_n, z)\} \quad (3.42)$$

Then the  $\mathcal{H}_\infty$  norm of block-diagonal transfer matrices is given by (3.26),

$$\|\mathcal{F}_l(P(z), K_c(z))\|_\infty = \max_{j \in \{1, \dots, n\}} \|\mathcal{F}_l(\tilde{p}(\nu_j, z), \tilde{k}_c(\nu_j, z))\|_\infty \quad (3.43)$$

Then by (3.38) and (3.43), each  $\tilde{k}_c(\nu_j, z)$  satisfies

$$\|\mathcal{F}_l(\tilde{p}(\nu_j, z), \tilde{k}_c(\nu_j, z))\|_\infty \leq \gamma \quad (3.44)$$

for each  $j \in \{1, \dots, n\}$ .

(iii)  $\Rightarrow$  (i): Simply write  $K_m(z) = F^T \text{diag}\{\tilde{k}_s(\nu_1, z), \dots, \tilde{k}_s(\nu_n, z)\} F$ .  $\square$

The advantages afforded by Theorem 2 are illustrated by its application to the requirement of robust stability for the cross-directional control problem described in Section 2.4. The uncertainty of the process model  $G(z)$  is modelled by an unstructured, stable, additive perturbation  $\delta G(z)$  in (2.26). The robust stability condition for general multivariable feedback systems was described in (2.27)–(2.29). However for symmetric circulant systems, it is possible to restate this condition in terms of the spatial frequency decomposition in Section 3.3.

If both the nominal plant transfer matrix  $G(z)$  and the feedback controller  $K(z)$  are symmetric circulant then the maximum singular value in (2.29) may be written in terms of the spatial frequency decomposition

$$\bar{\sigma} \left( K(e^{i\omega}) [I - G(e^{i\omega}) K(e^{i\omega})]^{-1} \right) = \max_{j=1, \dots, n} \left| \frac{\tilde{k}(\nu_j, e^{i\omega})}{1 - \tilde{g}(\nu_j, e^{i\omega}) \tilde{k}(\nu_j, e^{i\omega})} \right| \quad (3.45)$$

Then the robust stability condition (2.27)–(2.29) may be restated in terms of an upper bound on the magnitude of a two-dimensional function of spatial and dynamical frequencies  $\nu_j$  and  $\omega$ .

A stable closed-loop system composed of symmetric circulant  $G(z)$  in (2.1) and  $K(z)$  in (2.9) is robustly stable to the unstructured model perturbation  $\delta G(z)$  in (2.26) if

$$\left| \frac{\tilde{k}(\nu_j, e^{i\omega})}{1 - \tilde{g}(\nu_j, e^{i\omega}) \tilde{k}(\nu_j, e^{i\omega})} \right| < \frac{1}{l(\omega)} \quad (3.46)$$

for all spatial frequencies  $\nu_j \in \{\nu_1, \dots, \nu_n\}$  and dynamical frequencies  $\omega \in [-\pi, \pi]$ . It should be noted here that (3.46) defines the robust stability to a *multivariable* perturbation  $\delta G(z)$  in (2.26) on the process model  $G(z)$ . In other words, the model uncertainty generally disrupts the symmetric circulant structure of the process model. The result in (3.46) requires only that the *nominal* process model  $G(z)$  be diagonalized by the Fourier matrix  $F$  in (A.4).

The original, large scale problem is defined in terms of the  $n \times n$  transfer matrix model  $G(z)$  in (2.1) and  $n \times n$  feedback controller  $K(z)$  in (2.9) for the closed-loop performance specification (2.24) and robust stability specification (2.27). Section 3.4 showed that the closed-loop performance may be defined in terms of  $n$  decoupled single-input-single-output loops. This section has demonstrated the multivariable robust stability condition in terms of the same SISO feedback loops. A considerable reduction in complexity has been achieved by diagonalizing the problem.

### 3.6 Example

The following exercise is included to illustrate the use of the modal decomposition of Section 3.3 for the design of feedback controllers for systems composed of symmetric circulant transfer matrix blocks. The factorization of the controller  $K(z)$  into a structure (see Section 2.2) amenable to implementation is shown to be accommodated easily within this framework.

Consider a four-block problem which may arise in robust stabilization [23]. Given a symmetric circulant transfer matrix,  $G(z) \in \mathcal{C}^{75 \times 75}$ , which models an open-loop plant as  $y(z) = G(z)u(z)$  with  $n = 75$  actuators and sensors. Determine a transfer matrix,  $K(z) \in \mathcal{C}^{75 \times 75}$  to be used for feedback  $u(z) = K(z)v(z)$  where  $v(z) = y(z) - r(z)$ , such that the generalized stability margin  $\epsilon$  is maximized,

$$\epsilon_{\max}^{-1} = \inf_{K(z) \text{ stabilizing}} \|\mathcal{F}_l(P, K)\|_{\infty},$$

$$\mathcal{F}_l(P, K) = \begin{bmatrix} I \\ K(z) \end{bmatrix} (I - G(z)K(z))^{-1} \begin{bmatrix} I & G(z) \end{bmatrix}, \quad (3.47)$$

where the linear fractional transformation  $\mathcal{F}_l(P, K)$  is defined in (3.9). This is a very large,  $150 \times 150$ ,  $\mathcal{H}_\infty$  optimization problem. The first step in its solution is to write down the corresponding generalized plant  $P(z)$  as shown in (3.7),

$$P(z) = \left[ \begin{array}{cc|c} G(z) & 0 & G(z) \\ 0 & 0 & I \\ \hline G(z) & I & G(z) \end{array} \right], \quad (3.48)$$

where  $P(z) \in \mathcal{C}^{3n \times 3n}$  and the partitioning is such that

$$\begin{bmatrix} e_1(z) \\ e_2(z) \\ v(z) \end{bmatrix} = \begin{bmatrix} P_{11}(z) & P_{12}(z) \\ P_{21}(z) & P_{22}(z) \end{bmatrix} \begin{bmatrix} w_1(z) \\ w_2(z) \\ u(z) \end{bmatrix}, \quad (3.49)$$

where the feedback signal  $v(z) = y(z)$ , and the physical interpretation of the signals  $e(z)$  and  $w(z)$  is left as an exercise for the interested reader.

Since the transfer matrix  $G(z)$  is symmetric circulant ( $I$  and  $0$  also satisfy this condition), then  $P(z)$  in (3.48) is composed of symmetric circulant blocks. Then by Theorem 1, the  $\mathcal{H}_\infty$  optimal  $K(z)$  is also symmetric circulant. Then, since the transfer matrix on the right-hand-side of (3.47) is a  $2 \times 2$  block matrix, composed of four spatially-invariant blocks each of dimension  $75 \times 75$ , Theorem 1 may be used to simplify the optimization (3.47) to the solution of a family of 75 independent SISO four-block problems

$$\epsilon_{\max} = \min\{\epsilon(\nu_1), \dots, \epsilon(\nu_{75})\}, \quad (3.50)$$

where each  $\epsilon(\nu_j)$  is computed for a  $2 \times 2$  problem,

$$\begin{aligned} \epsilon(\nu_j)^{-1} &= \inf_{\tilde{k}(\nu_j, z) \text{ stabilizing}} \|\tilde{t}_{ew}(z)\|_\infty, \\ \tilde{t}_{ew}(z) &= \frac{1}{1 - \tilde{g}(\nu_j, z)\tilde{k}(\nu_j, z)} \begin{bmatrix} 1 & \tilde{g}(\nu_j, z) \\ \tilde{k}(\nu_j, z) & \tilde{k}(\nu_j, z)\tilde{g}(\nu_j, z) \end{bmatrix} \end{aligned} \quad (3.51)$$

then the multivariable  $K(z)$  optimal for the performance index (3.47) is constructed using

Theorem 1 and each SISO controller  $\tilde{k}(\nu_j, z)$  which resulted in solution of (3.51),

$$K(z) = F^T \tilde{K}(z) F, \quad \tilde{K}(z) = \text{diag}\{\tilde{k}(\nu_1, z), \dots, \tilde{k}(\nu_{75}, z)\} \quad (3.52)$$

where each of the modal controllers is a rational SISO transfer function with its coefficients parameterized through the spatial frequency variable  $\nu_j$ ,

$$\begin{aligned} \tilde{k}(\nu_j, z) &= \frac{\tilde{c}_0(\nu_j) + \tilde{c}_1(\nu_j)z^{-1} + \dots + \tilde{c}_{m_c}(\nu_j)z^{-m_c}}{1 + \tilde{s}_1(\nu_j)z^{-1} + \tilde{s}_2(\nu_j)z^{-2} + \dots + \tilde{s}_{m_s}(\nu_j)z^{-m_s}} \\ &= \frac{\tilde{c}(\nu_j, z)}{1 + \tilde{s}(\nu_j, z)} \end{aligned} \quad (3.53)$$

where

$$\begin{aligned} \tilde{c}(\nu_j, z) &= \tilde{c}_0(\nu_j) + \dots + \tilde{c}_{m_c}(\nu_j)z^{-m_c} \\ \tilde{s}(\nu_j, z) &= \tilde{s}_1(\nu_j)z^{-1} + \dots + \tilde{s}_{m_s}(\nu_j)z^{-m_s} \end{aligned} \quad (3.54)$$

The inverse Fourier transform in (3.52) is performed such that a multivariable controller of the form (2.13) is obtained.

$$\begin{aligned} C(z) &= F^T \text{diag}\{\tilde{c}(\nu_1, z), \dots, \tilde{c}(\nu_{75}, z)\} F \\ &= F^T \text{diag}\{\tilde{c}_0(\nu_1), \dots, \tilde{c}_0(\nu_{75})\} F + \dots + F^T \text{diag}\{\tilde{c}_{m_c}(\nu_1), \dots, \tilde{c}_{m_c}(\nu_{75})\} F z^{-m_c} \\ &= C_0 + \dots + C_{m_c} z^{-m_c} = \sum_{i=0}^{m_c} C_i \cdot z^{-i} \end{aligned} \quad (3.55)$$

A similar definition applies to  $S(z)$ . Then the multivariable controller may be written as,

$$u(z) = C(z)v(z) + S(z)u(z) \quad (3.56)$$

which is implementable as the real-time feedback control law,

$$\begin{aligned} u(t) &= C_0 v(t) + C_1 v(t-1) + \dots + C_{m_c} v(t-m_c) \\ &\quad - S_1 u(t-1) - \dots - S_{m_s} u(t-m_s) \end{aligned} \quad (3.57)$$

where  $C_i$  for  $i = 0, \dots, m_c$  and  $S_k$  for  $k = 1, \dots, m_s$  are all constant, real, symmetric

circulant matrices.

### 3.7 Graphical Interpretation

In the previous section it was shown that systems composed of symmetric circulant blocks may be decoupled into independent subsystems with the real Fourier matrix  $F$  in (A.4). In Theorems 1 and 2, it was shown that this diagonalization allowed a large scale multivariable design problem to be restated in terms of the design of a family of independent SISO problems, one for each spatial frequency  $\nu_j \in \{\nu_1, \dots, \nu_n\}$ . The goal of this section is to provide a more intuitive description of this class of dynamical systems. In Section 3.3, the modal decomposition of such systems may be interpreted as a description of the system's response to signals characterized by a spatial frequency  $\nu_j$  and a dynamical frequency  $\omega$ . The goal of this section is to change the multivariable interpretation of the spatially distributed system into a more intuitively understandable two-dimensional system in terms spatial and dynamical frequencies  $\nu_j$  and  $\omega$ .

In Appendix A, it is stated that circulant symmetric matrices have a certain relationship with signals which are a harmonic function of the spatial variable. The spatial frequency  $\nu$  of the input signal is preserved under transformation by a symmetric circulant matrix. For comparison, linear time-invariant SISO systems, have a similar relationship with signals which are a harmonic function of time. The dynamical frequency  $\omega$  of such a signal is preserved under transformation with a linear time-invariant (LTI) system. The frequency response of LTI systems is used to simultaneously display 'all' design relevant features. The Bode plot illustrates the magnitude and phase of a system's response as a continuous function of the dynamical frequency  $\omega$ . For example, in a closed-loop feedback system, the control-relevant concepts of disturbance attenuation, setpoint tracking, robust stability margins, and expected input magnitude, all find a natural representation in the frequency domain.

For multivariable systems, the generalization of the frequency response for linear, time-invariant systems is in terms of either the eigenvalue decomposition or the singular value decomposition [16, 56]. The SISO frequency domain specifications are restated for MIMO systems in terms of the eigenvalues and singular values of the closed-loop system.

The eigenvalue decomposition is used to determine the internal stability of the closed-loop system. The singular value decomposition is then used to represent the quality of the designed feedback in terms of performance, robustness etc. Two popular performance norms for MIMO systems,  $\mathcal{H}_2$  and  $\mathcal{H}_\infty$ , may be defined in terms of the closed-loop system singular values (2.23) and (2.28).

A natural question to ask is what (if any) features of traditional frequency domain design techniques generalize to the spatial frequency representation. First, it will be shown that the spatial frequency components of a multivariable system described by symmetric circulant transfer matrices possess all of the design-relevant attributes of both single variable Bode plots *and* multivariable sigma plots. Therefore, the spatial frequency components provide a useful measure of the quality of the performance of the closed-loop and may be used to direct the feedback controller design.

Second, for the design approach, it is important to produce a graphical representation of the spatial frequency decomposition that exposes the relevant properties of the feedback. A two-dimensional generalization of SISO system Bode plots is presented. The  $\omega\nu$ -plot of a symmetric circulant transfer matrix where the gain of the system is plotted as a two-dimensional surface as a function of the dynamical and spatial frequencies,  $\omega$  and  $\nu$ .

### 3.7.1 Singular Values, Eigenvalues, and Spatial Frequencies

In Section 3.3 it was demonstrated that a circulant symmetric transfer matrix  $A(z)$  could be transformed to a diagonal transfer matrix  $\tilde{A}(z)$  by using the real Fourier matrix  $F$ , such that  $FA(z)F^T = \tilde{A}(z) = \text{diag}\{\tilde{a}(\nu_1, z), \dots, \tilde{a}(\nu_n, z)\}$ . The diagonal elements of this transfer matrix is indexed by the spatial frequency  $\nu \in \{\nu_1, \dots, \nu_n\}$ . It may be interpreted as meaning that an input array in the shape of a sine wave of spatial frequency  $\nu_j$  will result in an output profile taking the shape of a sine wave of the same frequency  $\nu_j$ . For example, if the elements  $u_k$  of a vector  $u = [u_1, \dots, u_n]^T$  are given by a harmonic function

of the spatial variable, then the  $n \times n$  symmetric circulant matrix operator,

$$A(z) \begin{bmatrix} u_1 \\ \vdots \\ u_n \end{bmatrix} = \tilde{a}(\nu_j, z) \begin{bmatrix} u_1 \\ \vdots \\ u_n \end{bmatrix}, \quad u_k = \sin[(k-1)\nu_j] \quad (3.58)$$

where  $\tilde{a}(\nu_j, z)$  is a scalar  $1 \times 1$  transfer function. (A similar relationship holds for the cosine functions as shown in (A.5).) The spatial frequency  $\nu_j$  of the input signal is preserved under multiplication by the symmetric circulant matrix  $A(z)$  in (3.58).

From (3.58), it appears that the transfer function  $\tilde{a}(\nu_j, z)$  is an eigenvalue of the symmetric circulant transfer matrix  $A(z)$ . It is true in general that the unitarity of the real Fourier matrix  $F^T = F^{-1}$  results in a restatement of the diagonalization (3.14),

$$FA(z)F^{-1} = \tilde{A}(z) = \text{diag}\{\tilde{a}(\nu_1, z), \dots, \tilde{a}(\nu_n, z)\} \quad (3.59)$$

so that it is evident that the eigenvalues of the circulant symmetric matrix  $A(z)$  are given by  $\tilde{a}(\nu_j, z)$  with corresponding eigenvectors as the rows of the real Fourier matrix  $F$  [13].

The stability of a multivariable linear system is defined in terms of its eigenvalues [56]. However, in feedback control it is well-known that the eigenvalues of a multivariable system are not directly related to the quality of the feedback. Once a system has been determined to be stable, then the performance and the stability robustness are analyzed via the singular values of the system [16].

The singular values of symmetric circulant systems are discussed next. Circulant symmetric systems have an advantage over general multivariable systems in that their singular values are equivalent to the magnitude of the eigenvalues of the system [38].

Define a diagonal decomposition of the transfer matrix  $A(z)$  by

$$A(z) = U(z)\Sigma_A(z)V(z)^H, \quad (3.60)$$

such that the singular values  $\Sigma_A(z) = \text{diag}\{|\tilde{a}(\nu_j, z)|\}$ ,  $V(z) = F^T$ , and  $U(z) = F^T D(z)$ , where  $D(z) = \text{diag}\{d_j(z)\}$ ,  $d_j(z) = \tilde{a}(\nu_j, z)/|\tilde{a}(\nu_j, z)|$ . The singular values will not gen-

erally be in their usual descending order but rather according to their spatial frequency  $\nu_j = 2\pi(j - 1)/n$ .

This equivalence means that through the spatial frequency components of a symmetric circulant system combine the properties of the eigenvalue and singular value decompositions. The spatial frequency decomposition uses the stability of each of the eigenvalues  $\tilde{a}(\nu_j, z)$  to determine the nominal stability of the multivariable system  $A(z)$ . Then the robust stability and the performance of the system are analyzed through the magnitude of the singular values  $|\tilde{a}(\nu_j, z)|$  for  $j \in \{1, \dots, n\}$ .

### 3.7.2 Two Dimensional $\omega\nu$ -Plots

The conceptual benefits of a spatial frequency decomposition are explored next. In this section, it is demonstrated that the sigma plot of singular values for a symmetric circulant multivariable transfer matrix is a generalization of the Bode plots of the magnitude of the dynamical frequency response of SISO systems. The goal of this section is to restate the results of Sections 3.4, 3.5 to provide an intuitive graphical representation that will be useful from the perspective of design. The performance of a feedback system is commonly stated in terms of the  $\mathcal{H}_2$  and  $\mathcal{H}_\infty$  norms defined in (2.23) and (2.28). These may now be interpreted for symmetric circulant transfer matrices in terms of the two dimensional frequency domain decomposition.

As illustrated in Figure 3.3, the squared  $\mathcal{H}_2$ -norm of a *SISO* transfer function may be interpreted as the sum of the squared gain of the system across all dynamical frequencies. The squared  $\mathcal{H}_2$ -norm of a *MIMO* transfer matrix may be interpreted as the sum of the squared gain of the system across all dynamical frequencies and all singular values. The squared  $\mathcal{H}_2$ -norm of a *symmetric circulant* transfer matrix may be interpreted as the sum of the squared gain of the system across all dynamical and spatial frequencies. This corresponds to a sum across the discrete set of spatial frequencies  $\nu \in \{\nu_1, \dots, \nu_n\}$  and an integration over dynamical frequencies  $\omega \in [-\pi, \pi]$ ,

$$\|A(z)\|_2^2 = \frac{1}{2\pi} \int_{-\pi}^{\pi} \sum_{j=1}^n |\tilde{a}(\nu_j, e^{i\omega})|^2 d\omega \quad (3.61)$$

The  $\mathcal{H}_\infty$ -norm has an analogous interpretation. The squared  $\mathcal{H}_\infty$ -norm of a *SISO* transfer function may be interpreted as the supremum of squared gain of the system across all dynamical frequencies, and is illustrated in Figure 3.3. The squared  $\mathcal{H}_\infty$ -norm of a *MIMO* transfer matrix may be interpreted as the supremum squared of the largest singular value of the system taken across all dynamical frequencies. The squared  $\mathcal{H}_\infty$ -norm of a *symmetric circulant* transfer matrix may be interpreted as the supremum of the squared gain of the system across all dynamical and spatial frequencies.

$$\|A(z)\|_\infty^2 = \sup_{\omega \in [-\pi, \pi]} \max_{j \in \{1, \dots, n\}} |\tilde{a}(\nu_j, e^{i\omega})|^2 \quad (3.62)$$

To demonstrate these ideas, an example circulant-symmetric transfer matrix  $G(z)$  in (2.1) taken from a model of an industrial paper making process is considered [60]. Figure 3.4 contains an illustration of the transfer matrix decomposed with the real Fourier matrix  $F$  in (A.4) and plotted as a function of spatial and dynamical frequencies  $\nu$  and  $\omega$ . This plot will be referred to as a ‘surface’ although it is understood that the spatial frequency axis is defined only at discrete, evenly-spaced locations  $\nu \in \{\nu_1, \dots, \nu_n\}$ , and the dynamical frequency axis is defined at all points in the continuum  $\omega \in [-\pi, \pi]$ . The squared  $\mathcal{H}_2$ -norm of the transfer matrix  $G(z)$  is proportional to the volume enclosed by the surface. The squared  $\mathcal{H}_\infty$ -norm is given by the maximal height of the surface.

Another feature worth noting here is that the gain of the transfer matrix  $G(z)$  is very small at spatial frequencies  $\nu > 2.0$ . Since the spatial frequency components of the system may be interpreted as its singular values, then it can be seen from Figure 3.4 that a plant exhibiting high spatial frequency roll-off is in fact ill-conditioned. In other words, the plant gain is strongly dependent on the input direction. For the plant illustrated in Figure 3.4, an input signal with low spatial frequency  $\nu$  is much more easily passed through the system  $G(z)$  than an input signal of high spatial frequency. This is a common feature of physical spatially distributed control systems such as those occurring in paper and plastic sheet production [19, 58, 61]. In fact, it was pointed out by Heath in [34] that, for sheet forming processes, if there exist sufficient actuators to control all controllable variations, then the open-loop transfer matrix  $G(z)$  in (2.1) is likely to be ill-conditioned.

Ill-conditioned plants are traditionally difficult to control and are very sensitive to

modelling errors [55]. Figure 3.4 encourages a somewhat different interpretation of the conditioning of a distributed plant. The symmetry between the dynamical and the spatial frequencies indicates that the gain of the process has a 'roll-off' as a function of both frequencies. In other words, the high frequency components of the process are much harder to control than the low frequency components both dynamically and spatially.

It has long been known that the gain roll-off for high dynamical frequencies of physical plants must be accounted for in any practical feedback design technique [16]. All modern loop shaping based approaches account for this feature when designing feedback controllers that are robust to model uncertainty [56, 66]. In Chapter 4, loop shaping techniques are generalized to spatial and dynamical frequency domain approach which may be used to accommodate the ill-conditioned nature of these plants as roll-off in the spatial frequency domain.

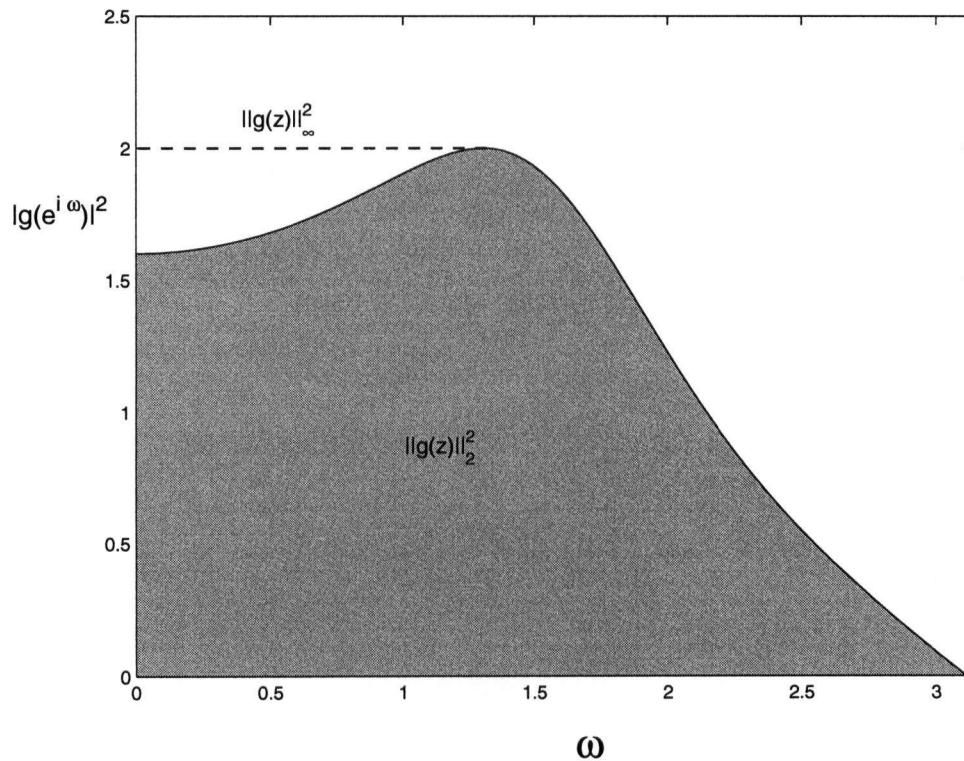


Figure 3.3: Geometric interpretation of the decomposition of a SISO transfer function  $g(z)$  in terms of dynamical frequencies  $g(e^{i\omega})$ . The  $\mathcal{H}_2$  and  $\mathcal{H}_\infty$  norms of the original transfer function  $g(z)$  may be represented in the frequency domain. As indicated, the square of the  $\mathcal{H}_\infty$ -norm,  $\|g(z)\|_\infty^2$ , is given by the maximum height of the curve. The square of the  $\mathcal{H}_2$ -norm,  $\|g(z)\|_2^2$ , is proportional to the area under the curve.

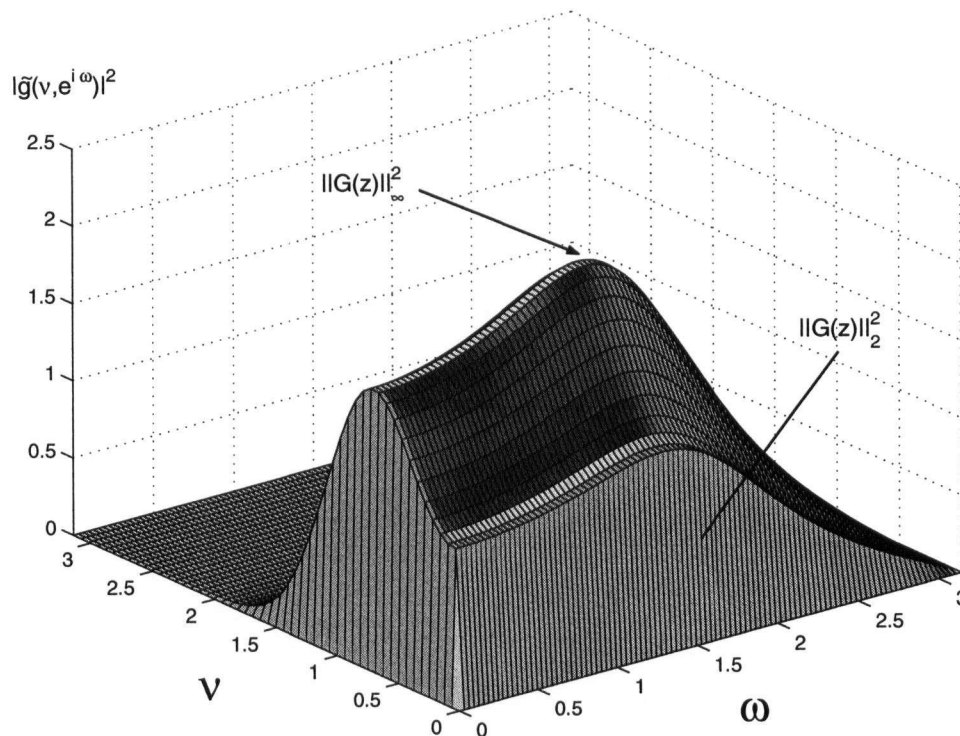


Figure 3.4:  $\omega\nu$ -plot for the symmetric circulant transfer matrix  $G(z)$  in terms of spatial and dynamical frequencies  $FG(e^{i\omega})F^T = \tilde{G}(e^{i\omega}) = \text{diag}\{\tilde{g}(\nu_j, e^{i\omega})\}$ . The  $\mathcal{H}_2$  and  $\mathcal{H}_\infty$  norms of the original transfer matrix  $G(z)$  may be represented in this domain. As indicated, the square of the  $\mathcal{H}_\infty$ -norm,  $\|G(z)\|_\infty^2$ , is given by the maximum height of the surface as indicated at  $(\nu, \omega) \approx (0.7, 1.3)$ . The square of the  $\mathcal{H}_2$ -norm,  $\|G(z)\|_2^2$ , is proportional to the volume bounded by the surface.

## Chapter 4

### Two Dimensional Loop Shaping

In this chapter, a constructive controller design technique is developed which addresses the design specifications of performance, robustness, and controller localization of Chapter 2. The feedback design proceeds in two steps; high-order controller synthesis followed by controller reduction.

First, the  $\omega\nu$ -plots introduced in Chapter 3 for describing the open-loop symmetric circulant transfer matrices are used to display the two dimensional spatial and dynamical frequency domain characteristics of the closed-loop transfer matrices. Traditional dynamical loop shaping techniques are extended to the two dimensional spatial and dynamical frequency domain and a non-localized feedback controller  $K(z)$  is synthesized to satisfy performance and robustness requirements.

Chapter 2 described the practical specification in which the implementation of the feedback is to be localized such that each actuator's input is restricted to depend only upon information from nearby sensors and actuators. Therefore the second design step is to reduce the 'spatial order' of the feedback by approximating the non-localized controller  $K(z)$  with a localized controller  $K_l(z)$ , such that the closed-loop shapes are not significantly degraded.

This chapter is divided into four sections. In Section 4.1 the traditional multivariable loop shaping concepts are reviewed. These specifications are modified, in Section 4.2, in order to better suit the spatially distributed problem. Section 4.3 contains a result that allows the designer to reduce the spatial order of the designed controller without compromising the internal stability of the feedback loop. Finally, in Section 4.4, a constructive design technique is presented in which one may synthesize localized feedback controllers which satisfy performance and robustness specifications.

#### 4.1 Traditional Loop Shaping

This section reviews the basic principles of multivariable frequency domain loop shaping for feedback controller design<sup>1</sup>. The performance and robustness specifications are stated in terms of the singular values of the closed-loop feedback system defined by  $G(z)$  in (2.1) and  $K(z)$  in (2.9).

For example, the following specifications are important when designing a practical feedback controller for disturbance attenuation,

1. Disturbance attenuation requires the norm of the sensitivity function  $\bar{\sigma}([I - GK]^{-1})$  to be small.
2. Limited control action requires  $\bar{\sigma}(K[I - GK]^{-1})$  to be small.
3. Robust stability for additive plant uncertainty  $G_p = G + \delta G_A$  requires  $\bar{\sigma}(K[I - GK]^{-1})$  to be small.
4. Robust stability for multiplicative plant uncertainty  $G_p = (I + \delta G_M)G$  requires  $\bar{\sigma}(GK[I - GK]^{-1})$  to be small.

It is well-known that these specifications are in conflict [16, 44, 56, 66]. One cannot simultaneously satisfy all performance and robustness requirements. For example, it can be shown that disturbance attenuation requires  $\underline{\sigma}(K(e^{i\omega}))$  to be large, while closed-loop robustness to additive model uncertainty requires  $\bar{\sigma}(K(e^{i\omega}))$  to be small.

The conflict is resolved by relaxing each of these specifications such that they apply only at the appropriate dynamical bandwidths. In the design of feedback controllers for physical systems it is common to find that the robustness requirements are important only at the high dynamical frequencies  $\omega$  where the small model gain and large model uncertainty combine such that the relative uncertainty is greater than 100%. One then proceeds by designing  $K(z)$  conservatively at high dynamical frequencies  $\omega$  with  $\bar{\sigma}(K(e^{i\omega}))$  small. Disturbance attenuation is then achieved by designing  $K(z)$  aggressively at low frequencies  $\omega$  with  $\underline{\sigma}(K(e^{i\omega}))$  large.

---

<sup>1</sup>These concepts may be found in a variety of sources and the interested reader is referred to [16, 44, 56, 66] and references therein.

For the relevant bandwidths, one can obtain open-loop approximations for the closed-loop specifications listed above,

1. Disturbance attenuation requires  $\underline{\sigma}(GK(e^{i\omega}))$  to be large where  $\underline{\sigma}(G(e^{i\omega}))$  is large, typically at low frequencies  $\omega$ .
2. Limited control action requires  $\bar{\sigma}(K(e^{i\omega}))$  to be small where  $\bar{\sigma}(G(e^{i\omega}))$  is small, typically at high frequencies  $\omega$ .
3. Robust stability for additive plant uncertainty  $G_p = G + \delta G_A$  requires  $\bar{\sigma}(K(e^{i\omega}))$  to be small where  $\underline{\sigma}(G(e^{i\omega})) \approx \bar{\sigma}(\delta G_A(e^{i\omega}))$  and/or  $\underline{\sigma}(G(e^{i\omega})) \leq \bar{\sigma}(\delta G_A(e^{i\omega}))$ , typically at high frequencies  $\omega$ .
4. Robust stability for multiplicative plant uncertainty  $G_p = (I + \delta G_M)G$  requires  $\bar{\sigma}(GK(e^{i\omega}))$  to be small where  $\bar{\sigma}(\delta G_M(e^{i\omega})) \approx 1$  and/or  $\bar{\sigma}(\delta G_M(e^{i\omega})) \geq 1$ , typically at high frequencies  $\omega$ .

The open-loop specifications 1–4 may be summarized as the requirement that the loop gain  $\underline{\sigma}(GK)$  be large at low frequencies and that  $\bar{\sigma}(GK)$  be small at high frequencies. These requirements are illustrated graphically in Figure 4.1, where the feedback  $K(z)$  must be designed such that the singular values  $\underline{\sigma}(GK)$  and  $\bar{\sigma}(GK)$  avoid the regions indicated.

The design procedure is complicated by the fact that the singular value loop shaping must be performed with an internally stabilizing  $K(z)$ . The requirement of closed-loop internal stability requires consideration of the phase of the system via the *eigenvalues* of  $GK$  and places limits on the achievable loop shape [16]. For example, time delay does not affect the singular value spectrum of a plant, since  $\sigma_j(z^{-2d}G) = \sigma_j(z^{-d}G)$  for all singular values  $j$ . However it is well-known that the achievable performance bandwidth of a closed-loop system with the plant  $G_2(z) = z^{-2d}G$  is roughly half of the bandwidth that can be achieved for a closed-loop system with the plant  $G_1(z) = z^{-d}G$ . The specifications on the loop shape must consider the properties of the plant  $G(z)$  and the capabilities of the controller  $K(z)$ .

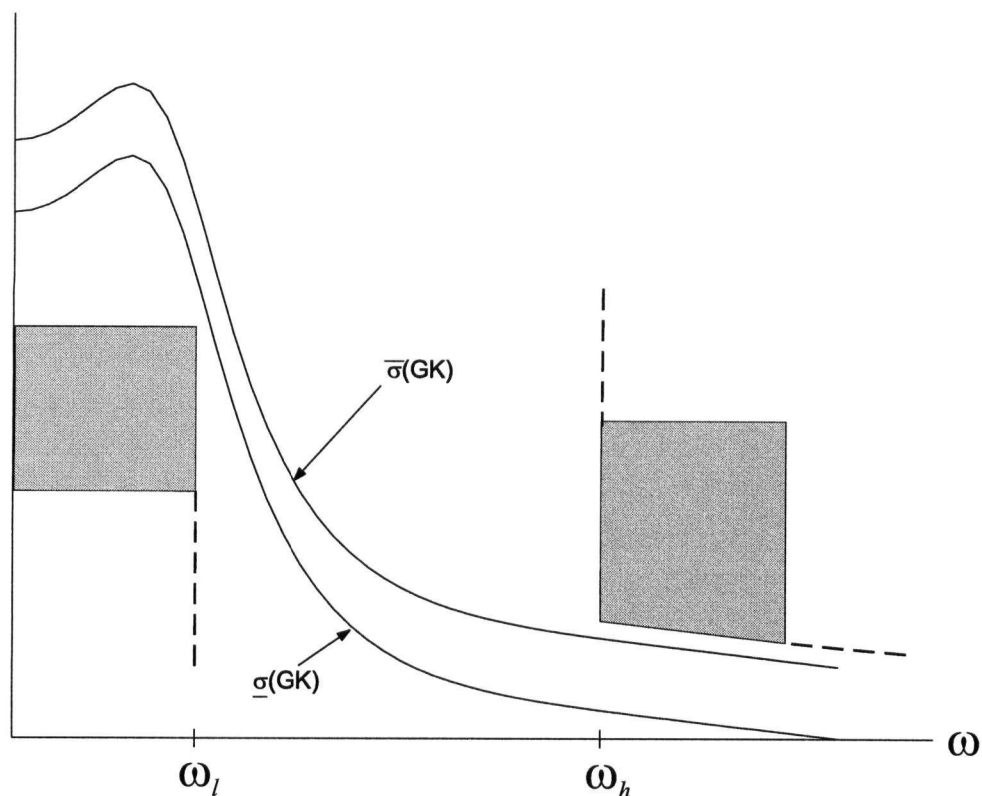


Figure 4.1: Traditional multivariable open-loop singular value shaping. The performance requirement places a lower bound on  $\underline{\sigma}(GK)$  for low frequencies  $\omega < \omega_l$ . The safety requirements (robust stability, limited control action, etc.) place an upper bound on  $\bar{\sigma}(GK)$  for high frequencies  $\omega > \omega_h$ .

As the requirement of internal stability is difficult to handle when shaping the open-loop singular values  $\bar{\sigma}(GK)$ ,  $\underline{\sigma}(GK)$ ,  $\bar{\sigma}(K)$ ,  $\underline{\sigma}(K)$  of the system, several loop shaping methodologies have emerged to handle this problem. These include the LQG/LTR techniques in which either  $(I - GK)^{-1}$ ,  $GK(I - GK)^{-1}$ , or  $(I - KG)^{-1}$ ,  $KG(I - KG)^{-1}$ , are shaped through the design of performance weights in an LQG optimization problem in which nominal stability is guaranteed [16].

The more sophisticated  $\mathcal{H}_2$  and  $\mathcal{H}_\infty$  mixed sensitivity techniques allow all relevant closed-loop transfer functions to be included directly in an optimization problem. As with the LTR methods, the loop shape is modified through the use of weighting functions in the optimization. With the added flexibility of these methods comes the risk of over-specification. One must still respect the trade off (Figure 4.1) required when designing

the optimization weights [8, 56, 66].

Finally the  $\mathcal{H}_\infty$  loop shaping [44, 66] technique performs controller design in two steps. The first step is to shape the open-loop singular values according to rules such as outlined above and in Figure 4.1. The second step uses  $\mathcal{H}_\infty$  synthesis to robustly stabilize the closed-loop.

## 4.2 Two Dimensional Frequency Domain Specifications

The rules described above for the shaping of MIMO loops are quite practical and apply to a wide variety of control design problems. However the general multivariable design problem as described above is not achievable for many spatially distributed problems. It can be seen from Figure 4.1 that the control loop's performance specifications must be satisfied for all singular values  $\sigma_j(GK)$  for  $j \in \{1, \dots, n\}$ . However, there exist many industrial examples of spatially-distributed control systems in which the process model  $G(z)$  is very ill-conditioned. The majority of cross-directional paper machine control systems have  $\sigma_j(G(e^{i\omega})) \approx 0$  for several singular values, even at the steady-state with  $\omega = 0$ . See Figure 2.4 for such an example. The model uncertainty compounds this problem and it is not uncommon to find industrial applications in which the relative uncertainty is larger than 100%, with the additive uncertainty  $\sigma_j(G(e^{i\omega})) < \bar{\sigma}(\delta G_A(e^{i\omega}))$  at  $\omega = 0$ , for over half of the  $n$  singular values.

In some multivariable control applications, the ill-conditioning of a plant transfer matrix  $G(z)$  is an indication that the process has been poorly designed, and that efforts may be better spent on process redesign rather than feedback compensation [55, 56]. However, for cross-directional control applications, it has been shown that if a process is well-designed in the sense that there are enough actuators to control the low spatial frequency components of the error, then it is likely the process model  $G(z)$  is ill-conditioned with vanishingly small gain for input directions corresponding to high spatial frequencies [19, 34].

The modification of the traditional MIMO loop shaping requirements of the previous section for ill-conditioned spatially-distributed processes may be interpreted as the relax-

ation of the performance requirement for some of the singular values (corresponding to high spatial frequency modes  $\nu_j$ ) at low dynamical frequency  $\omega$  [62].

It was shown in Chapter 3, that a symmetric circulant structure for feedback controllers  $K(z)$  in (2.9) is sufficient for a wide variety of control applications for spatially-distributed systems modelled by symmetric circulant transfer matrices  $G(z)$  in (2.1). Restricting the feedback controller  $K(z)$  in (2.9) to be symmetric circulant was shown in Chapter 3 to reduce the large design problem to that of designing a family of  $n$  SISO controllers one for each spatial frequency  $\nu_j \in \{\nu_1, \dots, \nu_n\}$ .

In addition to the design, the analysis of the closed-loop system is also simplified to consideration of the family of SISO problems. Repeated here are the expressions for the open-loop plant (analogous to (2.1))

$$\tilde{y}(\nu_j, z) = \tilde{g}(\nu_j, z)\tilde{u}(\nu_j, z) \quad (4.1)$$

and the feedback controller (analogous to (2.9))

$$\tilde{u}(\nu_j, z) = \tilde{k}(\nu_j, z)\tilde{v}(\nu_j, z), \quad (4.2)$$

where the feedback signal is the deviation from the reference signal  $\tilde{v}(\nu_j, z) = \tilde{y}(\nu_j, z) - \tilde{r}(\nu_j, z)$ . The notation of Chapter 3 has been used and the circulant symmetric transfer matrix  $G(z)$  in (2.1) is decoupled by the real Fourier matrix  $F$ , such that  $FG(z)F^T = \text{diag}\{\tilde{g}(\nu_1, z), \dots, \tilde{g}(\nu_n, z)\}$ . The corresponding definition is used for  $\tilde{k}(\nu_j, z)$  in (4.2).

Since, as discussed in Section 3.7, the singular values of a circulant symmetric transfer matrix are given by magnitude of SISO transfer functions such as (4.1), (4.2), then the multivariable loop shaping design specifications listed in Section 4.1 can be restated in terms of the individual feedback loops. The design specifications for these systems are then rewritten in terms of their spatial and dynamical frequencies,

1. Disturbance attenuation requires  $\left|1/[1 - \tilde{g}\tilde{k}(\nu_j, e^{i\omega})]\right|$  to be small.
2. Limited control action requires  $\left|\tilde{k}(\nu_j, e^{i\omega})/[1 - \tilde{g}\tilde{k}(\nu_j, e^{i\omega})]\right|$  to be small.

3. Robust stability for additive plant uncertainty  $G_p = G + \delta G_A$  requires

$$|\tilde{k}(\nu_j, e^{i\omega})/[1 - \tilde{g}\tilde{k}(\nu_j, e^{i\omega})]| \text{ to be small.}$$

4. Robust stability for multiplicative plant uncertainty  $G_p = (I + \delta G_M)G$  requires

$$|\tilde{g}\tilde{k}(\nu_j, e^{i\omega})/[1 - \tilde{g}\tilde{k}(\nu_j, e^{i\omega})]| \text{ to be small.}$$

As with the MIMO case in section 4.1, the closed-loop specifications for the decoupled system are in conflict and a trade off is required between performance and robustness. The design problem is to maintain the best performance possible without compromising the robustness margins of the closed-loop.

Qualitatively speaking, the performance specification may be satisfied, for a closed-loop stable system, by designing  $|\tilde{k}(\nu_j, e^{i\omega})|$  to be large at those frequencies  $\{\nu_j, \omega\}$  where  $|\tilde{g}(\nu_j, e^{i\omega})|$  is large and the relative uncertainty is small. The robustness of the closed-loop is a matter of designing  $|\tilde{k}(\nu_j, e^{i\omega})|$  to be small at those spatial and dynamical frequencies  $\{\nu_j, \omega\}$  where  $|\tilde{g}(\nu_j, e^{i\omega})|$  is small and/or the relative uncertainty is large. In this way, it will be shown that one can accommodate the large number of ill-conditioned spatially distributed applications exhibiting gain roll-off for high spatial frequencies  $\nu_j$  as well as high dynamical frequencies  $\omega$ .

With these trade-offs in mind, the closed-loop performance specifications above may be approximated (as with the MIMO case) in terms of open-loop design objectives.

1. Disturbance attenuation requires  $|\tilde{g}\tilde{k}(\nu_j, e^{i\omega})|$  to be large where  $|\tilde{g}(\nu_j, e^{i\omega})|$  is large, typically at low frequencies  $\nu$  and  $\omega$ .
2. Limited control action requires  $|\tilde{k}(\nu_j, e^{i\omega})|$  to be small where  $|\tilde{g}(\nu_j, e^{i\omega})|$  is small, typically at high frequencies  $\nu$  and  $\omega$ .
3. Robust stability for additive plant uncertainty  $G_p = G + \delta G_A$  requires  $|\tilde{k}(\nu_j, e^{i\omega})|$  to be small where  $|\tilde{g}(\nu_j, e^{i\omega})| \approx \bar{\sigma}(\delta G_A)$  and/or  $|\tilde{g}(\nu_j, e^{i\omega})| \leq \bar{\sigma}(\delta G_A)$ , typically at high frequencies  $\nu$  and  $\omega$ .
4. Robust stability for multiplicative plant uncertainty  $G_p = (I + \delta G_M)G$  requires  $|\tilde{g}\tilde{k}(\nu_j, e^{i\omega})|$  to be small where  $\bar{\sigma}(\delta G_M) \approx 1$  and/or  $\bar{\sigma}(\delta G_M) \geq 1$ , typically at high frequencies  $\omega$ .

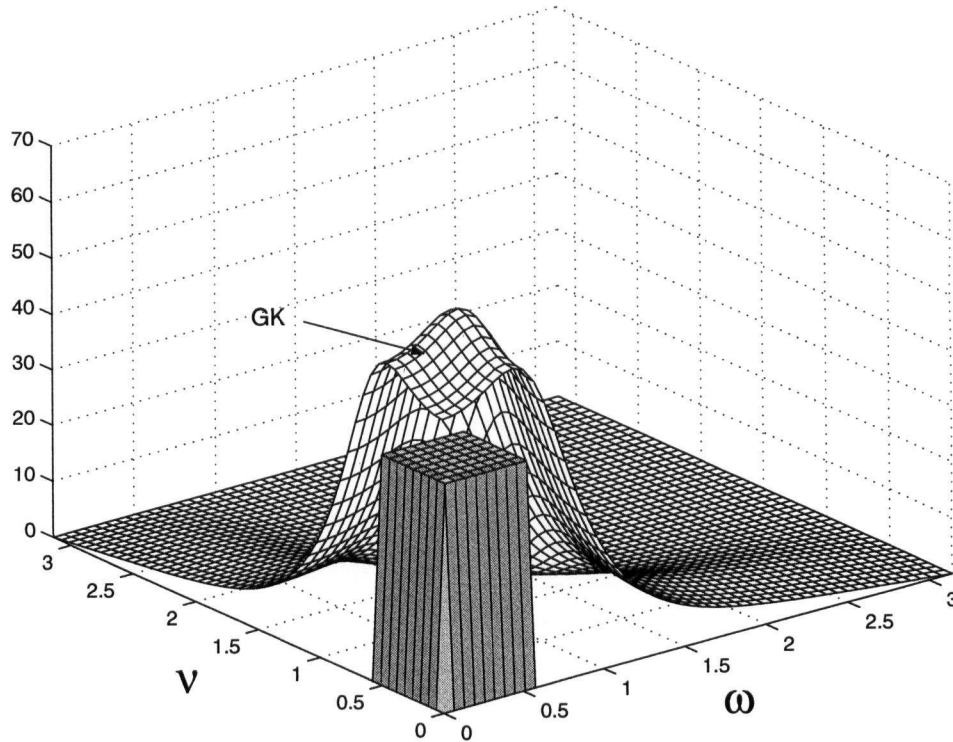


Figure 4.2: The analogous open-loop  $\omega\nu$ -surface shaping. Note that contrary to traditional loop shaping, the performance constraint is not selected to cover all singular values  $j \in \{1, \dots, n\}$ . The roll-off of the gain of the plant  $\tilde{g}(\nu_j, z)$  for high spatial frequencies  $\nu_j$  places a limit on the spatial bandwidth of a closed-loop system.

The open-loop specifications 1–4 above are analogous to the multivariable design requirements discussed in Section 4.1. The two dimensional design specifications are illustrated in Figure 4.2. The lower bound on the loop gain for performance at low frequencies is illustrated as applying to spatial frequencies  $\nu < 0.6$  and dynamical frequencies  $\omega < 0.6$ . The upper bound on the loop gain that applies at high spatial and dynamical frequencies  $\{\nu_j, \omega\}$  (analogous to Figure 4.1) is omitted for legibility.

In order to better illustrate the two dimensional frequency domain, contour plots in  $\{\nu_j, \omega\}$  are introduced. In an analogy to Figure 4.1, the relevant contours of the two dimensional loop gain is to be plotted on the same diagram as the design constraints indicated in requirements 1–4 above.

The two dimensional performance specification requires that the loop gain lie above a

performance boundary

$$|\tilde{g}(\nu_j, e^{i\omega})\tilde{k}(\nu_j, e^{i\omega})| > w_l \quad (4.3)$$

for low spatial and dynamical frequencies  $\{\nu_j, \omega\} \in \Omega_l$ .

In order to satisfy the requirement of robust stability, the loop gain is designed to lie below a robustness bound,

$$|\tilde{g}(\nu_j, e^{i\omega})\tilde{k}(\nu_j, e^{i\omega})| < w_h \quad (4.4)$$

for high spatial and dynamical frequencies  $\{\nu_j, \omega\} \in \Omega_h$ .

From the contour plots in Figures 4.3–4.5 it follows that the two dimensional loop shaping requires to design  $\tilde{k}(\nu_j, z)$  such that the contours  $|\tilde{g}(\nu_j, e^{i\omega})\tilde{k}(\nu_j, e^{i\omega})| = w_l$  and  $|\tilde{g}(\nu_j, e^{i\omega})\tilde{k}(\nu_j, e^{i\omega})| = w_h$  avoid the shaded areas  $\Omega_l$  and  $\Omega_h$ . The performance condition (4.3) is satisfied if the  $w_l$  contour does not intersect the set  $\Omega_l$ . The robustness condition (4.4) is satisfied if the  $w_h$  contour does not intersect the set  $\Omega_h$ .

Figure 4.3 illustrates an aggressive design satisfying the performance condition (4.3) but not the robustness condition (4.4). Figure 4.4 illustrates a conservative design satisfying the robustness condition (4.4) but not the performance condition (4.3). Figure 4.5 illustrates a design which has successfully traded off the conflicting requirements.

As with traditional loop shaping, these design specifications apply only to closed-loop systems that are nominally stable - a property only accessible through the eigenvalues of the system. The two dimensional loop shaping approach for these symmetric circulant systems has the advantage that the eigenvalues are very closely related to the singular values of the closed-loop. Section 3.7 showed that the eigenvalues of  $GK(e^{i\omega})$  are  $\tilde{g}(\nu_j, e^{i\omega})\tilde{k}(\nu_j, e^{i\omega})$  for  $\nu_j \in \{\nu_1, \dots, \nu_n\}$ , while the singular values of  $GK(e^{i\omega})$  are given by  $|\tilde{g}(\nu_j, e^{i\omega})\tilde{k}(\nu_j, e^{i\omega})|$ . This feature allows one to consider the loop shaping design of the large multivariable system in terms of the SISO problems defined by  $\tilde{g}(\nu_j, z)$  and  $\tilde{k}(\nu_j, z)$  for  $\nu_j \in \{\nu_1, \dots, \nu_n\}$ . The multivariable closed-loop internal stability of  $G(z)$  and  $K(z)$  is ensured by the internal stability of all  $n$  pairs of transfer functions  $\tilde{g}(\nu_j, z)$  and  $\tilde{k}(\nu_j, z)$ , while the closed-loop performance and robustness are analyzed by applying the above

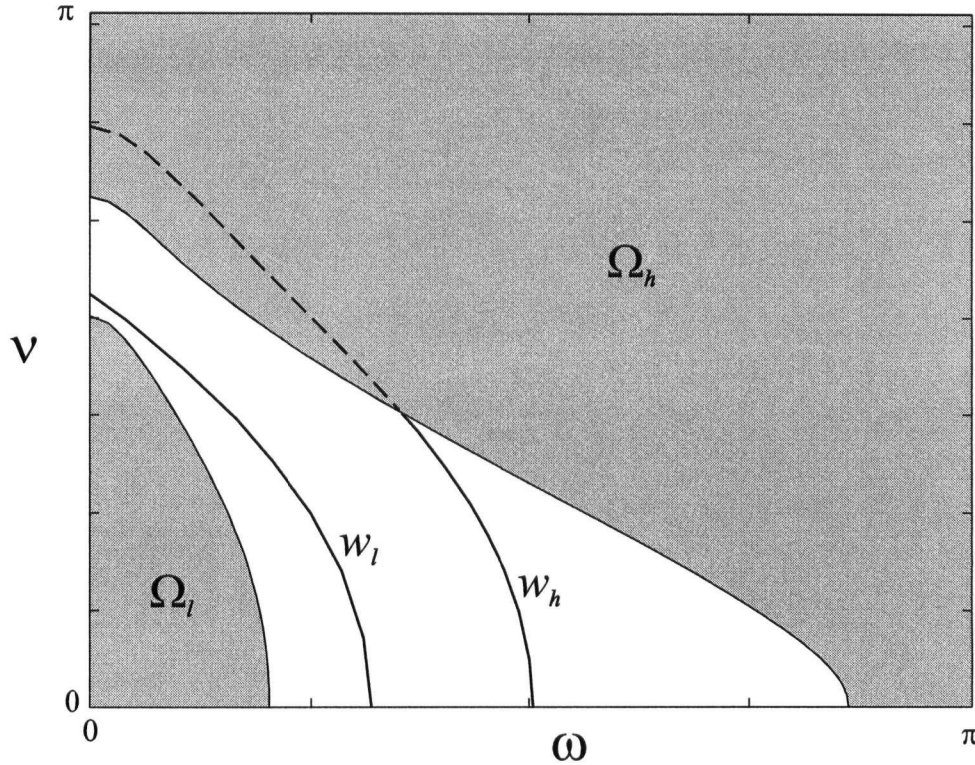


Figure 4.3: The  $\omega\nu$  contour plot shows that this design was too aggressive. The robustness condition (4.4) is not satisfied for all  $\{\nu_j, \omega\} \in \Omega_h$ , as the  $|\tilde{g}(\nu_j, e^{i\omega})\tilde{k}(\nu_j, e^{i\omega})| = w_h$  contour intersects  $\Omega_h$ .

specifications to the open-loop singular values  $|\tilde{g}(\nu_j, e^{i\omega})\tilde{k}(\nu_j, e^{i\omega})|$  and  $|\tilde{k}(\nu_j, e^{i\omega})|$ .

Chapter 5 contains a design example which relies on this close relationship between closed-loop eigenvalues and singular values to ensure stability while shaping the closed-loop transfer matrices in spatial and dynamical frequencies  $\nu_j$  and  $\omega$ .

### 4.3 Controller Spatial Order Reduction with Stability Requirement

In Chapter 3 it was shown that the two-dimensional frequency domain is an appropriate domain for the analysis and design of symmetric circulant feedback controllers for symmetric circulant processes. A wide range of practical design specifications in terms of performance and robustness may be specified in the  $\omega\nu$  domain.

In Chapter 2 it was stated that the goal was to design localized feedback controllers

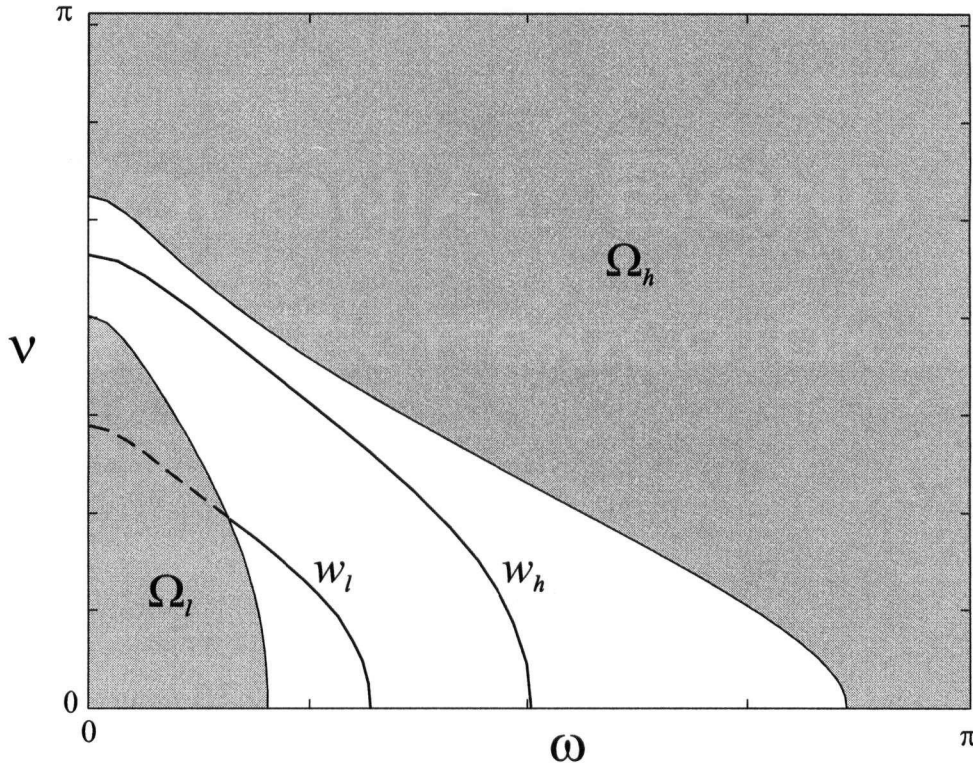


Figure 4.4: The  $\omega\nu$  contour plot shows that this design was too conservative. The performance condition (4.3) is not satisfied for all  $\{\nu_j, \omega\} \in \Omega_l$ , as the  $|\tilde{g}(\nu_j, e^{i\omega})\tilde{k}(\nu_j, e^{i\omega})| = w_l$  contour intersects  $\Omega_l$ .

$K(z) = [I + S(z)]^{-1}C(z)$  in which the factors  $C(z)$  and  $S(z)$  are band-diagonal Toeplitz symmetric transfer matrices. As discussed in Section 3.1, the first step in the design of the band-diagonal Toeplitz system is the design of banded symmetric circulant matrices  $C(z)$  and  $S(z)$ .

As shown in Chapter 3, the goal of the spatial frequency domain design techniques is the synthesis of a family of  $n$  single variable controllers  $\tilde{k}(\nu_j, z) = \tilde{c}(\nu_j, z)/[1 + \tilde{s}(\nu_j, z)]$  are designed, one for each  $\nu_j \in \{\nu_1, \dots, \nu_n\}$ . However, this frequency-by-frequency design generally results in a multivariable feedback controller  $K(z)$  defined by full (i.e. not banded) transfer matrix factors  $C(z) = F^T \text{diag}\{\tilde{c}(\nu_1, z), \dots, \tilde{c}(\nu_n, z)\}F$  and  $S(z) = F^T \text{diag}\{\tilde{s}(\nu_1, z), \dots, \tilde{s}(\nu_n, z)\}F$ , in spite of the localization of the process [4]. The development of optimization-based problem statements which *directly* synthesize an implementable feedback controller of low spatial order is currently the subject of much active

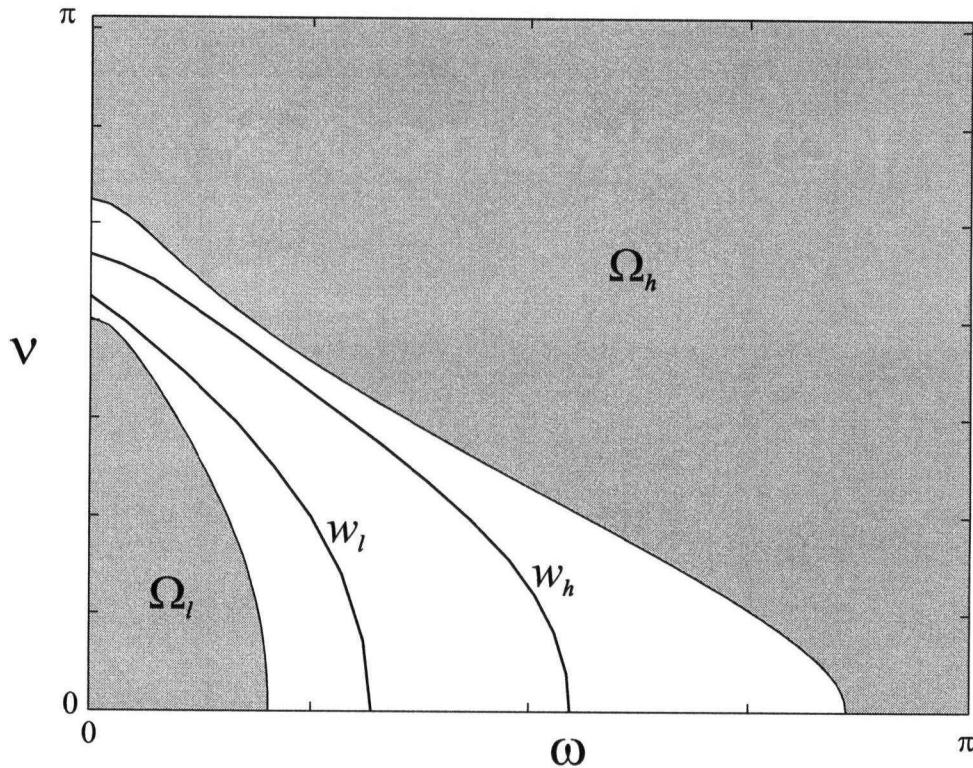


Figure 4.5: The  $\omega\nu$  contour plot illustrates a design which has successfully traded off the conflicting requirements.

research, but is still essentially an open problem [4, 11, 46].

In this work, a practical approach to low spatial order controller design is followed and is analogous to that used in the design of low dynamical order controllers [66]. One first synthesizes a high-order feedback controller to satisfy performance and robustness requirements and then approximates it with a lower order feedback controller.

In this section, it is assumed that we are given an internally stabilizing symmetric circulant feedback controller  $K(z)$  which satisfies all design requirements (possibly resulting from a two-dimensional loop shaping design), but whose factors  $C(z)$  and  $S(z)$  are full symmetric circulant matrices. A spatial order reduction is then achieved by approximating the factors  $C(z)$  and  $S(z)$  with banded symmetric circulant matrices  $C_l(z)$  and  $S_l(z)$ . A simple approximation technique is proposed, and a condition is derived for which closed-loop stability of the system with  $K_l(z) = [I + S_l(z)]^{-1}C_l(z)$  is guaranteed.

First, write the factors of the high-order, high-performance controller  $K(z) = [I +$

$S(z)]^{-1}C(z)$  as,

$$C(z) = \begin{cases} \text{toeplitz}\{c_1, c_2, \dots, c_{n/2}, c_{(n+2)/2}, c_{n/2}, \dots, c_2\} & n \text{ even} \\ \text{toeplitz}\{c_1, c_2, \dots, c_{(n+1)/2}, c_{(n+1)/2}, \dots, c_2\} & n \text{ odd} \end{cases} \quad (4.5)$$

where each element  $c_i(z)$  is generally non-zero (the argument  $z$  has been suppressed in (4.5) for legibility considerations). A similar definition holds for the denominator transfer matrix  $S(z)$ .

Next, if the full-matrix  $C(z)$  and  $S(z)$  in (4.5) are approximated with banded symmetric circulant transfer matrices by simply truncating the elements,

$$\begin{aligned} C_l(z) &= \text{toeplitz}\{c_1, c_2, \dots, c_{n_c}, 0, \dots, 0, c_{n_c}, \dots, c_2\} \\ S_l(z) &= \text{toeplitz}\{s_1, s_2, \dots, s_{n_s}, 0, \dots, 0, s_{n_s}, \dots, s_2\} \end{aligned} \quad (4.6)$$

where again the argument  $z$  has been suppressed in the elements in (4.6) to preserve legibility.

The controller perturbation introduced by the spatial order reduction is then given by,

$$\begin{aligned} \delta C_l(z) &= C(z) - C_l(z) \\ &= \begin{cases} \text{toeplitz}\{0, \dots, 0, c_{n_c+1}, \dots, c_{n/2}, c_{(n+2)/2}, c_{n/2}, \dots, c_{n_c+1}, 0, \dots, 0\} & n \text{ even} \\ \text{toeplitz}\{0, \dots, 0, c_{n_c+1}, \dots, c_{(n+1)/2}, c_{(n+1)/2}, \dots, c_{n_c+1}, 0, \dots, 0\} & n \text{ odd} \end{cases} \end{aligned} \quad (4.7)$$

a similar definition is used for  $\delta S_l(z) = S(z) - S_l(z)$ .

The following theorem presents a sufficient condition to be satisfied by the eliminated elements  $c_k(z)$  for  $k \geq n_c + 1$  and  $s_i(z)$  for  $n_s + 1$  in order to guarantee the preservation of closed-loop stability for the localized controller  $K_l(z) = [I + S_l(z)]^{-1}C_l(z)$ .

**Theorem 3 (Stability-Preserving Controller Localization)** *If the symmetric circulant controller  $K(z) = [I + S(z)]^{-1}C(z)$  in (4.5) is an internally stabilizing controller for a symmetric circulant plant  $G(z)$ , normalized such that  $\|G(z)\|_\infty = 1$ , then the closed-loop system with the symmetric circulant localized controller  $K_l(z) = [I + S_l(z)]^{-1}C_l(z)$  in (4.6) is stable if the truncated elements in (4.7) are small enough such that*

$$\sum_{k=n_c+1}^p |c_k(z)| + \sum_{i=n_s+1}^p |s_i(z)| < \frac{1}{2} |1 + \bar{s}(\nu_j, z) - \bar{g}(\nu_j, z)\bar{c}(\nu_j, z)| \quad (4.8)$$

for  $z = e^{i\omega}$  and all  $\omega \in [-\pi, \pi]$  and  $\nu_j \in \{\nu_1, \dots, \nu_n\}$ . The term  $p = (n+1)/2$  if  $n$  is odd, and  $p = (n+2)/2$  if  $n$  is even.

*Proof.* The small gain theorem is used to determine a sufficient condition for closed-loop stability in terms of the controller perturbations  $\delta C_l(z)$  and  $\delta S_l(z)$  defined by (4.7) [66],

$$\left\| \begin{bmatrix} \delta C_l & \delta S_l \end{bmatrix} \cdot \begin{bmatrix} -G \\ I \end{bmatrix} (I - KG)^{-1} (I + S)^{-1} \right\|_\infty < 1 \quad (4.9)$$

Since each of these transfer matrices in (4.9) is symmetric circulant, then the real unitary Fourier matrix  $F$  in (A.4), allows the condition (4.9) to be written in terms of the diagonal system by pre- and post-multiplication (i.e.  $\|(\cdot)\|_\infty = \|F(\cdot)F^T\|_\infty$ ). Then,

$$| -\delta\bar{c}_l(\nu_j, e^{i\omega}) \cdot \bar{g}(\nu_j, e^{i\omega}) + \delta\bar{s}_l(\nu_j, e^{i\omega}) | < | 1 + \bar{s}(\nu_j, e^{i\omega}) - \bar{c}(\nu_j, e^{i\omega})\bar{g}(\nu_j, e^{i\omega}) | \quad (4.10)$$

for all  $\nu_j \in \{\nu_1, \dots, \nu_n\}$  and  $\omega \in [-\pi, \pi]$ . Then using the fact that  $|\bar{g}(\nu_j, e^{i\omega})| \leq 1$ , we can write the left-hand-side of (4.10) as

$$| -\delta\bar{c}_l(\nu_j, e^{i\omega}) \cdot \bar{g}(\nu_j, e^{i\omega}) + \delta\bar{s}_l(\nu_j, e^{i\omega}) | \leq |\delta\bar{c}_l(\nu_j, e^{i\omega})| + |\delta\bar{s}_l(\nu_j, e^{i\omega})| \quad (4.11)$$

Then using the result in [13], the singular values of a symmetric circulant matrix  $\delta C_l(z) =$

$C(z) - C_l(z)$  defined by (4.7), are bounded by

$$\max_j |\delta \bar{c}_l(\nu_j, z)| = \bar{\sigma}(\delta C_l(z)) = \bar{\sigma}(C(z) - C_l(z)) \leq 2 \sum_{k=n_c+1}^p |c_k(z)| \quad (4.12)$$

where  $p = (n+1)/2$  if  $n$  is odd, and  $p = (n+2)/2$  if  $n$  is even. Writing a similar expression for  $\delta S_l(z)$  allows to write,

$$|\delta \bar{c}_l(\nu_j, e^{i\omega})| + |\delta \bar{s}_l(\nu_j, e^{i\omega})| \leq 2 \sum_{k=n_c+1}^p |c_k(z)| + 2 \sum_{i=n_s+1}^p |s_i(z)| \quad (4.13)$$

Combining results (4.10), (4.11), and (4.13) completes the proof.  $\square$

### Remarks:

1. The RHS of condition (4.8) is defined in the  $\omega\nu$  domain and is calculated using the properties of the plant and the full matrix non-localized controller  $\bar{k}(\nu_j, z)$ . The LHS is given directly in terms of the truncated matrix elements in the spatial domain.
2. Since the spatial order reduction only guarantees nominal stability of the closed-loop (4.8), the designer is still obliged to re-calculate the  $\omega\nu$  components of the system with the localized control  $K_l(z)$ , and verify that the low-order controller satisfies the design requirements.
3. The industrial rule of thumb is that the elements of the controller factors  $c_i(z)$  and  $s_i(z)$  in (4.5) are less important for larger  $i$ . This has recently been justified theoretically in [4] in which it is shown that a quadratic optimal problem statement for a spatially localized process will synthesize a feedback controller  $K(z)$  for which the gain of its elements decreased exponentially as a function of distance from the main diagonal.
4. Theorem 3 is a special case of the more general problem of analyzing controller perturbations which may be due to uncertainty in its implementation or due to deliberate reduction by the designer. This result can easily be expanded to include *dynamical* order reduction of  $C(z)$  and  $S(z)$  and techniques for stable order reduction may be found in [27, 66].

#### 4.4 Two Dimensional Loop Shaping Design Procedure

In this section, a procedure is presented for the design of a feedback controller  $K(z)$  in (2.9) to satisfy performance and robustness requirements, in which the feedback is localized such that each actuator's input is restricted to depend only upon information from nearby sensors and actuators.

However, it is not straightforward to *directly* design a localized controller  $K(z)$ , although currently there is much interest in the topic [4, 10, 46]. The proposed design procedure is more closely related to the traditional loop shaping procedure. The controllers produced by traditional loop shaping techniques (especially through  $\mathcal{H}_2$  and  $\mathcal{H}_\infty$  synthesis) result in controllers that have orders comparable to the generalized plant. But for practical reasons, a lower order is favored over a high order. The design often proceeds in two steps. First one synthesizes a high-performance, high order controller through a loop shaping procedure, and subsequently reduce the design to obtain a low order controller [56, 66].

The two dimensional loop shaping design proceeds in an analogous fashion. First, a high-performance controller is designed to satisfy the performance and robustness specifications described in Section 4.2 above. This controller will generally not be localized and the second step of the design is to reduce the spatial distribution of the feedback controller by approximating it with a localized controller that maintains closed-loop stability (Section 4.3). The localized controller is required to not significantly degrade the performance of the high-order controller obtained from the loop shaping.

Theorems 1 and 2 show that in terms of performance and robustness it is sufficient to consider symmetric circulant feedback controllers  $K(z)$  for many practical problem statements concerning symmetric circulant plants  $G(z)$ . Two dimensional loop shaping is used to trade off the performance and robustness specifications as described in section 4.2 and results in a family of feedback controllers  $\tilde{k}(\nu_j, z)$  one for each  $\nu_j \in \{\nu_1, \dots, \nu_n\}$ .

Each member of the family of controllers is factored as  $\tilde{k}(\nu_j, z) = \tilde{c}(\nu_j, z)/[1 + \tilde{s}(\nu_j, z)]$  for each  $\nu_j \in \{\nu_1, \dots, \nu_n\}$ . The multivariable feedback controller  $K(z) = [I + S(z)]^{-1}C(z)$  is obtained by computing the factors  $C(z) = F^T \text{diag}\{\tilde{c}(\nu_1, z), \dots, \tilde{c}(\nu_n, z)\}F$  and  $S(z) =$

$$F^T \text{diag}\{\tilde{s}(\nu_1, z), \dots, \tilde{s}(\nu_n, z)\}F.$$

Localized control was defined by restricting each actuator's input to depend only upon information from nearby sensors and actuators. As was discussed in Section 2.2 localized control is preferable over non-localized control for many practical reasons related to the implementation of the control law. However, the loop shaping design typically results in a controller  $K(z)$  that is not localized. In this case, a localized controller  $K(z) = [I + S(z)]^{-1}C(z)$  requires  $C(z)$  and  $S(z)$  to be banded transfer matrices with the majority of elements being zero.

The high-performance non-localized controller  $K(z)$  is approximated by a more practical localized controller by replacing  $C(z)$  and  $S(z)$  with banded transfer matrices  $C_l(z)$  and  $S_l(z)$  such that Theorem 3 is satisfied. The closed-loop performance and robustness requirements are then verified for the localized controller  $K_l(z) = [I + S_l(z)]^{-1}C_l(z)$ .

The design procedure is presented next. Two different options for controller synthesis are presented. These differ only in the details of how the closed-loop transfer matrices are shaped. The first option is an open-loop shaping procedure in which the parameters of the feedback controller  $K(z)$  are designed directly. One must consider the internal stability of the closed-loop while shaping the singular values. However, once closed-loop stability has been guaranteed, then open-loop shaping is straightforward and has an application in the case of a pre-defined controller structure. For example, Section 2.2 presents an industrial controller composed of a standard dead time compensator augmented with pre- and post-multiplication by spatially distributed transfer matrices. This particular example is not the only structure capable of controlling the papermaking process, but was arrived at via years of industrial experience. Indeed, one of the results of Chapter 5 is to illustrate that the industrial controller structure is able to successfully trade off the closed-loop requirements as defined in Section 4.2 above.

### Open-Loop Shaping

1. *Set up the problem.* Find a structure for the feedback controller  $K(z)$  with tuning parameters that can shape singular values  $\sigma_j(K(e^{i\omega}))$  and  $\sigma_j(GK(e^{i\omega}))$  while maintaining internal stability of the closed-loop.
2. *Diagonalize the problem.* Using Chapter 3 write  $G(z)$  and  $K(z)$  as the decoupled family  $\tilde{g}(\nu_j, z)$  and  $\tilde{k}(\nu_j, z)$  for  $\nu_j \in \{\nu_1, \dots, \nu_n\}$ .
3. *Controller synthesis.* Shape the closed-loop transfer matrices by manipulating the internally stabilizing  $\tilde{k}(\nu_j, z)$  such that the open-loop approximations  $|\tilde{g}(\nu_j, e^{i\omega})\tilde{k}(\nu_j, e^{i\omega})|$  and  $|\tilde{k}(\nu_j, e^{i\omega})|$  satisfy the specifications of Section 4.2.
4. *Factor the family of SISO controllers* such that  $\tilde{k}(\nu_j, z) = \tilde{c}(\nu_j, z)/[1 + \tilde{s}(\nu_j, z)]$  and construct transfer matrices  $C(z) := F^T \text{diag}\{\tilde{c}(\nu_1, z), \dots, \tilde{c}(\nu_n, z)\}F$  and  $S(z) := F^T \text{diag}\{\tilde{s}(\nu_1, z), \dots, \tilde{s}(\nu_n, z)\}F$ .
5. *Approximate* the full matrix factors  $C(z)$  and  $S(z)$  with banded  $C_t(z)$  and  $S_t(z)$  such that Theorem 3 is satisfied. Verify that the symmetric circulant controller  $K_t(z)$  satisfies the loop shaping design requirements.
6. *Check* the associated Toeplitz system satisfies condition (3.6) for internal stability, and implement the band-diagonal Toeplitz factors  $K_t(z) = [I + S_t(z)]^{-1}C_t(z)$ .

The second option, described below, is a closed-loop shaping procedure in which the performance weighting functions in an optimization problem are used to shape the closed-loop singular values. The ‘controller synthesis’ step can potentially be done in a number of ways depending on the specific problem requirements. Examples which consider some or all of these issues include generalized minimum variance predictive control [59, 61], mixed-sensitivity  $\mathcal{H}_2$  synthesis [4, 60], mixed-sensitivity  $\mathcal{H}_\infty$  synthesis [4],  $\mathcal{H}_\infty$  loop shaping [47], or  $\mu$ -synthesis [37]. The advantage over open-loop shaping is that these optimization techniques have been developed to guarantee an internally stable closed-loop system.

There is no need to select an appropriate controller structure. The controller design is achieved via careful shaping of the optimization weights.

The remainder of this work is dedicated to the industrial control problem and uses the open-loop shaping design approach described above. Therefore the closed-loop shaping approach is not expanded on further. An example of its application to a mixed-sensitivity  $\mathcal{H}_2$  loop shaping design procedure is described in [60].

### Closed-Loop Shaping

1. *Set up the problem.* Select appropriate inputs and outputs and write the generalized plant  $P(z)$  in terms of  $G(z)$  and weighting functions.
2. *Diagonalize the problem.* Using Chapter 3 write the generalized transfer matrix  $\mathcal{F}_l(P(z), K(z))$  as the decoupled family  $\mathcal{F}_l(\tilde{p}(\nu_j, z), \tilde{k}(\nu_j, z))$  for  $\nu_j \in \{\nu_1, \dots, \nu_n\}$ .
3. *Controller synthesis.* Shape the closed-loop transfer matrices to satisfy the specifications of Section 4.2, by adjusting the relevant performance weights in  $\|\mathcal{F}_l(\tilde{p}(\nu_j, z), \tilde{k}(\nu_j, z))\|_2 \rightarrow \min$ , for each  $\nu_j \in \{\nu_1, \dots, \nu_n\}$ .
4. *Factor* the family of SISO controllers such that  $\tilde{k}(\nu_j, z) = \tilde{c}(\nu_j, z)/[1 + \tilde{s}(\nu_j, z)]$  and construct transfer matrices  $C(z) := F^T \text{diag}\{\tilde{c}(\nu_1, z), \dots, \tilde{c}(\nu_n, z)\}F$  and  $S(z) := F^T \text{diag}\{\tilde{s}(\nu_1, z), \dots, \tilde{s}(\nu_n, z)\}F$ .
5. *Approximate* the full matrix factors  $C(z)$  and  $S(z)$  with banded  $C_l(z)$  and  $S_l(z)$  such that Theorem 3 is satisfied. Verify that the symmetric circulant controller  $K_l(z)$  satisfies the loop shaping design requirements.
6. *Check* the associated Toeplitz system (3.5) satisfies condition (3.6) for internal stability, and implement the band-diagonal Toeplitz factors  $K_t(z) = [I + S_t(z)]^{-1}C_t(z)$ .

## Chapter 5

### Industrial Paper Machine Control

This chapter presents many of the issues involved when applying the loop shaping design approach developed in Chapter 4 to the control of industrial paper machine processes as described in Chapter 1.

Section 5.1 presents an overview of the functioning of a prototype software tool developed for the tuning of cross-directional paper making processes. The process is modelled by existing software [32] as the linear transfer matrix  $G(z)$  described in (2.1)–(2.8). The performance and robustness specifications in (2.24) and (2.27) are diagonalized as in Chapter 3 and then restated in terms of the loop shaping criteria in Chapter 4. The function of the tuning tool is to generate parameters of the industrial cross-directional controller  $K(z)$  in Figure 2.3 and (2.9), (2.15) according to the principles of the open-loop shaping procedure described in Section 4.4.

Section 5.2 describes the inaugural field trial of the prototype tuning tool for tuning the feedback controller for the basis weight of a newsprint machine in a Canadian paper mill. The main steps in the execution of the testing procedure of the controller tuning tool are presented. The success of this field test provides an industrial validation of the controller analysis and design concepts presented in Chapters 3 and 4.

#### 5.1 Prototype Tuning Tool

A prototype tuning tool has been developed in Matlab for the industrial cross-directional control problem. Currently there exists a software tool (described in [32]) that identifies the parameters of the open-loop process model  $G(z)$  in (2.7)–(2.8). However, there existed no tools that allow the design of the free parameters of the industrial feedback controller  $K(z)$  in (2.15)–(2.19). The industrial problem requirements are such that the tuning tool

must be capable of using the knowledge provided by the identified process model  $G(z)$  in order to generate parameters of the controller  $K(z)$  such that acceptable closed-loop performance is achieved for any of the CD processes in Section 1.1.

Above all, an acceptable controller design requires guarantees of stability for the closed-loop. In an industrial setting, this means, not only the nominal stability of the closed-loop is satisfied, but that some margin for model uncertainty has been allowed. Secondary to the requirement of closed-loop stability is the performance specification in which the feedback controller should counteract the effect of the disturbances on the paper sheet. This section provides an overview of the functioning of the prototype tuning tool. Details of its operation may be found in Section 5.2.1, which presents the data from the tuning tool's inaugural field trial.

The tuning tool relies on the two dimensional loop shaping concepts developed in Chapters 3 and 4. Following a successful model identification session, the parameters of the process model  $G(z)$  are available and controller design may begin.

1. The variables of the tuning tool are first initialized with the identified parameters of the process model  $G(z)$  defined in (2.7)–(2.8).
2. The circulant extension of the process model is constructed (see Section 3.1), and the process model is diagonalized such that subsequent design may proceed with the family of SISO process models  $\tilde{g}(\nu_j, z)$ , one for each  $\nu_j \in \{\nu_1, \dots, \nu_n\}$ , where  $n$  is the number of actuators in the process.
3. The tuning tool calculates default values for the parameters of the diagonalized feedback controller  $\tilde{k}(\nu_j, z)$ . These default values are based on the diagonalized process model  $\tilde{g}(\nu_j, z)$ , and are quite conservative.
4. The designer is presented with several tuning 'knobs' through which the performance and robustness of the closed-loop design may be accessed. Section 5.2.3 explains the functioning of the tuning knobs in some detail.
5. (Automated) The tuning tool then calculates parameters for the controller  $\tilde{k}(\nu_j, z)$  based on the process model  $\tilde{g}(\nu_j, z)$ , and the positions of the tuning knobs. This

calculation is performed such that the (user-specified) robust stability margin is achieved (as defined by the additive unstructured perturbation in Section 2.4).

6. (Automated) The tuning tool then automatically forms the multivariable controller  $K(z)$ , from an inverse Fourier transform of the family of SISO controllers  $\tilde{k}(\nu_j, z)$ , and truncates the high-order elements in order to obtain a (user-specified) spatial order, as described in Section 4.3.
7. The user evaluates the design based on the trade-off between the performance, robustness, and spatial order of the controller. If the design is unacceptable, then return to Step 4.
8. Following the completion of a successful design in terms of the spatial frequency components of the symmetric circulant extension, the software then performs a final stability check on the 'true' truncated Toeplitz system (see Section 3.1).
9. The tuning tool then saves the tuning parameters for the spatial filter, the Dahlin controller, and the actuator profile smoothing into a file *tune.mat*.

Following the successful generation of the file *tune.mat* in Step 9 above, the designer is then free to implement the generated controller tuning parameters. As the prototype tuning tool exists only as Matlab m-files, the procedure for this implementation is currently 'manual' (i.e. the designer must walk over to the operator station and type the numbers in by hand).

The following section presents a demonstration of the procedure for the tuning of a CD controller for an industrial paper machine process in a working paper mill. More detail for the inner workings of each of the software-implemented operations of the controller design will be presented.

## 5.2 Field Test: Consistency Profiling for Newsprint

This section describes the first field trial of the prototype tuning tool described in Section 5.1. The purpose of such a trial is to begin the validation procedure for the controller analysis and design techniques introduced in Chapters 3 and 4.

The inaugural test site for the prototype tuning tool was selected to be a Canadian paper mill producing newsprint. As described in Chapter 1, newsprint is a lightweight paper product and mill in question was producing 45gsm (grams per square metre) paper for the duration of our site visit. The testing of the tuning tool was limited to the design of the control for the basis weight profile only. This paper machine uses the consistency profiling actuators (see Section 1.1.1) to flatten the basis weight of the produced paper sheet. This particular machine has  $n = 226$  consistency profiling actuators spaced on  $x_a = 35\text{mm}$  centres and distributed across the 7.91m wide paper sheet. The actuators change the weight profile by injecting low consistency whitewater into the pulp slurry as it exits the headbox. An increase in the flow of water injected by an actuator reduces the local concentration of pulp fibres and thus locally reduces the basis weight.

A commonly-occurring form of closed-loop instability in industrial CD control occurs as a slowly developing steady-state actuator profile of a very high spatial frequency [36, 65]. This phenomenon is well known to papermakers and is referred to as actuator picketing, due to the fact that the actuators profile slowly develops a steady-state 'picket-fence' appearance. In the language of Chapters 3 and 4 this signal has a high spatial frequency  $\nu$  and a low dynamical frequency  $\omega$ . It is caused by the application of a large control signal in a low gain direction of the process that is swamped by the model uncertainty, typically at high spatial frequency  $\nu$ .

Cross-directional controllers with large gain in the direction of high spatial frequency modes result from the application of a controller design rule-of-thumb without due consideration of the process. Usually feedback control is expected to remove the steady-state error from a closed-loop process. It is well-known that this may be accomplished by designing a feedback controller  $K(z)$  with integral action [56]. A multivariable controller with integral action has infinite gain in all directions at steady-state  $\omega = 0$ . However, the closed-loop stability of such a configuration cannot be guaranteed for the majority of industrial CD control processes. It was discussed in Section 2.4 that the sign of the gain of the CD process is uncertain at certain input directions. In Chapter 4 it was stated that robust stability requires the loop gain to be small at those spatial and dynamical frequencies  $\{\nu_j, \omega\}$  for which the gain of the process  $|\bar{g}(\nu_j, e^{i\omega})|$  is small. Figure 5.2 illustrates

the gain roll-off of  $\tilde{g}(\nu_j, z)$  for the newsprint model considered here.

Indeed, initially this mill had tuned their CD basis weight controller in Figure 2.3 with integral control action. The subsequent appearance of a picketing actuator profile resulted in the field engineers' implementation of the 'Actuator Profile Smoothing' feature of the industrial controller (see Figure 1.7). The functioning of this feature may be observed from Figure 2.3 in which it may be seen that an integrating controller corresponds to setting the  $n \times n$  matrix  $S = I$ . The smoothing function is included in the industrial controller specifically to combat actuator picketing. Setting  $S \neq I$  according to the spatial filter parameters described in (2.18)–(2.19) in Section 2.2 removes integral control action at high spatial frequencies. The smoothing function, defined by  $S$  is very effective at reducing controller gain at high spatial frequencies. Care must be taken not to introduce an overly-conservative controller while attempting to reduce actuator picketing. Such an example is presented in Figure 5.7 where the closed-loop performance was unnecessarily degraded.

The configuration of the control system at the mill was standard. The operator's computer (an NT station) is connected to the control processor via a LAN network connection. The operator's computer contains an 'operator station' and the industrial model identification software. The operator station is used to implement the day-to-day maintenance of the control system. It is mainly used to monitor the scanned paper profiles and to take the controller off-line in the event of problems (sheet breaks etc.). The tuning parameters of the feedback controller are also accessed via the operator station. The model identification software (described in [32]) is an off-line identification tool. Its function is to send excitation signals to the actuators profile and to record the measured response of the paper profile.

Prior to departing for the field trial, the prototype tuning tool was installed on a laptop NT machine and tested at Honeywell-Measurex's Devron division in Vancouver. All of the tuning calculations were to be performed on this laptop station. The procedure followed for the field trial of the prototype tuning tool is outlined as follows:

1. A local TCP-IP address was secured within the mill in order to connect the laptop computer to the network.

2. The industrial model identification software tool was used to log closed-loop data for the system running with the controller tuned by mill personnel.
3. The real-time control system was taken off-line by freezing the consistency profiling actuators at a constant profile.
4. The model identification software tool [32] was then used to send an excitation signal to the actuator profile (see Figure 5.1) and the profile response was logged.
5. The control system (still with the original controller tuning) was placed back on-line to maintain the paper quality.
6. The industrial model identification software, was used to identify the parameters of the spatial and dynamical response of the process model  $G(z)$  in (2.1) with parameters (2.7), (2.8).
7. The output of the model identification experiment was saved as *model.mat*.
8. The file *model.mat* was transferred across the network into the laptop computer containing the prototype tuning tool m-files.
9. A new set of feedback controller parameters were generated and saved as *tune.mat*, using the prototype tuning tool described in Section 5.1.
10. The real-time control system was taken off-line by freezing the consistency profiling actuators at a constant profile.
11. The new controller tuning parameters were keyed into the industrial controller database using the operator station.
12. The control system was placed back on-line, this time with the feedback controller defined by the new tuning numbers.
13. Closed-loop data were logged using the model identification tool over the course of several hours.

The data collected from this field trial are reported in the following subsections.

### 5.2.1 Process Model

The nominal model for the weight process has been identified from industrial paper machine data and has the output disturbance form (2.20) shown in Figure 2.2,

$$y(z) = G_t(z)u(z) + D_t(z)d(z) \quad (5.1)$$

where  $y(z), u(z) \in \mathcal{C}^{226}$  are the  $\mathcal{Z}$ -transforms of the measurement vector (error profile) and the control vector (actuator profile) respectively,  $D_t(z) \in \mathcal{C}^{226 \times 226}$  represents the transfer matrix shaping filter through which the vector of white noise disturbances  $d(z) \in \mathcal{C}^n$  enters the process,  $G_t(z) \in \mathcal{C}^{226 \times 226}$  is the process transfer matrix containing both the dynamic and the spatial responses of the system to the actuator array.

The two transfer matrices in (5.1) are given by the factors,

$$G_t(z) = (I - A_t z^{-1})^{-1} (B_t \cdot z^{-d}) \quad D_t(z) = (I - H_t z^{-1})^{-1} (I - E_t z^{-1}) \quad (5.2)$$

where the dead time  $d = 3$  (the sample time was  $T = 25s$ ). The matrices  $A_t, B_t, H_t, E_t \in \mathcal{R}^{226 \times 226}$  are all symmetric band-diagonal constant matrices,

$$\begin{aligned} B_t &= \text{toeplitz}\{b_1, \dots, b_5, 0, \dots, 0\} & E_t &= \text{toeplitz}\{\alpha_1, 0, \dots, 0\} \\ A_t &= \text{toeplitz}\{a_1, 0, \dots, 0\} & H_t &= \text{toeplitz}\{h_1, 0, \dots, 0\} \end{aligned} \quad (5.3)$$

where  $a_1 = \alpha_1 = 0.8221$ ,  $h_1 = 0.9990$ , and

$$\begin{aligned} b_1 &= -0.0814 \\ b_2 &= -0.0455 \\ b_3 &= -0.0047 \\ b_4 &= 0.0017 \\ b_5 &= 0.0003 \end{aligned} \quad (5.4)$$

The circulant extension to the process model (5.2), is obtained by writing the circulant

symmetric matrices according to the procedure in Section 3.1),

$$\begin{aligned} B &= \text{toeplitz}\{b_1, \dots, b_5, 0, \dots, 0, b_5, \dots, b_2\} & E &= E_t \\ A &= A_t & H &= H_t \end{aligned} \quad (5.5)$$

The design will then proceed based on the system defined with the circulant symmetric model,

$$G(z) = [I - Az^{-1}]^{-1}Bz^{-3} \quad D(z) = D_t(z) \quad (5.6)$$

where the circulant symmetric process model in (5.6) has been normalized such that  $\|G(z)\|_\infty = 1$ . The true process  $G_p(z)$  is assumed to belong to the set  $\Pi_g$  that is defined

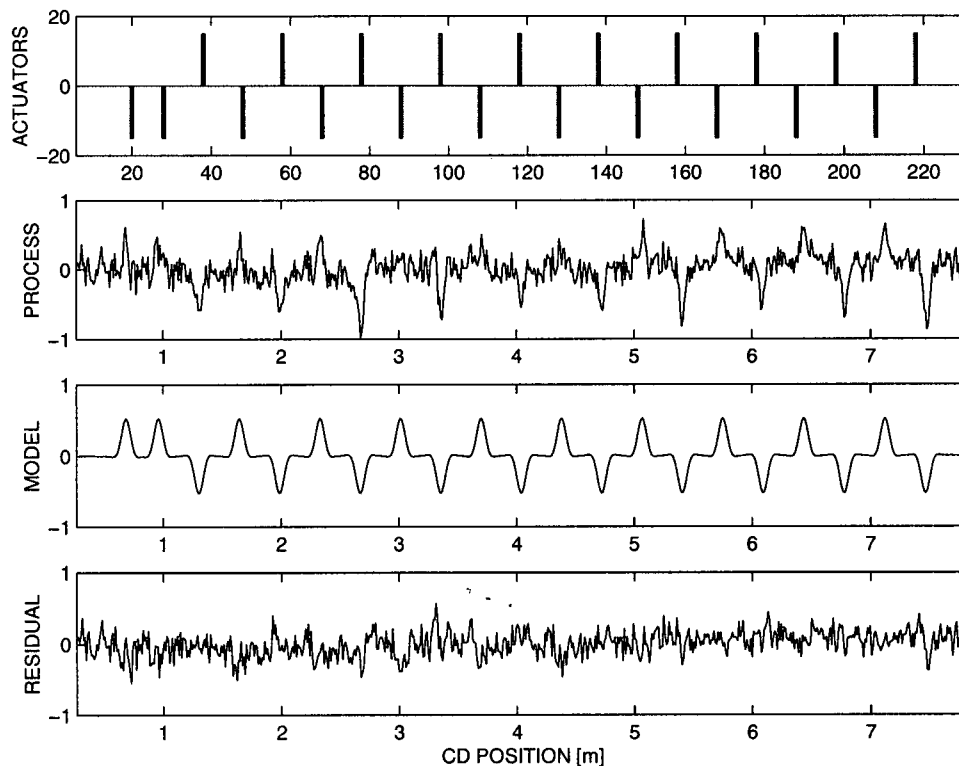


Figure 5.1: Model identification: The upper plot illustrates the actuator profile shape used to excite the process during the model identification. The second plot indicates the 'true' measured basis weight response profile. The last plot indicates the modelled response. The lower plot contains the residual signal due to process disturbances and model uncertainty.

as in (2.26) by an additive unstructured perturbation on the nominal model,

$$\Pi_g = \{G(z) + \delta G_A(z) : \bar{\sigma}(\delta G_A(e^{i\omega})) < l(\omega)\} \quad (5.7)$$

where  $G(z)$  is the nominal circulant model given in (5.6).

In this example the level of model uncertainty is estimated as

$$l(\omega) = 0.1 \cdot \|G(z)\|_\infty = 0.1 \quad (5.8)$$

The relationship between the nominal process model and the uncertainty is illustrated in Figure 5.2 where the contour plot of the two-dimensional frequency response is shown. For the process under consideration, a process model-mismatch of  $l(\omega) = 0.1 \cdot \|G(z)\|_\infty$  defines the 100% relative uncertainty bound on the model by the 0.1 contour. This bound is especially relevant to the design of control systems, as no benefit can be guaranteed from the feedback for those spatial and dynamical frequencies  $\nu_j$  and  $\omega$  outside the 0.1 contour, and provides an upper bound on the spatial and dynamical closed-loop bandwidths that may be achieved with feedback control.

### 5.2.2 Design Specifications

The industrial requirements for the feedback in the cross-directional control of a paper-making process may be summarized as “tune the existing controller to make the paper sheet as uniform as possible”.

1. *Controller Structure.* The controller structure is given by (2.11)

$$K_t(z) = [I + S_t(z)]^{-1} C_t(z) \quad (5.9)$$

in this case, the transfer matrix factors are  $226 \times 226$ . The industrial implementation of the feedback controller is illustrated in Figure 2.3 and given by (2.15)

$$\begin{aligned} C_t(z) &= S_t \cdot K_w \cdot c(z) = C_t \cdot c(z) \\ S_t(z) &= -S_t \cdot z^{-1} \end{aligned} \quad (5.10)$$

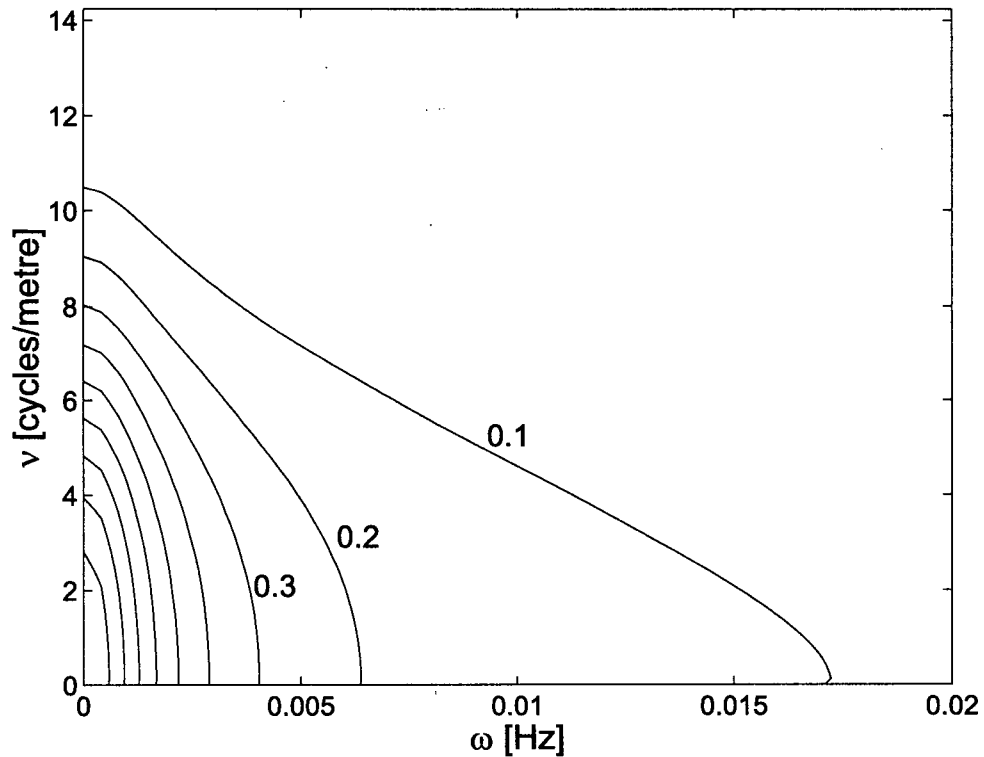


Figure 5.2: Contour plot of the open-loop basis weight frequency response  $|\tilde{g}(\nu_j, e^{i\omega})|$  for the model in (5.1)–(5.8). The area outside the 0.1 contour indicates the region of the  $\omega\nu$ -plane for which there is more than 100% relative model uncertainty. Even at steady-state, over a quarter of the spatial frequencies (60 out of 226 singular vectors) are uncontrollable.

where  $S, K_w \in \mathcal{R}^{n \times n}$  are symmetric band-diagonal Toeplitz matrices, defined in (2.15)–(2.19).

The design procedure requires the use of the circulant extension to the feedback controller  $K_t(z)$  in (5.9). This is obtained by writing the circulant symmetric matrices,

$$\begin{aligned} C &= \text{toeplitz}\{c_1, \dots, c_{n_c}, 0, \dots, 0, c_{n_c}, \dots, c_2\} \\ S &= \text{toeplitz}\{s_1, \dots, s_{n_s}, 0, \dots, 0, s_{n_s}, \dots, s_2\} \end{aligned} \quad (5.11)$$

The loop shaping design will proceed based on the controller defined with the cir-

culant symmetric matrices in (5.11)

$$K(z) = [I - Sz^{-1}]^{-1}C \cdot c(z) \quad (5.12)$$

with  $C$ ,  $S$ , and  $c(z)$  as defined in (5.11) and (2.15)–(2.19).

2. *Performance.* As described in Chapter 1, paper is sold based on the quadratic variance of the error profile  $v(t) = y(t) - r(t)$ . This metric for paper quality lead to the measure for feedback controller performance in (2.24) in terms of the  $\mathcal{H}_2$ -norm of the closed-loop transfer matrix

$$\| [I - G(z)K(z)]^{-1}D(z) \|_2 \rightarrow \text{small} \quad (5.13)$$

This requirement is a restatement of the loop shaping specifications of Section 4.1 that the sensitivity function

$$\sigma_j \left( [I - G(e^{i\omega})K(e^{i\omega})]^{-1} \right) \rightarrow \text{small} \quad (5.14)$$

for singular values  $j \in \{1, \dots, 226\}$  and  $\omega \in [-\pi, \pi]$ , where the exogenous disturbances are important. In the case of the disturbance transfer matrix with parameters as in (5.2), the gain of  $D(z)$  is largest at low dynamical frequencies  $\omega$ . Thus, for the exogenous white noise signal  $d(t)$  in (5.1), the performance condition (5.14) is most important at low dynamical frequencies  $\omega$ .

3. *Robust Stability.* As stated in Section 4.1, an advantage of the loop shaping control design techniques is their ability to quantify the trade off between performance and robustness. It is not possible to satisfy the performance condition (5.14) for all singular values  $j \in \{1, \dots, 226\}$  and all dynamical frequencies  $\omega \in [-\pi, \pi]$ . Disturbance attenuation will always be sacrificed for closed-loop stability. An internally stable closed-loop defined by  $G(z)$  and  $K(z)$  is robustly stable for all  $G_p(z) \in \Pi_g$  in (5.7) if

$$\bar{\sigma} \left( K(e^{i\omega})[I - G(e^{i\omega})K(e^{i\omega})]^{-1} \right) < \frac{1}{l(\omega)} = \frac{1}{0.1} = 10.0 \quad (5.15)$$

for  $l(\omega) > 0$  in (5.7) and all  $\omega \in [-\pi, \pi]$ .

### 5.2.3 Two Dimensional Open-Loop Shaping

#### Set up the problem

The structure of the industrial multivariable paper machine controller  $K(z)$  was described in (2.15)–(2.19) above. It remains to be shown that the existing controller structure is capable of shaping the singular values of  $\sigma_j(K(e^{i\omega}))$  and  $\sigma_j(GK(e^{i\omega}))$  while maintaining internal stability of the closed-loop. In order to demonstrate these features, the plant  $G(z)$  in (5.5), (5.6) and the controller  $K(z)$  in (5.11), (5.12) will be diagonalized with the real Fourier matrix  $F$  in (A.4). As noted in Section 3.7.1, this diagonalization allows the simultaneous examination of both the eigenvalues and singular values of a circulant symmetric system.

First, the plant  $G(z)$  in (5.5), (5.6) is diagonalized

$$\tilde{g}(\nu_j, z) = \frac{\tilde{b}(\nu_j)z^{-d}}{1 - \tilde{a}(\nu_j)z^{-1}} \quad (5.16)$$

where  $FG(z)F^T = \text{diag}\{\tilde{g}(\nu_1, z), \dots, \tilde{g}(\nu_{226}, z)\}$  is formed by computing  $FBF^T = \text{diag}\{\tilde{b}(\nu_1), \dots, \tilde{b}(\nu_{226})\}$  and  $FAF^T = \text{diag}\{\tilde{a}(\nu_1), \dots, \tilde{a}(\nu_{226})\}$ .

Next, the industrial controller  $K(z)$  in Section 2.2 is diagonalized as

$$\tilde{k}(\nu_j, z) = \frac{\tilde{c}(\nu_j)}{1 - \tilde{s}(\nu_j)z^{-1}} \cdot c(z) \quad (5.17)$$

where  $FK(z)F^T = \text{diag}\{\tilde{k}(\nu_1, z), \dots, \tilde{k}(\nu_{226}, z)\}$  is formed by diagonalizing  $FCF^T = \text{diag}\{\tilde{c}(\nu_1), \dots, \tilde{c}(\nu_{226})\}$  and  $FSF^T = \text{diag}\{\tilde{s}(\nu_1), \dots, \tilde{s}(\nu_n)\}$ .

Next, it is important to determine bounds on the spectra  $\tilde{c}(\nu_j)$  and  $\tilde{s}(\nu_j)$ , as well as tuning parameters  $\{d_c, a_c, \alpha_c\}$  for the dynamical part  $c(z)$  in (5.17) such that closed-loop stability is guaranteed with the plant  $\tilde{g}(\nu_j, z)$  in (5.16).

The dynamical part of the controller  $c(z)$  is restricted to setting the controller parameters  $\{d_c, a_c, \alpha_c\}$  in (2.16) in terms of the model parameters  $\{d, a_1, \alpha_1\}$

given in (5.2) as  $\{d, a_1, \alpha_1\} = \{3, 0.8221, 0.8221\}$ . This setting of the parameters for  $c(z)$  is motivated by stability considerations and the fact that minimum variance control is achieved for certain values of  $\tilde{c}(\nu_j)$  and  $\tilde{s}(\nu_j)$  in (5.17) [18]. In fact, the proposed loop shaping design procedure may be interpreted as the detuning of a minimum variance controller for robustness considerations [59].

The loop shaping will proceed by assigning the remaining degrees of freedom; the two spectra  $\tilde{c}(\nu_j)$  and  $\tilde{s}(\nu_j)$  in (5.17) for  $\nu_j \in \{\nu_1, \dots, \nu_{226}\}$ . It may be shown that closed-loop stability is guaranteed for  $\tilde{k}(\nu_j, z)$  and  $\tilde{g}(\nu_j, z)$  in (5.16) and (5.17) if,

$$0 < \tilde{s}(\nu_j) \leq 1, \quad 0 \leq \tilde{r}(\nu_j) \quad (5.18)$$

with

$$\tilde{c}(\nu_j) = \frac{\tilde{b}(\nu_j)}{\tilde{b}(\nu_j)^2 + \tilde{r}(\nu_j)} \quad (5.19)$$

for all spatial frequencies  $\nu_j \in \{\nu_1, \dots, \nu_{226}\}$

The design can then safely proceed by shaping the open-loop transfer functions  $|\tilde{g}(\nu_j, z)\tilde{k}(\nu_j, z)|$  and  $|\tilde{k}(\nu_j, z)|$  via the spectra  $\{\tilde{r}(\nu_j), \tilde{s}(\nu_j)\}$  according to the closed-loop stability condition (5.18).

## Two Dimensional Frequency Domain Specifications

This step presents the performance and robust stability design specifications which are required to be met during the loop shaping step of the design.

The frequency domain design specifications on the feedback are derived as bounds on the shape of controller gain  $|\tilde{k}(\nu_j, z)|$  rather than loop gain  $|\tilde{g}(\nu_j, z)\tilde{k}(\nu_j, z)|$  as was developed in Figures 4.3–4.5. The design procedure is identical, but the robustness requirement for an ill-conditioned plant with additive uncertainty is more easily stated in terms of requirements on  $|\tilde{k}(\nu_j, z)|$  [44, 56].

1. *Performance.* The design procedure requires the performance specification in (5.14) to be rewritten in terms of the open-loop transfer function  $\tilde{k}(\nu_j, z)$ .

First, the requirement is quantified by requiring 90% attenuation of disturbances,

$$\left| \frac{1}{1 - \tilde{g}(\nu_j, e^{i\omega})\tilde{k}(\nu_j, e^{i\omega})} \right| < \tilde{p}(\nu_j, \omega) = 0.1 \quad (5.20)$$

for the low spatial and dynamical frequencies in  $\{\nu_j, \omega\} \in \Omega_l$  where, in engineering units,

$$\Omega_l = \left\{ \{\nu_j, \omega\} : |\nu_j| < 5.5\text{m}^{-1}, |\omega| < 10^{-4.6}\text{Hz} \right\} \quad (5.21)$$

The closed-loop specification (5.20) is satisfied by the open-loop requirement

$$|\tilde{k}(\nu_j, e^{i\omega})| > w_l = \left( \frac{1}{0.1} + 1 \right) \cdot \frac{1}{0.5} = 22.0 \quad (5.22)$$

for the low spatial and dynamical frequencies in  $\{\nu_j, \omega\} \in \Omega_l$  in (5.21).

The set of low frequencies  $\Omega_l$  in (5.21) for which condition (5.22) must be satisfied is illustrated in Figure 5.3. The design satisfies the open-loop performance condition (5.22) if the contour(s) of  $|\tilde{k}(\nu_j, e^{i\omega})| = 22.0$  lie in the white space of Figure 5.3.

2. *Robust stability.* Next, the requirement of closed-loop robust stability (5.15) is rewritten as the two dimensional closed-loop condition

$$\left| \frac{\tilde{k}(\nu_j, e^{i\omega})}{1 - \tilde{g}(\nu_j, e^{i\omega})\tilde{k}(\nu_j, e^{i\omega})} \right| < \frac{1}{l(\omega)} = 10.0 \quad (5.23)$$

for spatial frequencies  $\nu$  and dynamical frequencies  $\omega$ .

The closed-loop specification (5.23) is satisfied for the high spatial and dynamical frequencies in  $\{\nu_j, \omega\} \in \Omega_h$  where,

$$\Omega_h = \left\{ \{\nu_j, \omega\} : |\tilde{g}(\nu_j, e^{i\omega})| < 0.1 \right\} \quad (5.24)$$

by the open-loop requirement

$$|\tilde{k}(\nu_j, e^{i\omega})| < w_h = \frac{1}{2 \cdot l(\omega)} = 1/(2 \cdot 0.1) = 5.0 \quad (5.25)$$

for the high spatial and dynamical frequencies in  $\{\nu_j, \omega\} \in \Omega_h$  in (5.24).

The set of high frequencies  $\Omega_h$  in (5.24) for which condition (5.25) must be satisfied is illustrated in Figure 5.3. The design satisfies the open-loop robust stability condition (5.25) if the contour(s) of  $|\tilde{k}(\nu_j, e^{i\omega})| = 5.0$  lie in the white space of Figure 5.3.

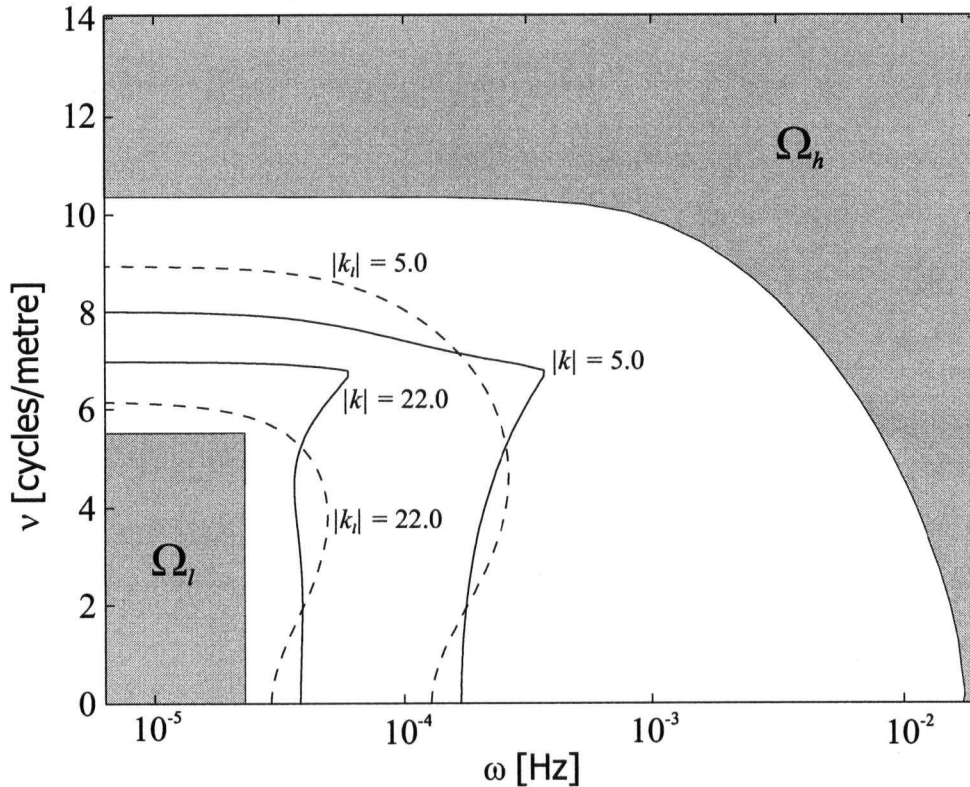


Figure 5.3: Contour plots in  $\omega\nu$  of the sets  $\Omega_l$  in (5.21) and  $\Omega_h$  in (5.24). The performance condition (5.22) is satisfied if the contour(s)  $|\tilde{k}(\nu_j, e^{i\omega})| = 22.0$  lie outside the set  $\Omega_l$ . The robust stability condition (5.25) is satisfied if the contour(s)  $|\tilde{k}(\nu_j, e^{i\omega})| = 5.0$  lie outside the set  $\Omega_h$ . The contours of the full-matrix controller  $K(z)$  obtained in the 'Controller Synthesis' step are illustrated as the solid lines. The contours of the controller  $K_l(z)$  obtained by spatial order reduction are illustrated as the dashed lines.

### Controller Synthesis

In this step, the procedure is presented for synthesizing the two spectra  $\tilde{c}(\nu_j)$  and  $\tilde{s}(\nu_j)$  for the controller  $\tilde{k}(\nu_j, z)$  in (5.17) via the available degrees of freedom to satisfy design specifications of nominal stability (5.18), nominal performance (5.22), and robust stability (5.25).

The available degrees of freedom for spectrum  $\tilde{s}(\nu_j)$  are the order of the Blackman window  $n_s$  and the blend factor  $\lambda$  in (2.18). The spectrum  $\tilde{c}(\nu_j)$  has  $n = 226$  degrees of freedom and is defined by the spectrum  $\tilde{r}(\nu_j) \geq 0$  with  $\nu_j \in \{\nu_1, \dots, \nu_{226}\}$  in (5.18), (5.19).

Following the selection of the order of the Blackman window  $n_s$  in (2.18), the design of the control system is specified completely by the value of the tuning knob  $\lambda$  in (2.18). The only remaining degree of freedom is the spectrum  $\tilde{r}(\nu_j)$  in (5.19). It is then automatically calculated such that the conflicting specifications imposed by (5.18), (5.22), (5.25) are simultaneously satisfied.

1. *Performance.* In order to satisfy the performance condition in (5.22), it is required that

$$\tilde{r}(\nu_j) \rightarrow 0^+ \quad \tilde{s}(\nu_j) \rightarrow 1^- \quad (5.26)$$

for low spatial frequencies  $\nu_j < 5.5\text{m}^{-1}$  as defined by the set  $\Omega_l$  in (5.21) and Figure 5.3.

A value of  $\tilde{r}(\nu_j) = 0$  corresponds to a model-inverse gain for the controller given by  $\tilde{c}(\nu_j) = \tilde{b}(\nu_j)^{-1}$  in (5.19) and should only be used at low spatial frequencies  $\nu_j$  where  $|\tilde{b}(\nu_j)|$  is large. Setting  $\tilde{s}(\nu_j) = 1$  leads to integrating dynamics in  $\tilde{k}(\nu_j, z)$  in (5.17).

2. *Robust Stability.* In order to satisfy the robust stability condition in (5.25), it is required that

$$\tilde{r}(\nu_j) > 0 \quad \tilde{s}(\nu_j) < 1 \quad (5.27)$$

for high spatial frequencies  $\nu_j > 5.5\text{m}^{-1}$  as defined by the set  $\Omega_h$  in (5.24) and Figure 5.3.

A value of  $\tilde{r}(\nu_j) > 0$  corresponds to a more conservative controller gain as  $|\tilde{c}(\nu_j)| < |\tilde{b}(\nu_j)^{-1}|$  in (5.19) and is especially important at high spatial frequencies for which

the open-loop process gain rolls off and  $|\tilde{b}(\nu_j)| \rightarrow 0$ . The quantity  $\tilde{s}(\nu_j) < 1$  corresponds to the removal of integral control action in  $\tilde{k}(\nu_j, z)$  in (5.17), as the controller pole  $\tilde{s}(\nu_j)$  is moved away from the unit circle. Integrating control results in  $|\tilde{k}(\nu_j, e^{i\omega})| \rightarrow \infty$  as  $\omega \rightarrow 0$ , this is undesirable at high spatial frequencies  $\nu_j$  for which an integrating  $\tilde{k}(\nu_j, z)$  violates the robust stability condition (5.25).

For practical controller design, it has been found sufficient to restrict the robust stability analysis to evaluating condition (5.25) along the  $\nu$ -axis of Figure 5.3. The gain of the Dahlin controller  $c(z)$  in (2.16) rolls off quickly for high dynamical frequencies  $\omega$ . The contours of  $|\tilde{k}(\nu_j, e^{i\omega})| = w_h$  are still examined for all  $\omega\nu$ , but the robust design of the spectrum  $\tilde{r}(\nu_j)$  only requires to examine the  $\nu$ -axis.

It can be shown that  $|\tilde{k}(\nu_j, e^{i0})|$  will satisfy (5.25) for  $\{\nu_j, 0\} \in \Omega_h$  in (5.24) if, for  $z = e^{i\omega}$  and  $\omega = 0$ ,

$$\begin{aligned} \tilde{r}(\nu_j) &> 2 \cdot l(\omega) \cdot \left| \frac{c(z) \cdot \tilde{b}(\nu_j)}{1 - \tilde{s}(\nu_j)z^{-1}} \right| - \tilde{b}(\nu_j)^2 \\ &\approx \frac{0.0047}{\lambda} \cdot |\tilde{b}(\nu_j)| - \tilde{b}(\nu_j)^2 \end{aligned} \quad (5.28)$$

where  $l(w)$  is the level of model uncertainty in (5.8),  $c(z)$  in (2.16) tuned as in (5.17), and  $\tilde{s}(\nu_j) \approx 1 - \lambda$  for high spatial frequencies  $\nu_j > 10\text{m}^{-1}$  (see Figure 5.4).

3. *Controller Localization.* The matrix  $S = F^T \text{diag}\{\tilde{s}(\nu_1), \dots, \tilde{s}(\nu_{226})\}F$  is automatically a banded circulant matrix defined by the Blackman window of order  $n_s$  in (2.18). However, the localization of the matrix  $C = F^T \text{diag}\{\tilde{c}(\nu_1), \dots, \tilde{c}(\nu_{226})\}F$  with  $\tilde{c}(\nu_j)$  defined by spectra  $\tilde{b}(\nu_j)$  and  $\tilde{r}(\nu_j)$  in (5.19) remains an issue. Theorem 3 shows that it is desirable to keep the magnitude of the elements of  $\delta C = C - C_l$  small, in other words the full matrix  $C$  be as close as possible to a banded matrix  $C_l$ . An empirical rule for this is that the localization of  $C$  is related to the smoothness of  $\tilde{c}(\nu_j)$ . Therefore, in anticipation of the truncation of the elements of  $C$ , it is desirable to design  $\tilde{r}(\nu_j)$  such that

$$|\tilde{r}(\nu_j) - \tilde{r}(\nu_{j+1})| \rightarrow \text{small} \quad (5.29)$$

for  $j \in \{1, \dots, 225\}$ .

Note that the satisfaction of conditions (5.26)–(5.29) requires some trade off. The performance specification of (5.26) requires  $\tilde{s}(\nu_j) \rightarrow 1$ , which means that the tuning knob  $\lambda \rightarrow 0$ . However, notice that  $\lambda$  appears in the denominator of the robust stability condition (5.28), meaning that a small value of  $\lambda$  results in a large value of  $\tilde{r}(\nu_j)$  needed at high frequencies  $\nu_j$  to satisfy the robust stability condition. However, the performance requirement (5.26) already has  $\tilde{r}(\nu_j) = 0$  at low frequencies  $\nu_j$ . Such a large difference in  $\tilde{r}(\nu_j)$  at the low spatial frequencies and the high spatial frequencies leads to a violation of the localization constraint (5.29).

The controller tuning proceeded as follows:

- the order of the Blackman window in (2.18) (and hence  $S$ ) was selected as  $n_s = 4$  for spatial bandwidth considerations.
- for each iteration of  $\lambda$ , the spectrum  $\tilde{r}(\nu_j)$  was automatically calculated such that the performance condition (5.28) was satisfied at low  $\nu_j < 5.5\text{m}^{-1}$  and the robust stability condition (5.28) was satisfied at high  $\nu_j > 10\text{m}^{-1}$ .
- the tuning knob  $\lambda$  in (2.18) was manually iterated until an acceptable trade off between performance (5.26), and the localization of  $C$  in (5.29) was achieved.

The resulting tuning parameters for the spectrum  $\tilde{s}(\nu_j)$  were  $n_s = 4$  and  $\lambda = 0.01$ . The spectrum  $\tilde{s}(\nu_j)$  is illustrated in Figure 5.4. The tuning spectrum  $\tilde{r}(\nu_j)$  and the corresponding controller gain spectrum  $\tilde{c}(\nu_j)$  in (5.19) are both illustrated in Figure 5.4.

The central row of the full circulant matrix  $C = F^T \text{diag}\{\tilde{c}(\nu_1), \dots, \tilde{c}(\nu_{226})\}F$  is plotted in Figure 5.5. The size of the elements of  $C$  decay quickly as a function of their distance from the central element. This almost-localized structure facilitates the elimination of the smaller elements of  $C$  to satisfy Theorem 3.

In summary, at the end of this step we are left with the settings for the dynamical controller for  $c(z)$  in (2.16) and the spectra  $\tilde{c}(\nu_j)$ ,  $\tilde{s}(\nu_j)$  in (5.17), such that the controller  $\tilde{k}(\nu_j, z)$  satisfies the performance requirement (5.22) and the robust stability requirement (5.25) are satisfied as illustrated in Figure 5.3.

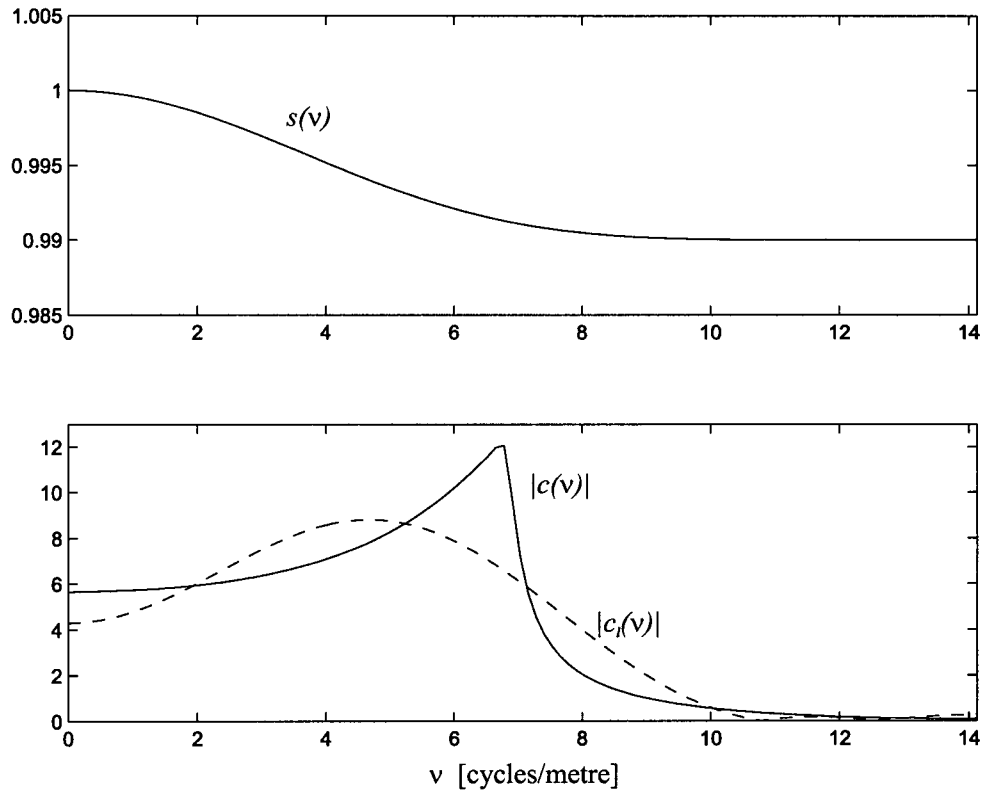


Figure 5.4: The spectra  $\tilde{s}(\nu_j)$  and  $\tilde{c}(\nu_j)$  resulting from the controller synthesis for the controller  $\tilde{k}(\nu_j, z)$  in (5.17) and (5.19). The dashed line represents the spectrum of  $\tilde{c}_i(\nu_j)$  obtained by spatial order reduction.

### Controller Spatial Order Reduction

The previous step produced spectra  $\tilde{c}(\nu_j)$  and  $\tilde{s}(\nu_j)$  such that the controller  $\tilde{k}(\nu_j, z)$  in (5.17) is stable and satisfied the design requirements for performance (5.22) and robust stability (5.25). The multivariable controller is constructed from these spectra by writing,

$$\begin{aligned} C &= F^T \text{diag}\{\tilde{c}(\nu_1), \dots, \tilde{c}(\nu_{226})\} F, \\ S &= F^T \text{diag}\{\tilde{s}(\nu_1), \dots, \tilde{s}(\nu_{226})\} F \end{aligned} \quad (5.30)$$

where  $C, S \in \mathcal{R}^{226 \times 226}$  are both symmetric circulant matrices.

It was stated in Section 5.2.2 the final goal of the design is band-diagonal Toeplitz matrices  $C_t$  and  $S_t$ . Section 4.3 describes the first step towards that goal as the spatial order reduction of the circulant matrices  $C$  and  $S$  by truncating elements to obtain banded

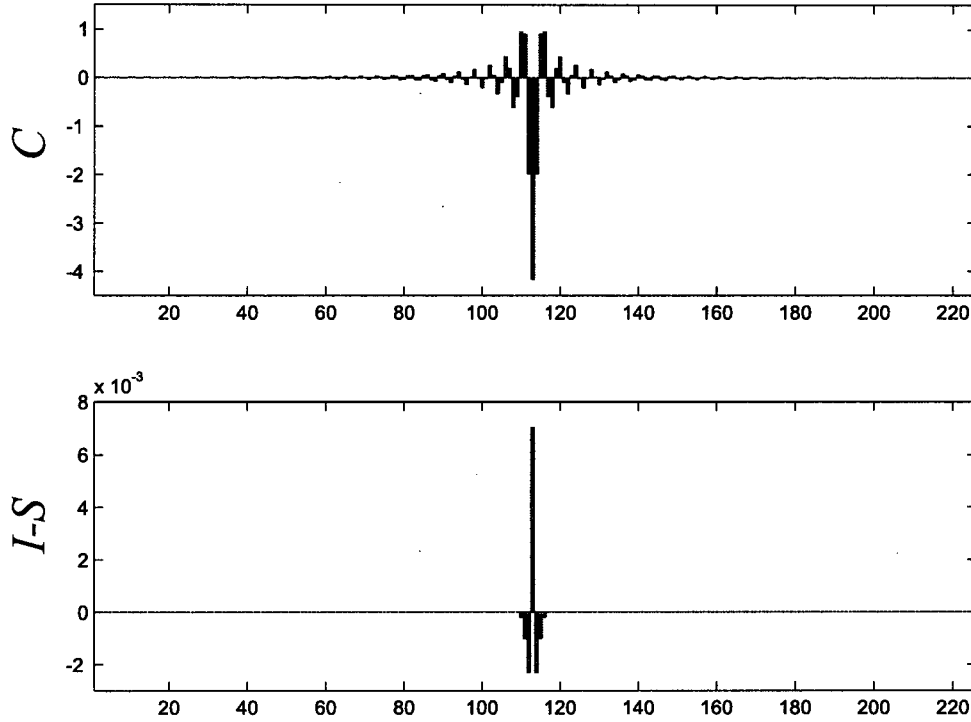


Figure 5.5: The central row of the full circulant matrices  $C(113, :)$  and  $I - S(113, :)$  resulting from the spectrum  $\tilde{c}(\nu_j)$  and  $\tilde{s}(\nu_j)$  in Figure 5.4 and  $C = F^T \text{diag}\{\tilde{c}(\nu_1), \dots, \tilde{c}(\nu_{226})\}F$  and  $S = F^T \text{diag}\{\tilde{s}(\nu_1), \dots, \tilde{s}(\nu_{226})\}F$ .

circulant matrices  $C_l$  and  $S_l$ .

Due to the parameterization of the industrial controller, the matrix  $S$  in (2.18) is already banded with  $n_s = 4$  and is given for  $\lambda = 0.01$  as the  $226 \times 226$  constant matrix,

$$S_l = S = \text{toeplitz}\{s_1, \dots, s_4, 0, \dots, 0, s_4, \dots, s_2\} \tag{5.31}$$

where,

$$\{s_1, s_2, s_3, s_4\} = \{0.9930, 0.0023, 0.0010, 0.0002\} \tag{5.32}$$

However, the  $226 \times 226$  symmetric circulant matrix  $C$ , illustrated in Figure 5.5, has no non-zero elements,

$$C = \text{toeplitz}\{c_1, \dots, c_{113}, c_{114}, c_{113}, \dots, c_2\} \tag{5.33}$$

but the magnitude of  $|c_k|$  in (5.33) decreases rapidly away from the centre.

It is desired to truncate these smaller elements of  $C$  in (5.33) to obtain a banded  $226 \times 226$  symmetric circulant matrix with  $n_c = 7$  in (5.11).

$$C_l = \text{toeplitz}\{c_1, \dots, c_7, 0, \dots, 0, c_7, \dots, c_2\} \quad (5.34)$$

such that closed-loop stability is maintained. The perturbation on the controller  $K(z)$  introduced by the spatial order reduction is then,

$$\begin{aligned} \delta C_l &= \text{toeplitz}\{0, \dots, 0, c_8, \dots, c_{113}, c_{114}, c_{113}, \dots, c_8, 0, \dots, 0\} \\ \delta S_l &= 0_{226 \times 226} \end{aligned} \quad (5.35)$$

As discussed in Section 4.3, closed-loop stability must be verified following the spatial order reduction of a controller. In this case, only the gain matrix  $C$  was required to be reduced to  $C_l$  in (5.34). This fact allows for the evaluation of the closed-loop stability based on the gain margin for each of the 226 SISO loops. Calculation of the gain margin is less conservative than the small gain theorem based condition in Theorem 3, and is used to verify the stability of the closed-loop system with  $C_l$  in (5.34) with

$$\{c_1, \dots, c_7\} = \{-4.1226, -1.9487, 0.9150, 0.9408, 0.0027, 0.0011, 0.0002\} \quad (5.36)$$

The multivariable controller is then written as

$$K_l(z) = [I - S_l z^{-1}]^{-1} C_l \cdot c(z) \quad (5.37)$$

with banded circulant factors  $C_l$  and  $S_l$ . The central rows of the banded circulant matrices  $C_l$  and  $S_l$  are illustrated in Figure 5.6.

Since only stability has been guaranteed for the closed-loop with circulant symmetric controller  $K_l(z)$  with the circulant plant defined by the transfer matrix  $G(z)$  in (5.6). The satisfaction of the design requirements of disturbance attenuation (5.22) and robust stability (5.25), is verified for the reduced order controller  $K_l(z)$  by plotting the appropriate

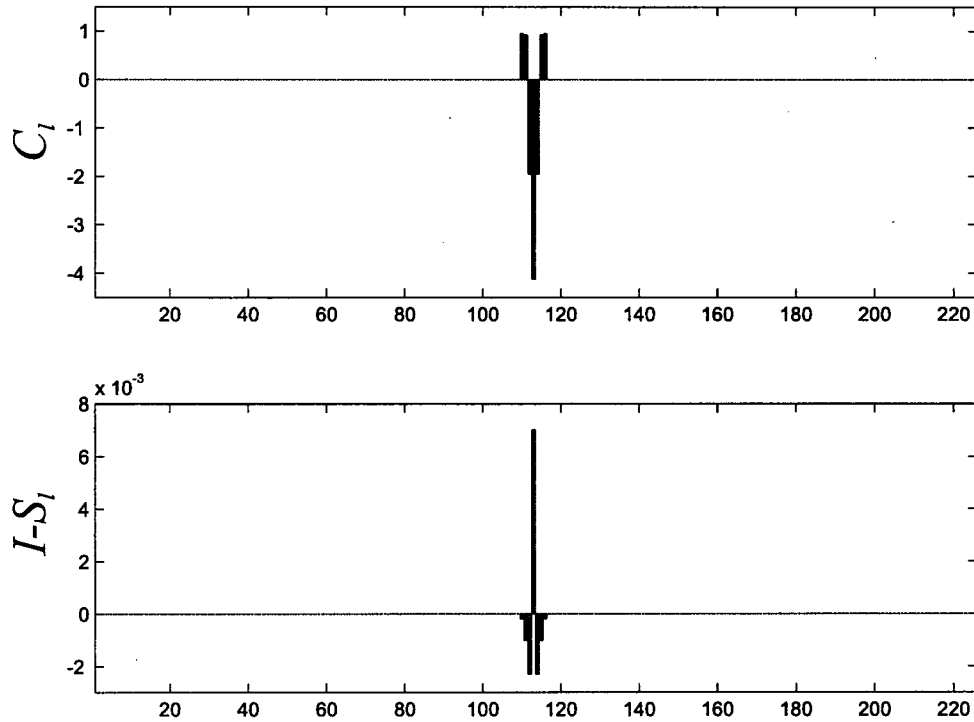


Figure 5.6: The central row of the banded circulant matrix  $C_l(113, :)$  resulting from the spatial order reduction (5.34). The central row of the banded circulant matrix  $I - S_l(113, :)$  is also shown, due to the structure of the industrial controller  $S_l = S$  and no spatial order reduction was required.

$\omega\nu$  contours of  $|\tilde{k}_l(\nu_j, e^{i\omega})|$  in Figure 5.3.

The design requirements (5.22) and (5.25) have been satisfied with a controller  $K_l(z)$  in (5.37) which may be implemented such that each actuator in the array requires information only from  $2n_c - 1 = 13$  measurement locations and  $2n_s - 1 = 7$  actuators. In other words, to realize the control law  $K_l(z)$  each actuator requires only about 6% of the  $n = 226$  available measurements and information from about 3% of the  $n = 226$  actuators in the array!

### Implementation

The previous step produced banded circulant matrices  $C_l$  in (5.34) and  $S_l$  in (5.31) which, when used in the feedback controller  $K_l(z)$  in (5.37), satisfy the design requirements (5.22) and (5.25) for the circulant process model  $G(z)$  in (5.6) defined in terms of the banded

circulant matrices  $B, A \in \mathcal{R}^{226 \times 226}$  in (5.2), (5.5).

The final step in the controller design is to verify that the controller formed by extracting the band-diagonal Toeplitz matrices from  $C_l$  and  $S_l$ , i.e.

$$\begin{aligned} C_t &= \text{toeplitz}\{c_1, \dots, c_7, 0, \dots, 0\} \\ S_t &= \text{toeplitz}\{s_1, \dots, s_4, 0, \dots, 0\} \end{aligned} \quad (5.38)$$

such that

$$K_t(z) = [I - S_t z^{-1}]^{-1} C_t c(z) \quad (5.39)$$

stabilizes the more accurate process model  $G_t(z)$  in (5.3) with band-diagonal Toeplitz factors given by  $B_t$  and  $A_t$  in (5.2). The Toeplitz system matrices  $\{B_t, A_t, C_t, S_t\}$  are obtained by trimming the 'ears' from the circulant matrices  $\{B, A, C_l, S_l\}$ , as shown in Figure 3.1.

In Section 3.1 it was shown that closed-loop stability of the band-diagonal Toeplitz system is given by the invertibility of the  $2n \times 2n$  transfer matrix  $L_t(z)$  defined in 3.5. These factors are realized here by the  $452 \times 452$  transfer matrix,

$$\begin{aligned} L_t(z) &:= \begin{bmatrix} I - S_t z^{-1} & C_t c(z) \\ B_t z^{-d} & I - A_t z^{-1} \end{bmatrix} \\ &= \begin{bmatrix} I - S_l z^{-1} & C_l c(z) \\ B z^{-d} & I - A z^{-1} \end{bmatrix} - \begin{bmatrix} -\delta S_t z^{-1} & \delta C_t c(z) \\ \delta B_t z^{-d} & 0_{226 \times 226} \end{bmatrix} \end{aligned} \quad (5.40)$$

where  $B$  and  $A$  in (5.5),  $S_l$  in (5.31),  $C_l$  in (5.34), and  $c(z)$  in (2.16). The matrix  $\delta B_t = B - B_t$ , and similar definition apply to  $\delta C_t$  and  $\delta S_t$ . The matrix  $\delta A_t = 0_{226 \times 226}$  due to the fact the circulant  $A$  and the band-diagonal Toeplitz  $A_t$  both being given by  $A = A_t = 0.8221 \cdot I_{226 \times 226}$ .

The invertibility of the first term in (5.40) is guaranteed by the internal stability of the circulant symmetric controller  $K_l(z)$  in (5.37) and the circulant symmetric plant model  $G(z)$  in (5.6). The second term in (5.40) contains the 'ears' of each of the relevant transfer

matrices. Following the verification of invertibility of  $L_t(z)$  in (5.40), the two matrices  $C_t$  and  $S_t$  are implemented as factors in the controller  $K_t(z)$  in (5.39).

#### 5.2.4 Paper Mill Results

This section presents data obtained from a paper machine describing and comparing the closed-loop performance obtained by tuning the industrial controller in (5.9) with two different feedback controller designs. The first of these is denoted by  $K_b(z)$  and has been designed using the empirical tuning rules for paper machine control. The second set of results displays the closed-loop performance of  $K_t(z)$  in (5.39), resulting from the two dimensional loop shaping procedure in Section 5.2.3. Both of these controllers were implemented on a paper machine whose model is described in Section 5.2.1.

The controller designed with traditional empirical tuning rules is given by (5.9) with

$$K_b(z) = [I - S_b z^{-1}]^{-1} C_b c_b(z) \quad (5.41)$$

this design has  $n_s = 2$  and  $\lambda = 0.1$  in (2.18), such that

$$S_b = \text{toeplitz}\{0.9595, 0.0202, 0, \dots, 0\} \quad (5.42)$$

The matrix  $C_b = -6.5494 \cdot S_b$  and the parameters of the dynamical controller  $c_b(z)$  given by  $c(z)$  in (2.16) with parameters  $\{d_c, a_c, \alpha_c\} = \{3, 0.7316, 0.8365\}$ .

The two dimensional frequency components of the controller are calculated from the circulant extension of  $K_b(z)$  as in (5.5) and diagonalizing with the Fourier matrix  $F$  in (A.4)

$$\tilde{k}_b(\nu_j, z) = \frac{\tilde{c}_b(\nu_j)}{1 - \tilde{s}_b(\nu_j)z^{-1}} \cdot c_b(z) \quad (5.43)$$

The relevant  $\omega\nu$ -contours defining performance  $|\tilde{k}_b(\nu_j, e^{i\omega})| = 22.0$  in (5.22) and robust stability  $|\tilde{k}_b(\nu_j, e^{i\omega})| = 5.0$  in (5.25) are plotted in Figure 5.7 along with the sets  $\Omega_l$  in (5.21) and  $\Omega_h$  in (5.24). The performance criterion is violated since the contour  $|\tilde{k}_b(\nu_j, e^{i\omega})| = 22.0$  intersects the set  $\Omega_l$ . In this case, the empirical approach, in an effort to maintain

closed-loop robust stability, has resulted in an overly conservative controller.

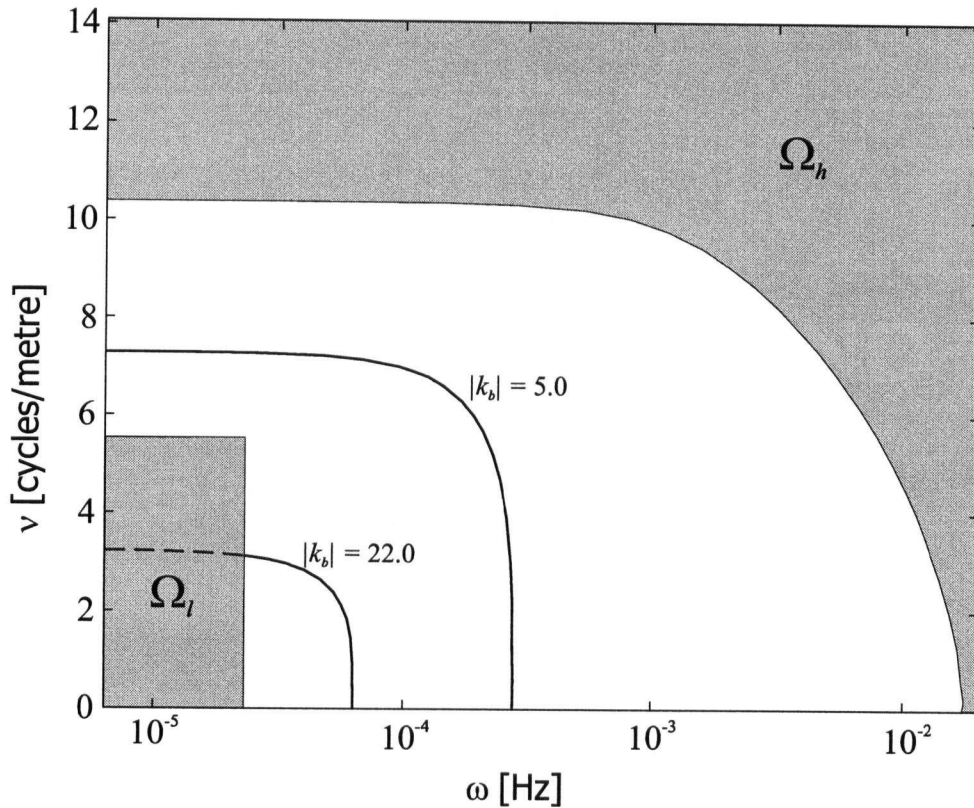


Figure 5.7: An  $\omega\nu$  contour plot showing the controller  $|\tilde{k}_b(\nu_j, z)|$  in (5.43) relative to the sets  $\Omega_l$  in (5.21) and  $\Omega_h$  in (5.24). The performance criterion is violated since the contour  $|\tilde{k}_b(\nu_j, e^{i\omega})| = 22.0$  intersects the set  $\Omega_l$ .

Figure 5.8 displays the closed-loop steady-state ( $\omega = 0$ ) error profiles for the controllers  $K_b(z)$  in (5.41) and  $K_t(z)$  in (5.39), respectively. The profiles shown are the high-resolution measured profiles obtained from the scanning sensor as described in Chapter 1.1. The paper sheet is measured at 693 locations evenly-spaced across the 7.91m wide paper sheet. The high resolution error profile  $v_h(t) \in \mathcal{R}^{693}$  is related to the low resolution error profile  $v(t) = y(t) - r(t) \in \mathcal{R}^{226}$  by a linear spatial downsampling transformation,

$$v(t) = C_m^T v_h(t) \quad (5.44)$$

where  $C_m \in \mathcal{R}^{693 \times 226}$ .

While it is difficult to quantitatively compare the closed-loop profiles in Figure 5.8,

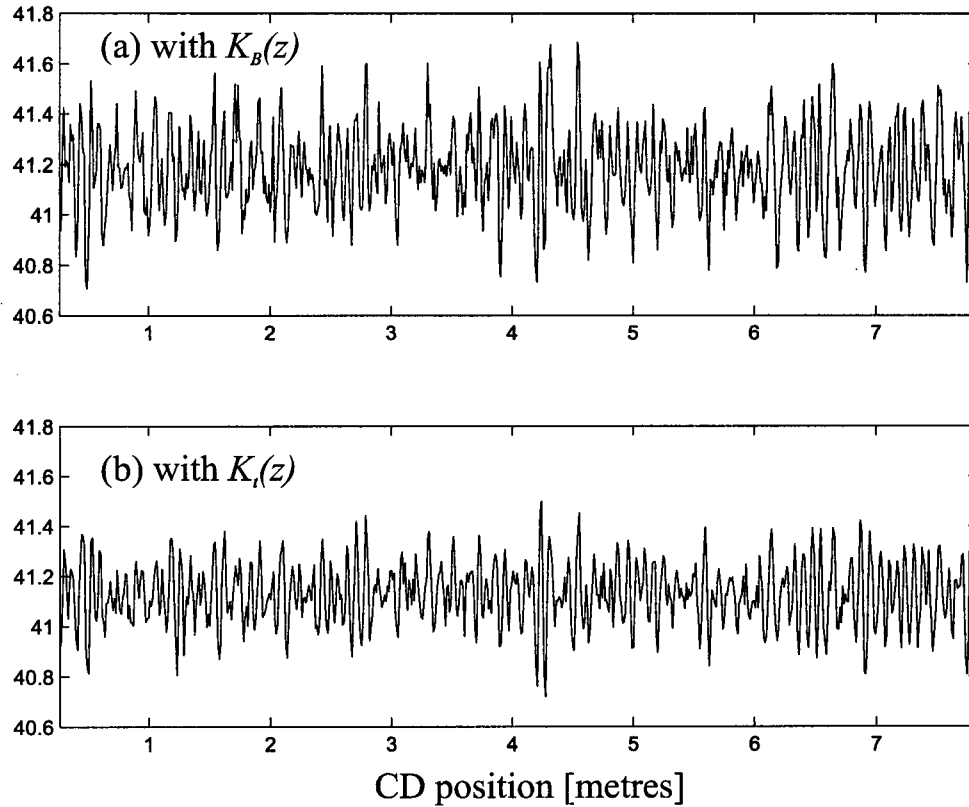


Figure 5.8: The steady-state of the measured paper profiles under closed-loop control, (a) with the controller  $K_b(z)$  in (5.41) which was designed according to the more traditional industrial tuning rules, and (b) with the controller  $K_t(z)$  in (5.39) which was designed according to two dimensional loop shaping procedure in Chapter 4.

there is much information available in the spatial frequency content of these signals. Figure 5.9 contains the steady state spatial frequency components of the error profile  $\tilde{v}(\nu_j, z) = \tilde{y}(\nu_j, z) - \tilde{r}(\nu_j, z)$  with  $z = e^{i\omega}$  and  $\omega = 0$ .

The spectra in Figure 5.9 indicate that the two controllers  $K_b(z)$  and  $K_t(z)$  provide approximately the same performance for higher spatial frequencies  $\nu > 8\text{m}^{-1}$ . In Figure 5.2 it can be seen that the open-loop gain of the process  $\tilde{g}(\nu_j, z)$  in (5.16) rolls off as a function of spatial frequency. The process is much harder to control at high spatial frequencies and both controllers have this bandwidth limitation.

At very low spatial frequencies  $\nu < 1\text{m}^{-1}$  the closed-loop performance is not significantly different for  $K_b(z)$  and  $K_t(z)$ . The contour plots in Figures 5.3 and 5.7 predicted that each of these controllers would achieve over 90% attenuation of disturbances for these

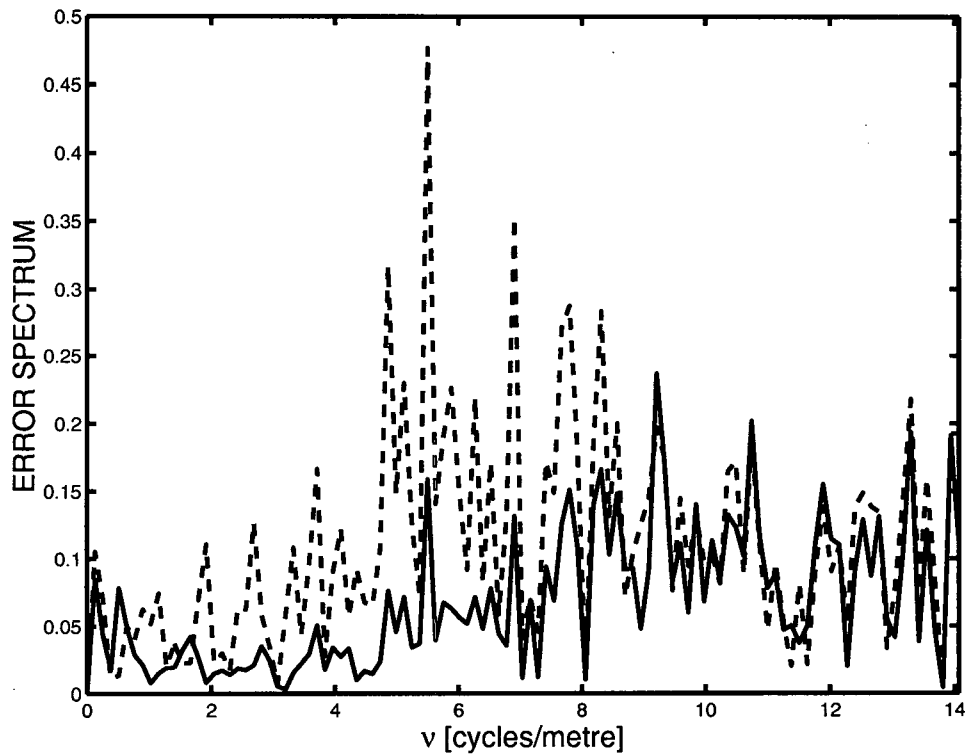


Figure 5.9: Spatial frequency power spectra of the steady-state error profiles of the closed-loop system with the controller  $K_b(z)$  in (5.41) shown as the dashed line, and the controller  $K_t(z)$  in (5.39) shown as the solid line.

low spatial frequencies.

It is the mid-range spatial frequencies  $2\text{m}^{-1} < \nu < 7\text{m}^{-1}$  where the greatest difference in closed-loop performance is realized. The contour plots in Figure 5.3 and Figure 5.7 indicated that the controller  $K_t(z)$  would achieve approximately twice the closed-loop spatial bandwidth of the more conservative controller  $K_b(z)$ . It can be seen easily in Figure 5.9 the performance of the controller  $K_t(z)$  is significantly better than that of the controller  $K_b(z)$  for these mid-range spatial frequencies.

## Chapter 6

### Conclusions

This work has concentrated on the analysis and design of feedback control for dynamical systems that are distributed in one spatial dimension and controlled by an array of identical actuators. The cross-directional control of paper machines is an industrially important example of such a process and it has played a central role in shaping this work. This Chapter summarizes the goals, approach, and results contained in this thesis.

Chapter 1 illustrated the broad range of cross-directional processes occurring in industrial paper machine applications. The spatial response of the process to a single actuator can be as narrow as two actuator-widths, or as wide as about a third of the paper sheet. The dynamics of these processes are also diverse. Relative to the sample time, the actuators can respond almost instantaneously or be slow enough to be described as an integrating process. Process deadtime due to the transport delay of the paper sheet from the actuator array to the scanning sensor must also be considered. Time delays as long as five sample times have been observed in working mills.

There exists a large body of theoretical work in advanced control which may possibly be applied to the cross-directional control problem, as discussed in Section 1.3. In addition to the theoretical work directed specifically at cross-directional control of flat sheet processes, there have also been many advances in multivariable control, robust control, and spatially distributed systems, that can be collected and applied to the cross-directional control problem.

However, in spite of the existing control theory, the state of the art for industrial paper machine control is to design the cross-directional controller using empirical rules-of-thumb. This is a complex task and, as a result, many paper machines are running with poorly-tuned feedback controllers. The two most common problems associated with profile control represent the two extremes associated with feedback controller design.

First, the closed-loop may be conservatively designed, resulting in an underactive control which does not do enough to remove variation in the process. This was the situation faced by the mill as described in Chapter 5. The second problem faced by papermakers is that of closed-loop instability. The cross-directional controller is often designed without calculation of a stability margin, and the incautious application of empirical tuning rules has led to a large number of paper machines with a marginally-stable closed-loop. This is a potentially dangerous situation as the process model uncertainty, inevitably occurring when modelling real-world problems, easily destabilizes such a closed-loop system. This instability always results in operator intervention and often results in financial loss for the mill due to culled paper.

In order to reconcile the above issues, in Chapter 3 a general framework is presented for the analysis of dynamical systems that are distributed in one spatial dimension and controlled by an array of identical actuators. Within this framework, Chapter 4 developed a constructive technique for the design of practical feedback controllers for such processes. Referred to as two dimensional loop shaping, the analogy to the traditional 'one dimensional' loop shaping is preserved in order to allow the transfer of knowledge and experience from a design technique that is familiar to most control engineers. This technique is graphical in nature and allows the designer to view the trade-off between the conflicting criteria of closed-loop stability and aggressive closed-loop performance of the control system.

As spatially distributed systems tend to involve a large number of input and output variables, the feedback control can potentially involve a large amount of computation - both offline for controller design and also online for real-time implementation. Here the offline computations, involved in the design of the controller, are kept low by exploiting the natural structure of the process. The real-time computation is negligible due to the low complexity of the resulting feedback control law.

As stated above, the analysis and design techniques developed and presented in this work were motivated by the need to tune cross-directional controllers for industrial paper machines. The two dimensional loop shaping technique is applied as a tool for the design of feedback controllers for paper machine cross-directional processes. This framework

for analysis and design was shown to be well-suited to address the wide variety of such processes for which a cross-directional controller must perform well.

The theoretical component of this work has been balanced by the requirements of tuning an industrial paper machine in a working mill. This practical control problem was maintained as an example throughout this work. Chapter 5 contains the details of the inaugural field trial on an industrial paper machine in a Canadian mill producing newsprint-grade paper. The analysis of the control system indicated that the mill had tuned their controller to be overly conservative. The industrial controller was then retuned using the tool that was developed based on the two dimensional loop shaping technique described in Chapters 3 and 4. The results of the 'before' and 'after' closed-loop performance of the control system were recorded and analyzed. The design technique was validated when the retuned control system was found to remove significantly more variation from the product without compromising the closed-loop stability margins of the system.

## Bibliography

- [1] Calculation and partitioning of variance using paper machine scanning sensor measurements. Technical information paper, Technical Association of the Pulp and Paper Industry, TIP 1101-01 1996.
- [2] R. Abraham and J. Lunze. Modelling and decentralized control of a multizone crystal growth furnace. *Int. J. Robust and Nonlinear Control*, 2:107–122, 1992.
- [3] J.U. Backstrom, C. Gheorghe, G.E. Stewart, and R.N. Vyse. Constrained model predictive control for cross directional multi-array processes. In *Control Systems 2000*, pages 331–336, Victoria, BC, May 2000.
- [4] B. Bamieh, F. Paganini, and M. Dahleh. Distributed control of spatially-invariant systems. *IEEE Trans. Automat. Contr.*, to appear.
- [5] L.G. Bergh and J.F. MacGregor. Spatial control of sheet and film forming processes. *The Canadian Journal of Chemical Engineering*, 65:148–155, February 1987.
- [6] R.W. Brockett and J.L. Willems. Discretized partial differential equations: Examples of control systems defined on modules. *Automatica*, 10:507–515, 1974.
- [7] S.-C. Chen and R.G. Wilhelm Jr. Optimal control of cross-machine direction web profile with constraints on the control effort. In *Proc. of American Control Conf.*, USA, June 1986.
- [8] R.Y. Chiang and M.G. Safonov. *Matlab Robust Control Toolbox - Version 2*. The MathWorks, Inc., 1997.
- [9] K. Cutshall. Cross-direction control. In *Paper Machine Operations, Pulp and Paper Manufacture, 3rd ed., vol. 7*, pages 472–506, Atlanta and Montreal, Chap. XVIII 1991.

- [10] R. D'Andrea. Linear matrix inequalities, multidimensional system optimization, and control of spatially distributed system: An example. In *Proc. of American Control Conf.*, pages 2713–2717, San Diego, CA, USA, June 1999.
- [11] R. D'Andrea and G.E. Dullerud. Distributed control of spatially interconnected systems. *IEEE Trans. Automat. Contr.*, submitted.
- [12] R. D'Andrea, G.E. Dullerud, and S. Lall. Convex  $l_2$  synthesis for multidimensional systems. In *Proc. of IEEE Conference on Decision and Control*, pages 1883–1888, Tampa, FL, USA, December 1998.
- [13] P.J. Davis. *Circulant Matrices*. Wiley, New York, 1979.
- [14] G. Ayres de Castro and F. Paganini. Control of distributed arrays with recursive information flow: Some case studies. In *Proc. of IEEE Conference on Decision and Control*, pages 191–196, Phoenix, AZ, USA, December 1999.
- [15] N. Denis and D.P. Looze.  $\mathcal{H}_\infty$  controller design for systems with circulant symmetry. In *Proc. of IEEE Conference on Decision and Control*, pages 3144–3149, Phoenix, AZ, USA, December 1999.
- [16] J.C. Doyle and G. Stein. Multivariable feedback design: Concepts for a classical/modern synthesis. *IEEE Trans. Automat. Contr.*, AC-26(1):4–16, February 1981.
- [17] G.E. Dullerud, R. D'Andrea, and S. Lall. Control of spatially varying distributed systems. In *Proc. of IEEE Conference on Decision and Control*, pages 1889–1893, Tampa, FL, USA, December 1998.
- [18] G.A. Dumont. Analysis of the design and sensitivity of the Dahlin regulator. Technical report, Pulp and Paper Research Institute of Canada, PPR 345 1981.
- [19] S.R. Duncan. *The Cross-Directional Control of Web Forming Processes*. PhD thesis, University of London, UK, 1989.
- [20] S.R. Duncan. The design of robust cross-directional control systems for paper making. In *Proc. of American Control Conf.*, pages 1800–1805, Seattle, WA, USA, June 1995.

- [21] S.R. Duncan and G.F. Bryant. The spatial bandwidth of cross-directional control systems for web processes. *Automatica*, 33(2):139–153, 1997.
- [22] S.J. Elliott. Down with noise. *IEEE Spectrum*, pages 54–61, June 1999.
- [23] M.J. Englehart and M.C. Smith. A four-block problem for  $\mathcal{H}_\infty$  design: Properties and applications. *Automatica*, 27(5):811–818, 1991.
- [24] A.P. Featherstone and R.D. Braatz. Input design for large-scale sheet and film processes. *Ind. Eng. Chem. Res.*, 37:449–454, 1998.
- [25] C.R. Fuller, S.J. Elliott, and P.A. Nelson. *Active Control of Vibration*. Academic Press, London, 1996.
- [26] D.H. Gay and W.H. Ray. Identification and control of distributed parameter systems by means of the singular value decomposition. *Chem. Eng. Sci.*, 50(10):1519–1539, 1995.
- [27] T.T. Georgiou and M.C. Smith. Optimal robustness in the gap metric. *IEEE Trans. Automat. Contr.*, 35(6):673–686, June 1990.
- [28] J. Ghofraniha. *Cross-Directional Response Modelling, Identification and Control of the Dry Weight Profile on Paper Machines*. PhD thesis, Department of Electrical and Computer Engineering, University of British Columbia, Vancouver, Canada, 1997.
- [29] G.C. Goodwin, B.M. Carny, and W.J. Edwards. Analysis of thermal camber control in rolling mills. In *Proc. IFAC World Congress*, pages 160–164, Tallinn, USSR, 1990.
- [30] D.M. Gorinevsky. On regularized feedback update of distributed-parameter systems in control and nonlinear estimation applications. In *Proc. of American Control Conf.*, pages 1823–1827, Albuquerque, NM, USA, June 1997.
- [31] D.M. Gorinevsky. Honeywell opportunities in control of distributed micro electro-mechanical systems. In *Meeting on Distributed-Parameter System Control*, Cupertino, CA, USA, February 1999.

- [32] D.M. Gorinevsky, E.M. Heaven, C. Sung, and M. Kean. Integrated tool for intelligent identification of CD process alignment shrinkage and dynamics. *Pulp and Paper Canada*, 99(2):40–60, 1998.
- [33] D.M. Gorinevsky, E.M. Heaven, and R.N. Vyse. Performance analysis of cross-directional control using multivariable and spectral models. *IEEE Trans. on Control Systems Technology*, to appear.
- [34] W.P. Heath. Orthogonal functions for cross-directional control of web forming processes. *Automatica*, 32(2):183–198, 1996.
- [35] W.P. Heath and P.E. Wellstead. Self-tuning prediction and control for two-dimensional processes. part 1: Fixed parameter algorithms. *Int. J. Control*, 62(1):65–107, 1995.
- [36] E.M. Heaven, I.M. Jonsson, T.M. Kean, M.A. Manness, and R.N. Vyse. Recent advances in cross-machine profile control. *IEEE Control Systems Magazine*, pages 36–46, October 1994.
- [37] M. Hovd, R.D. Braatz, and S. Skogestad. Optimality of SVD controllers. Technical report, Norwegian University of Science and Technology, December 1996.
- [38] M. Hovd and S. Skogestad. Control of symmetrically interconnected plants. *Automatica*, 30(6):957–973, 1994.
- [39] D.W. Kawka. *A Calendering Model for Cross-Direction Control*. PhD thesis, McGill University, Montreal, Canada, 1998.
- [40] K. Kristinnson and G.A. Dumont. Cross-directional control on paper machines using gram polynomials. *Automatica*, 32(4):533–548, 1996.
- [41] D.L. Laughlin, M. Morari, and R.D. Braatz. Robust performance of cross-directional control systems for web processes. *Automatica*, 29(6):1395–1410, 1993.
- [42] W.S. Levine and M. Athans. On the optimal error regulation of a string of moving vehicles. *IEEE Trans. Automat. Contr.*, 11(3):355–361, August 1966.

- [43] P. Lundstrom, S. Skogestad, and J.C. Doyle. Two-degree-of-freedom controller design for an ill-conditioned distillation process using  $\mu$ -synthesis. *IEEE Trans. Contr. Syst. Technol.*, 7(1):12–21, January 1999.
- [44] D. McFarlane and K. Glover. A loop shaping design procedure using  $\mathcal{H}_\infty$  synthesis. *IEEE Trans. Automat. Contr.*, AC-37(6):759–769, June 1992.
- [45] A.V. Oppenheim and R.W. Schaffer. *Discrete-Time Signal Processing*. Prentice Hall, New Jersey, 1989.
- [46] F. Paganini. A recursive information flow system for distributed control arrays. In *Proc. of American Control Conf.*, pages 3821–3825, San Diego, CA, USA, June 1999.
- [47] G. Papageorgiou and K. Glover. A systematic procedure for designing non-diagonal weights to facilitate  $\mathcal{H}_\infty$  loop shaping. In *Proc. of IEEE Conference on Decision and Control*, pages 2127–2132, San Diego, CA, USA, December 1997.
- [48] T.F. Patterson and J.M. Iwamasa. Review of web heating and wet pressing literature. In *TAPPI Papermakers Conf.*, Atlanta, GA, USA, March 1999.
- [49] J. Reinschke.  *$\mathcal{H}_\infty$  Control of Spatially Distributed Systems*. PhD thesis, Department of Engineering, University of Cambridge, England, 1999.
- [50] A. Rigopoulos. *Application of Principal Component Analysis in the Identification and Control of Sheet-Forming Processes*. PhD thesis, Georgia Institute of Technology, USA, 1999.
- [51] J. Ringwood. Multivariable control using the singular value decomposition in steel rolling with quantitative robustness assessment. *Control Eng. Practice*, 3(4):495–503, 1995.
- [52] T. Samad. Issues in design and control of multi-vehicle aerospace systems. In *Meeting on Distributed-Parameter System Control*, Cupertino, CA, USA, February 1999.
- [53] C.M. Satter and R.E. Freeland. Inflatable structures technology applications and requirements. In *Proc. of AIAA Space Programs and Technologies Conference*, Huntsville, AL, USA, September 1995.

- [54] B. Shu and B. Bamieh. Robust  $\mathcal{H}_2$  control of vehicular strings. *ASME Journal on Dynamics, Measurement and Control*, submitted.
- [55] S. Skogestad, M. Morari, and J.C. Doyle. Robust control of ill-conditioned plants: High-purity distillation. *IEEE Trans. Automat. Contr.*, 33(12):1092–1105, December 1988.
- [56] S. Skogestad and I. Postlethwaite. *Multivariable Feedback Control: Analysis and Design*. Wiley, New York, 1996.
- [57] G.A. Smook. *Handbook for Pulp and Paper Technologists*. Angus Wilde Publications Inc., Vancouver, 2 edition, 1992.
- [58] G.E. Stewart, D.M. Gorinevsky, and G.A. Dumont. Design of a practical robust controller for a sampled distributed parameter system. In *Proc. of IEEE Conference on Decision and Control*, pages 3156–3161, Tampa, FL, USA, December 1998.
- [59] G.E. Stewart, D.M. Gorinevsky, and G.A. Dumont. Robust GMV cross directional control of paper machines. In *Proc. of American Control Conf.*, pages 3002–3007, Philadelphia, PA, USA, June 1998.
- [60] G.E. Stewart, D.M. Gorinevsky, and G.A. Dumont.  $\mathcal{H}_2$  loopshaping controller design for spatially distributed systems. In *Proc. of IEEE Conference on Decision and Control*, pages 203–208, Phoenix, AZ, USA, December 1999.
- [61] G.E. Stewart, D.M. Gorinevsky, and G.A. Dumont. Spatial loopshaping: A case study on cross-directional profile control. In *Proc. of American Control Conf.*, pages 3098–3103, San Diego, CA, USA, June 1999.
- [62] G.E. Stewart, D.M. Gorinevsky, G.A. Dumont, C. Gheorghe, and J.U. Backstrom. The role of model uncertainty in cross-directional control systems. In *Control Systems 2000*, pages 337–345, Victoria, BC, May 2000.
- [63] W.A. Strauss. *Partial Differential Equations: An Introduction*. Wiley, New York, 1992.

- [64] A.J. Thake, J.F. Forbes, and P.J. McLellan. Design of filter-based controllers for cross-directional control of paper machines. In *Proc. of American Control Conf.*, pages 1488–1493, Albuquerque, NM, USA, June 1997.
- [65] R. Vyse, C. Hagart-Alexander, E.M. Heaven, J. Ghofraniha, and T. Steele. New trends in CD weight control for multi-ply applications. In *TAPPI Update on Multiply Forming Forum*, Atlanta, Georgia, USA, February 1998.
- [66] K. Zhou, J.C. Doyle, and K. Glover. *Robust and Optimal Control*. Prentice Hall, New Jersey, 1996.

# Appendix A

## Fourier Matrices

The complex Fourier matrix is defined as follows [38],<sup>1</sup>

$$\mathcal{F}^H = \frac{1}{\sqrt{n}} [m_1 \ m_2 \ \cdots \ m_n] \quad (\text{A.1})$$

where the vectors  $m_k \in \mathcal{C}^{n \times 1}$  are given by,

$$m_k = [1 \ v_k \ v_k^2 \ \cdots \ v_k^{n-1}]^T, \quad v_k = e^{2\pi(k-1)i/n} \quad (\text{A.2})$$

In other words, the  $k^{\text{th}}$  row of  $\mathcal{F}$  contains the  $k^{\text{th}}$  spatial harmonic and has frequency  $\nu_k$ . The complex Fourier matrix  $\mathcal{F} \in \mathcal{C}^{n \times n}$  in (A.1) may then be used to diagonalize any  $n \times n$  circulant matrix,

$$A = \mathcal{F}^H \Sigma_A \mathcal{F}, \quad \Sigma_A = \text{diag}\{a(\nu_1), \dots, a(\nu_n)\} \quad (\text{A.3})$$

The subset of circulant *symmetric* matrices may be diagonalized with a pure real Fourier matrix. The real Fourier matrix  $F$  is constructed from the complex Fourier transform matrix  $\mathcal{F}$  in (A.1) by the following unitary operations,

$$\begin{aligned} F(1, :) &= \frac{1}{n} [1, 1, \dots, 1] \\ F(k, :) &= \frac{1}{\sqrt{2}} (\Im m[\mathcal{F}(k, :)] - \Im m[\mathcal{F}(n+2-k, :)]) \\ F(n+2-k, :) &= \frac{1}{\sqrt{2}} (\Re e[\mathcal{F}(k, :)] + \Re e[\mathcal{F}(n+2-k, :)]) \end{aligned} \quad (\text{A.4})$$

for  $k = 2, \dots, p$ , where  $p = (n+1)/2$  if  $n$  is odd and  $p = n/2$  if  $n$  is even. The  $j^{\text{th}}$  row of  $F$  contains the  $j^{\text{th}}$  spatial harmonic and has frequency  $\nu_j = 2\pi(j-1)/n$ . The real Fourier

---

<sup>1</sup>The unitary, complex Fourier matrix  $\mathcal{F}$  may be created, for example, using the MATLAB command  $\mathcal{F} = \text{fft}(\text{eye}(n))/\text{sqrt}(n)$ .

matrix  $F$  is unitary, satisfying the property  $F^T F = I$ .

More intuitively, the rows of the real Fourier matrix  $F$  in (A.4) may be re-written in terms of the familiar trigonometric functions,

$$F(j, k) = \begin{cases} \sqrt{\frac{1}{n}} & j = 1 \\ \sqrt{\frac{2}{n}} \cdot \sin[(k-1)\nu_j] & j = 2, \dots, p \\ \sqrt{\frac{2}{n}} \cdot \cos[(k-1)\nu_j] & j = p+1, \dots, n \end{cases} \quad (\text{A.5})$$